POLITECNICO DI MILANO

M.Sc. IN CIVIL ENGINEERING

ANALYSIS OF GPR RESPONSE TO THIN LAYERS

SUPERVISOR

Dr. DIEGO AROSIO

THESIS BY

SEYED REZA HOSSEINI

July 2014

POLITECNICO DI MILANO

M.Sc. IN CIVIL ENGINEERING

ANALYSIS OF GPR RESPONSE TO THIN LAYERS

A Master thesis submitted to Department of Civil and Environmental Engineering in partial fulfillment of the requirements for the degree of Master of Science in Civil Engineering.

Submitted by:

Seyed Reza Hosseini

Student ID: 749436

Supervised by:

Dr. Diego Arosio

Department of Civil and Environmental Engineering, Politecnico di Milano

Piazza L. da Vinci, 32, 20133 Milano

Acknowledgement

I would like to express my special appreciate to my advisor professor Diego Arosio, for his patient guidance, enthusiastic encouragement and useful critiques of this research work.

I would also like to thank all of my Iranian and international friends who supported me, and intended me to strive towards my goal. I had great and unforgettable time in Italy; such moments would not have been possible without them.

Finally, I take this opportunity to express my sincere gratitude to my beloved family who were always encouraging me with their best wishes and inspiring me to follow my dreams.

Seyed Reza Hosseini

Politecnico di Milano

July 2014

CONTENT

Abstract

Detection and location of discontinuities like fractures within resistive rock masses by means of Ground Penetrating Radar (GPR) is an effective geophysical method. Investigation with GPR is based on the propagation and reflection of electromagnetic waves. Thanks to the high resolution of this investigation technique, it is possible to detect fractures in mines and over unstable rock slopes. It may also help to improve the production of ornamental rock slabs in the quarrying industry.

In most cases, rock fractures could be considered as beds whose thickness is smaller than the resolution limits (i.e., a thin bed) which are embedded in a homogeneous medium. In the last decade, preliminary studies on GPR response to thin beds have been carried out to determine aperture and filling material of rock fractures.

In this work, GPR experiments and numerical simulations were performed with a high frequency antenna on quarried blocks to compare synthetic and real data. Two rock blocks were placed one in front of the other, to simulate the presence of an air-filled rock fracture. Simulations were performed separately with sandstone blocks (Pietra Giuggiulena, Sicily, Italy) and marble blocks (Carrara, Massa-Carrara, Italy).

The results suggest that, for apertures smaller than one eighth of the dominant wavelength ($\lambda d/8$), a quasi-linear relationship exists between thickness and reflection amplitude. It was found that below this thickness, the information is encoded in the amplitude of the thin-bed response and may be used to determine bed thickness. In addition, the trend of the reflection coefficient as a function of bed thickness was compared with Chung and Lawton (1995) equation, and a good match was observed for thicknesses below $\lambda d/8$.

Key words: Ground Penetrating Radar (GPR), Thin bed, Rock fracture, GprMax, Resolution.

List of Tables

List of Figures

Symbols and Notations

E	Electric field	[V/m]
f	Frequency	[Hz]
f_c	Central frequency	[Hz]
f_d	Dominant frequency	[Hz]
I	Current	[A]
j_c	Conduction current density	[A/m^2]
j_d	Displacement current density	[A/m^2]
j_t	Total current density	[A/m^2]
R_{12}	Reflection coefficient at the interface of two semi-infinite media (1) and (2)	-
R	Reflection coefficient	-
t	Time	[s]
t_0	Relaxation time	[s]
T	Period	[s]
T_{12}	Transmission coefficient at the interface of two semi-infinite media (1) and (2)	-
T_x	Radiation pattern term of the receiving antenna	-
V	Velocity of electromagnetic waves	[m/s]
α	Attenuation (propagation formulation)	[dB/m]
β	Phase term (propagation formulation)	[rad/m]
ε_e	Effective permittivity	[F/m]
$\varepsilon', \varepsilon''$	Real and imaginary parts of the permittivity	[F/m]
ε_o	Permittivity of the vacuum = 8.84 10-12 F/m	[F/m]
ε_r	Dielectric constant	-
λ	Wavelength	[m]
μ	Magnetic permeability	[H/m]
μ_0	Magnetic permeability of the vacuum = $4\pi 10^{-7}$ H/m	[H/m]
μ_r	Relative magnetic permeability	-
ρ	Free charge density	[C/m^3]
σ	Conductivity	[S/m]
σ', σ''	Real and imaginary parts of the conductivity	[S/m]
ω	Angular frequency	[rad/s]

Objective and Outline of the Study

Detection and location of fractures is crucial in many fields of earth sciences and geoengineering, e.g. hydrology, geology, mining industry, environmental sciences and civil engineering. In most cases rock fractures can be considered as beds whose thickness is smaller than the resolution limit (i.e., a thin bed), and can be imagined as layers embedded in a homogeneous formation, giving rise to reflected signals from the top and the bottom of the bed having opposite polarities.

The fundamental objective of this thesis consist in considering GPR experiments and numerical simulations performed with high frequency antenna on quarried Sandstone and Marble blocks to compare analytical expressions of thin bed response to real and synthetic GPR datasets.

This document is divided into two major chapters. The first one is devoted to general description about Ground Penetrating Radar, related theory and useful definitions. A summary of previous works on thin beds is also provided in this chapter.

Chapter 2 is dedicated to a complete explanation of experimental set up, acquisition and analysis of synthetic and real data. This chapter is separated into two parts addressing the analysis of data regarding experiments with Sandstone and Marble blocks respectively.

At the end, conclusions and final comments of these investigations are presented.

CHAPTER 1

GPR AND ROCK DISCONTINUITIES

1.1. Introduction to GPR

Radar is an object-detection system is a part of the electromagnetic spectrum to determine the range, altitude, direction, or speed of both moving and fixed objects such as aircraft, ships, spacecraft, guided missiles, motor vehicles, weather formations, and terrain. The radar antenna transmits pulses of radio waves, which bounce off any object in their path. The object returns a tiny part of the wave's energy to a dish or antenna, which is usually located at the same site as the transmitter.

The history of RADAR began in 1886 with a German Physicist by name Heinrich Hertz when he demonstrated that electromagnetic waves can be reflected off solid objects. In 1895 Alexander Popov, a physics instructor at the Imperial Russian Navy School in Kronstadt (Russian town), developed an apparatus using a tube that could detect distant lightning strikes. Christian Hulsmeyer, a German researcher, was the first to use radio waves to detect the presence of distant metallic objects.

The term RADAR is an acronym which was coined in mid-1930‘s by British and American scientists who conducted experiments with devices to locate objects such as ships and aircrafts by the reflection of radio waves. The process was originally called Radio Location, but as subsequent experiments proved to be successful a well-structured name was chosen; RAdio Detection and Ranging. Hence, the name RADAR. A radar system usually operates in the ultra-high-frequency (UHF) or the microwave part of the radio frequency (RF) spectrum. Radar is something that is in use all around us, although it is normally invisible. It has diverse applications in numerous fields including traffic control, radar astronomy, military applications, flight control systems, meteorology, outer space surveillance, marine applications, geology, geophysics, etc. Police uses radar to detect the speed of passing motorists. Air traffic control uses radar to track planes both on the ground and in the air, and also to guide planes in for smooth landings. In Radar astronomy, radar is used to observe nearby astronomical objects by reflecting microwaves off target objects and analyzing the echoes. The military uses it to detect the enemy and to guide weapons in locating their targets. Meteorologists use radar to track storms hurricanes and tornadoes and also important tool in weather forecasting and helps make the forecasts more accurate. NASA (National Aeronautical and Space Administration), uses radar to map the Earth and other planets, to track satellites and space debris and to help with things like docking and maneuvering. In marine applications, radars are used to measure the bearing and distance of ships to prevent collision with other ships, to navigate and fix their positions at sea when within range of shore or other fixed references such as islands, buoys and light ships. The automatic opening of the doors when one enters a supermarket is also common application of radar in everyday life. Ground Penetrating Radar (GPR) as a geophysical technique is a high frequency electromagnetic method that uses radio pulses to image the subsurface. The frequencies used are the Ultra High Frequencies (UHF) or the Very High Frequencies (VHF) of the microwave band of the radio spectrum. Precisely, GPR works within the range from 10MHz to 2GHz. It is a nondestructive

and noninvasive method that can use electromagnetic wave propagation and scattering to image, locate and quantitatively identify changes in electrical and magnetic properties in the subsurface.

The first attempt in applying GPR was made in 1920s in Austria, to determine the thickness of the ice in the glacier. The aspects of the technology remained mainly forgotten until 1950s, when US Air Force radar on board technicians noticed that their radar pulses were penetrating the glacial ice flying over Greenland. A number of mishap occurred since airborne radar analysts were detecting the bedrock surface below the ice interpreting it as a ground surface, neglecting the ice above and almost causing planes to crash into glaciers. Realization that radar is able to penetrate ice led to various experiments with ice and other materials, such as soil and water. As a result, the first GPR prototype was designed in 1967 by NASA and sent on a mission to the Moon to determine surface conditions prior to arrival of manned vehicle. In the 1970s it was recognized the ability of GPR to detect and locate buried objects, such as pipes, tunnels, mine shafts etc. At the same time, geologist and hydrologists began to investigate buried and surface soil units. The development has been continued in future, both in the field of the GPR devices design and processing techniques. The advancements in the field of portable computers have strongly influenced the field. The existence of numerous lossy dielectric material environments combined with the broad radio frequency spectrum led to a wide range of GPR applications. It is often said that applications of GPR are limited only by the imagination of the people and availability of suitable instrumentation and processing techniques. Similar methodology can be applied to glaciology and to nondestructive testing of concrete structures; the spatial scale of applications varies from kilometers to centimeters.

GPR has become a very significant technique in subsurface exploration over the last few years. Ground penetrating radar provides high-resolution images of shallow non-conductive soils, rocks or structures. Apart from the nature of the waves, the principle is very comparable to reflection seismic techniques. Ground penetrating radar is based on the propagation and reflection of high frequency (20MHz-2GHz) electromagnetic waves. The electromagnetic waves which transmitted from an antenna (Tx) are reflected on layers and objects in subsurface. These reflections are received with another antenna (Rx). The material properties that control electromagnetic energy transfer through media are electrical conductivity, relative dielectric permittivity and relative magnetic permeability.

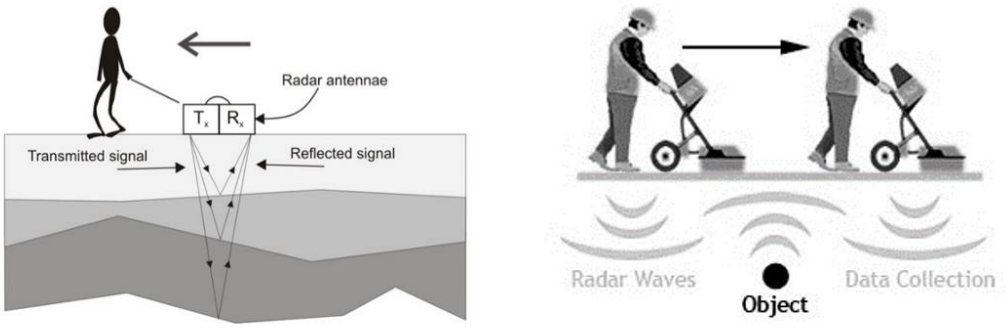

Figure 1-1, Simplified illustration of the operation of GPR

In Table 1-1, there is a list of different geophysical methods and their dependent physical properties. These properties for GPR are Permittivity and Electric conductivity.

Geophysical Method	***Dependent Physical Property***
Gravity	Density
Magnetic	Susceptibility
Seismic refraction	Elastic moduli; density
Seismic reflection	Elastic moduli; density
DC-Resistivity	Resistivity
Induced polarization (IP)	Resistivity; capacitance
Electromagnetic (EM)	Conductance; inductance
EM-VLF	Conductance; inductance
EM- ground penetrating radar	Permittivity; conductivity
Magneto-telluric (MT)	Resistivity

Table 1-1. Geophysical Methods for Subsurface Investigation

The transmitting antenna radiates a short high frequency electromagnetic pulse into the subsurface, where it is Refracted, Diffracted and Reflected primarily as it encounters changes in dielectric Permittivity and Electric conductivity.

1.2. Theory

The EM field generated by the transmitter is produced by oscillating charges. In a nutshell, these charges generate electric fields that in time will generate magnetic fields and vice versa. The continuous generation of electric and magnetic fields constitutes electromagnetic, sinusoidal shaped waves that propagate in the vacuum at a velocity c, the speed of light, equal to 0.299 m/ns. Electromagnetic waves can be classified according to their frequency, wavelength or quantum energy as shown in Figure 1-2.

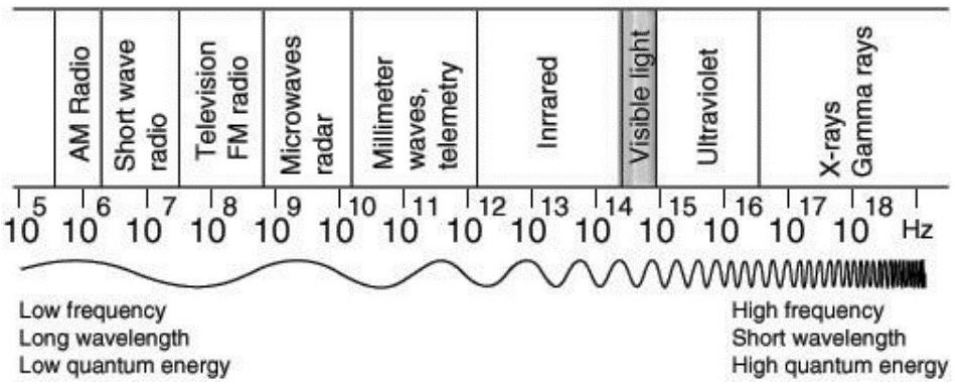

Figure 1-2, Electromagnetic spectrum from low frequency, long wavelength and low quantum energy (radio waves) to high frequency, short wavelength and high quantum energy (X-rays, Gamma rays).

The main material properties that control transfer of electromagnetic energy through a media are Electrical Conductivity, Relative Magnetic Permeability and Relative Dielectric Permittivity. In the following, these three parameters are explained individually. In the following the expressions for Reflection coefficients, Transmission coefficient, Velocity of the electromagnetic wave and Electromagnetic impedance are mentioned.

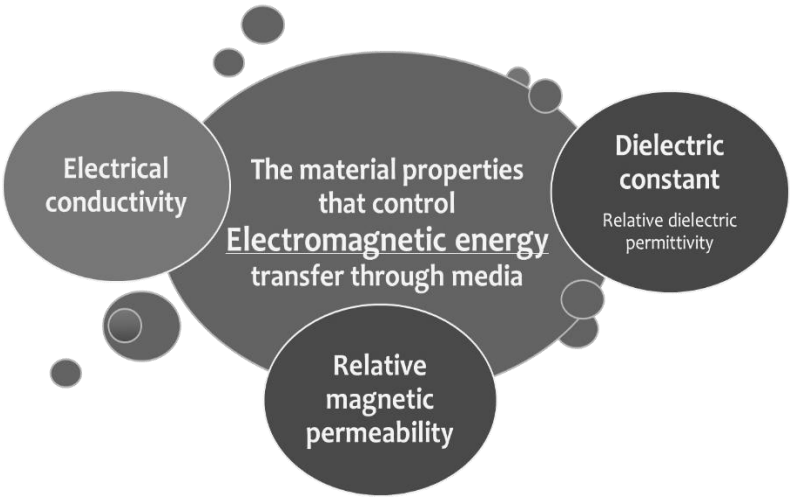

Figure 1-3, The material properties that control electromagnetic energy transfer through media

Dielectric constant (Relative dielectric permittivity) (εr)

Dielectric constant is a measure of the capacity of a material to store a charge when an electric field is applied. Relative dielectric constant is a dimensionless number and commonly represented by the Greek letter (ε_r). The application of an electric field to a material results in a local redistribution of bound charges. The displacement currents are related to the electric field by

$$j_d = \varepsilon \frac{\partial E}{\partial t} \qquad (1\text{-}1)$$

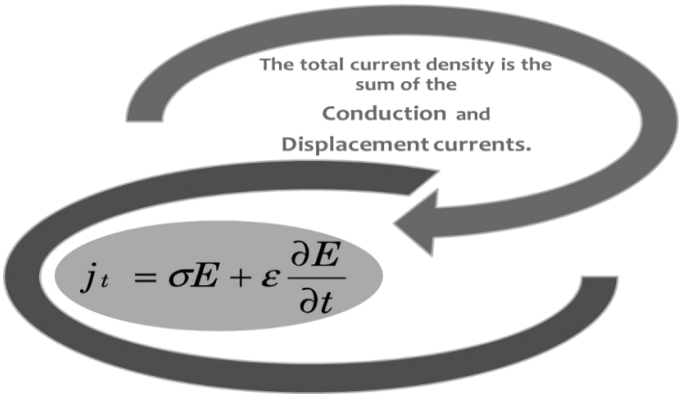

Figure 1-4, The total current density is the sum of the conduction and displacement current

For a generic dielectric, permittivity is a complex number.

$$\varepsilon = \varepsilon' - j\varepsilon'' \qquad (1\text{-}2)$$

The imaginary parts represent the energy dissipation. The relative dielectric constant (ε_r) is defined as the ratio of the permittivity divided by the permittivity in vacuum.

$$\varepsilon_r = \frac{\varepsilon}{\varepsilon_o} \qquad (1\text{-}3)$$

The permittivity in vacuum is ε_0 =8.85 10^{-12} *farad* per *meter*. Dielectric constant controls the strength of the signal reflection. How much signals is reflected and how much passes through depends largely on difference of dielectric constant between the two layers. We assume to work in a medium with a very small conductivity and constant relative magnetic permeability.

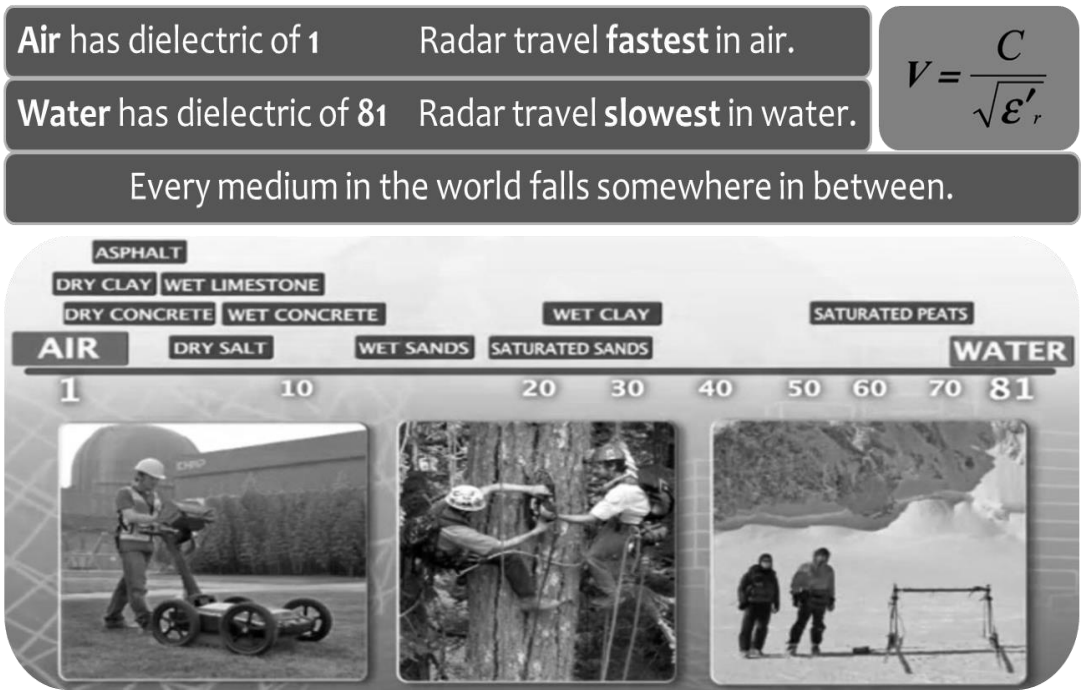

Figure 1-5, Dielectric constant of different mediums

Electrical conductivity (σ)

The application of an electric field to a material causes the displacements of free charged particles such as electrons or ions. A measure of the ability of a material to conduct current is the *electrical conductivity*. It is the reciprocal of electrical resistivity ($\sigma=1/\rho$) and commonly represented by the Greek letter σ. Its SI unit is *siemens* per *meter* ($S \cdot m^{-1}$). The conductive currents are related to the electric field by

$$j_c = \sigma E \qquad (1\text{-}4)$$

The electric conductivity is complex.

$$\sigma = \sigma' + i\sigma'' \qquad (1\text{-}5)$$

Electrical conductivity represents the energy dissipation during charge distribution. It controls the signal penetration depth. As conductivity increases, the penetration depth decreases. This is because the electromagnetic energy is more quickly dissipated into heat, causing a loss in signal strength at depth. We assume to work in a medium with a very small conductivity and negligible imaginary part of dielectric constant.

$$\text{thus} \quad \varepsilon'' = 0 \quad , \quad \sigma \ll \varepsilon' \omega$$
$$\text{and} \quad \alpha \cong \omega \sqrt{\mu \varepsilon'} \, \frac{\sigma}{2\omega\varepsilon'} \qquad (1\text{-}6)$$

The conductivity of soils and rocks is mainly due to the pore fluids. Common rock forming minerals (SiO2, silicates, carbonates) have a very low conductivity ($s=10^{-10}\_10^{-4}$ S/m) while the pore fluids may be very conductive (typically 10^{-2} to 1 S/m). The fracture density in rocks and the porosity in soils thus play a major role.

Relative magnetic permeability (μ_r)

Relative magnetic permeability (μ_r) is defined as the ratio of the permeability of a specific medium to the permeability of free space.

$$\mu = \frac{\mu_r}{\mu_0} \qquad (1\text{-}7)$$

The permittivity of free space is equal to $\mu_0 = 4\pi \times 10^{-7}$ *henry* per *meter*.

This parameter is often ignored in GPR studies because many natural, near-surface materials are assumed to have a very weak magnetic response. In geology, the magnetic properties have not a relevant role because they do not considerably vary from rock to rock. However, sands and soils exhibit significant magnetic responses in laboratory measurements and GPR data acquired through such materials require consideration of magnetic field storage and loss effects.

Velocity (V)

Velocity of the electromagnetic wave is always given by:

$$V = \frac{\omega}{\beta} = \sqrt{\frac{1}{\varepsilon' \mu}} \qquad (1\text{-}8)$$

Considering relative permittivity and relative magnetic permeability:

$$V = \sqrt{\frac{1}{\varepsilon_0 \varepsilon'_r \mu_0 \mu_r}} \qquad (1\text{-}9)$$

If *C* indicates the speed of light:

$$V = \frac{C}{\sqrt{\varepsilon'_r \mu_r}} \qquad (1\text{-}10)$$

Finally, since the relative magnetic permeability of non-magnetic rock formations is approximately one, we generally have:

$$V = \frac{C}{\sqrt{\varepsilon'_r}} \qquad (1\text{-}11)$$

From this expression, we conclude that the velocity of radar waves is affected by dispersion because permittivity is generally a non-constant function of frequency within the bandwidth of the radar systems.

Electromagnetic impedance (Z), Reflection (R) and Transmission coefficients (T)

When a wave comes to a surface that separates two media with different electromagnetic characteristics, the energy will be partially reflected and partially transmitted. The quantity of reflected and transmitted energy, for normal incidence, depends on the Reflection coefficients R and Transmission coefficient T.

$$T = \frac{2Z_1}{Z_1 + Z_2} \qquad (1\text{-}12)$$

$$R = \frac{Z_2 - Z_1}{Z_2 + Z_1} \qquad (1\text{-}13)$$

In addition, these quantities depend on the electromagnetic impedance Z1 and Z2 of the media.

$$Z^2 = \frac{j\omega\mu}{j\omega\varepsilon + \sigma} \qquad (1\text{-}14)$$

Since μ is generally constant in rock formations, reflections are normally produced by ε or σ variations within the inspected space. One can consider three different situations for electromagnetic impedance that the third case is interesting for GPR applications. We assume to work in a medium with a very small conductivity and with a negligible imaginary part of permittivity:

1. For $\boldsymbol{\varepsilon'' = 0}$ and $\boldsymbol{\sigma = 0}$

$$Z = \sqrt{\frac{\mu}{\varepsilon'}} \qquad (1\text{-}15)$$

2. For $\boldsymbol{\varepsilon'' \ll \varepsilon'}$ and $\boldsymbol{\sigma = 0}$

$$Z \cong \sqrt{\frac{\mu}{\varepsilon'}} \left(1 + j\frac{\varepsilon''}{2\varepsilon'}\right) \qquad (1\text{-}16)$$

3. For $\boldsymbol{\varepsilon'' = 0}$ and $\boldsymbol{\sigma \ll \varepsilon'\omega}$

$$Z \cong \sqrt{\frac{\mu}{\varepsilon'}} \left(1 + j\frac{\sigma}{2\omega\varepsilon'}\right) \qquad (1\text{-}17)$$

Properties of different materials and soil types

The Table 1-2 contains a list of materials and their relative permittivity values, conductivities and wave velocities. According to the general tendency of the materials, water content decreases the velocity of waves: Water, compared to any other material in the list has the greatest relative permittivity.

Material	Relative permittivity (ε_r or κ^*)	Conductivity (σ) [S/m]	Attenuation constant [dB/m]	Velocity [mm/ns]
Air	1 1	0 3×10^{-15}	0 5.07×10^{-12}	300
Water/ Freshwater	81 80	10^{-6} - 10^{-2} 5×10^{-4}	0.01 9.39×10^{-2}	33
Sea Water	80	3×10^{3}	103	10
Sand, dry **Sand (dry, 3% moisture)**	2 - 6 3.3	10^{-7} - 10^{-3} 1×10^{-5}	0.01 - 1 9.30×10^{-3}	165
Sand (moist, 20% moisture)	10.6	7.5×10^{-5}	3.89×10^{-2}	92
Sand, wet **Sand (wet, 40% moisture)**	10 - 30 24.5	10^{-3} - 10^{-2} 4.5×10^{-4}	0.5 - 5 1.54×10^{-1}	61
Saturated Sand	20 - 30	0.1 - 1.0	0.03 -0.3	60
Silts	5 - 30	1 - 100	1 - 100	70
Clay	5 - 40	2 - 1000	1 - 100	60
Kerosene	1.8 2.09		-	-
Gasoline	2.0	1×10^{-6}		
LNAPL-saturated sand	3.0	1×10^{-6}		

Table 1-2, Common dielectric permittivity and conductivity of some materials

Loss factor

Other useful parameter is the loss tangent or more appropriately the loss factor, P, which is used to describe the loss component of a material and is related to conductivity, permittivity and attenuation coefficient by the following equation

$$P = \left(\frac{\sigma' + \omega\varepsilon''}{\omega\varepsilon' - \sigma''} \right) \qquad (1\text{-}18)$$

This practically useful parameter help us to assess how 'lossy' a lossy dielectric is and, therefore, can provide a guide to physical effects of attenuation on the GPR wave. The loss factor can be used as a limiting expression for the appropriateness of low-loss assumptions and describes the ratio of EM energy loss ($\sigma' + \omega\varepsilon''$) to energy storage ($\omega\varepsilon' - \sigma''$). For relatively dry, low conductivity materials, this will be much less, than 1 and the loss factor can then approximated to (Daniels, 1996)

$$P \cong \left(\frac{\sigma'}{\omega\varepsilon'}\right) \quad (1\text{-}19)$$

This is considered to be the 'low-loss' condition and allows the velocity and wavelength to be approximated to

$$V(m/s) = \left(\frac{c}{\sqrt{\varepsilon\mu}}\right) \quad (1\text{-}20)$$

$$\lambda(m) = \frac{v}{f} \quad (1\text{-}21)$$

Where *f is* the frequency of the propagation wave in the material (in Hertz or cycles per second). For most GPR users, the low-loss condition is a useful and convenient approximation for common materials, and when used in combination with Table 1-2 (Typical relative permittivity and static conductivity values), it provides an appropriate method for calculation of GPR. From this, initial frequency of target depth and resolution can be determined for a particular survey and provides the first step in GPR section interpretation.

What is important to realize is that, in general, the attenuation of a GPR signal is proportional to, and strongly controlled by, the frequency, whilst the velocity is not so dependent on frequency in relative terms. As such, higher frequencies attenuate significantly more than low frequencies, and there is a relative loss of the high-frequency signal component as the wave propagates. The frequency dependence of the attenuation also explains why, relatively speaking, lower-frequency GPR signals penetrate further than higher frequencies.

Convolutional model

Acquisition and processing are often described by means of the convolutional model. A basic model of seismic reflection. Often represented by the Figure 1-6, or a variant of it.

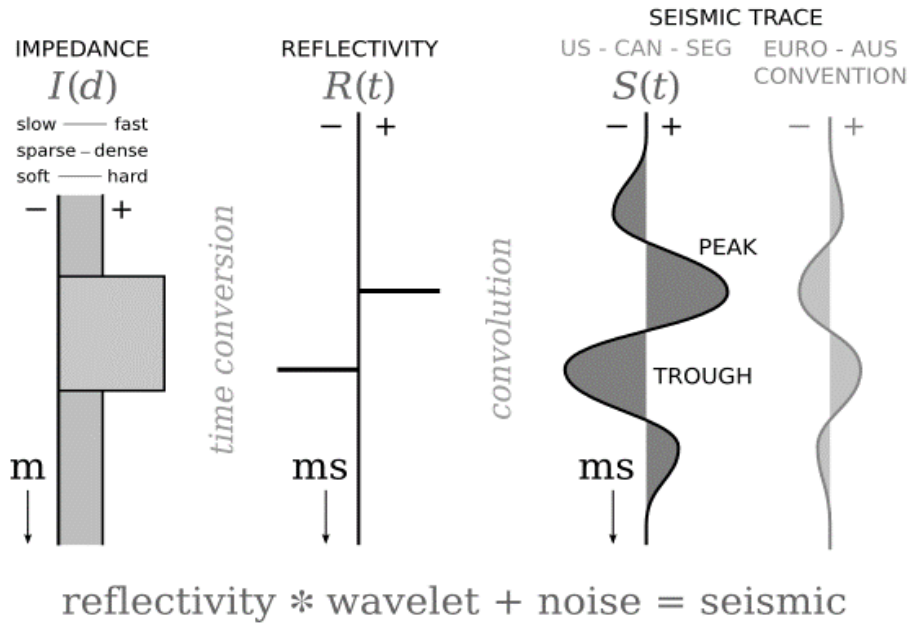

Figure 1-6, Convolutional model

In a nutshell, we have geology on the left: some sort of hard (fast, dense) bed, surrounded by softer material. Instead of 'hardness', we use impedance, *I*, which is the product of density and velocity (of sound waves) in the material. This is transformed to the time domain, and represented by only the impedance contrasts. We call this a reflectivity series, *R*. Now we can convolve this with a wavelet, and this gives us a synthetic, *S*, which is a model seismic trace. It gives us an idea of what a seismic reflection might look like at this interface. There are two traces to illustrate that American geophysicists generally display the seismic with opposite polarity, compared to their European cousins.

1.3. Interaction with subsurface materials

Reflection, Refraction, Diffraction

When electromagnetic waves travelling through the subsurface encounter a buried discontinuity separating materials of a different physical and chemical properties, part of the wave is reflected off the boundary and back to the surface. These subsurface discontinuities may be the interfaces between archaeological features and the surrounding matrix, void spaces, or buried stratigraphic boundaries and discontinuities. The proportion and direction of the reflected electromagnetic waves wave are dependent upon the properties and shape of the deposit off which they are reflected.

The part of the EM wave that is not reflected at subsurface discontinuities changes velocity, and in doing so is refracted and bent at the interface, resulting in a change in the direction of the wave through the ground. The angle at which the wave will be refracted can be predicted based on Snell's Law of Refraction.

In physics, 'diffraction' refers to the bending of waves around objects, or the spreading of waves as they pass through narrow openings. In GPR theory, diffraction is more commonly applied to the phenomenon that produces point source hyperbolas. The hyperbolic image produced from point source reflectors is due to the fact that GPR energy is emitted in a cone, which radiates outwards with depth. As such, energy is reflected from objects that are not directly below the antenna; the reflection, however, is recorded as being directly below the antenna, and at a greater depth due to the oblique transmission of the wave. Only the apex of the hyperbola denotes the actual location of the point source.

Multiples, ringing, and reverberation

Multiples or "ring-down" occur when electromagnetic waves encounter highly-reflective or impermeable objects (such as metals), and are due to multiple reflections between the metal object and the surface. The result is multiple stacked reflections being imaged below the metal object. Ringing refers to system noise produced from the antennas, and is visible in reflection profiles as horizontal banding, usually in the upper portion of the profile. Reverberation, like ring-down, produces multiples in reflection profiles, but it is a result of system noise produced from 'ringing antennae', which reverberate when, spaced too closely.

Background Noise and Clutter

Not all waveforms collected are due to subsurface reflections. Especially in the case of unshielded antenna, reflections may be collected from nearby above ground objects, such as buildings and trees; these generally produce high amplitude linear reflections. Background noise may also be generated by other nearby sources of EM waves, including televisions, cell phones, and radio transmission antennas; GPR survey can be especially compromised by background signals in areas near airports, military bases, or busy roads. The GPR antennae also contribute to background noise, in a way that they produce an EM field that obscures signals within 1.5 wavelengths of the antenna. Background noise produced from subsurface reflections is termed clutter, and refers to point targets and small discontinuities that reflect energy and obscure the signals of other more important reflected waves. Clutter can be minimized is we select antennas of lower frequency, which will not detect small objects.

Attenuation

As the GPR pulse propagates in the geologic medium, it suffers attenuation. High frequency components of the pulse suffer more pronounced effects of attenuation than low frequency components resulting in resolution loss in radargrams. The quality of the GPR images is then strongly dependent on an adequate correction of the attenuation effects. It is important to note that attenuation occurs when EM waves are emitted to the ground as the result of four general factors.

The first one is coupling losses, which occur when the radar antennas are not placed in direct contact with the ground, or when the ground surface is uneven, allowing radar energy to be scattered and lost before it effectively "couples" with the ground. This loss factor can be mostly overcome by making sure that GPR instrumentation is moved slowly and carefully along the ground surface, with antenna attached to the ground.

Another factor is spherical divergence or geometric spreading which occurs when energy is moving into the ground. Energy propagates radially away from the source and decreases in amplitude with increasing distance. The loss of amplitude can be considered by reference to Figure 1-7. The total energy (E) is spread out over a spherical shell with a radius (r) that increases with time. The energy is spread out over the surface of the sphere such that the energy density (i.e. energy per unit area) is $E/4\pi r^2$. Sometime later, when the shell has radius R, the energy density is $E/4\pi R^2$. As R > r, the energy density is now smaller. The energy thus diminishes in proportion to $1/r^2$. Amplitude, which is proportional to the square root of the energy density, thus varies in proportion to 1/r.

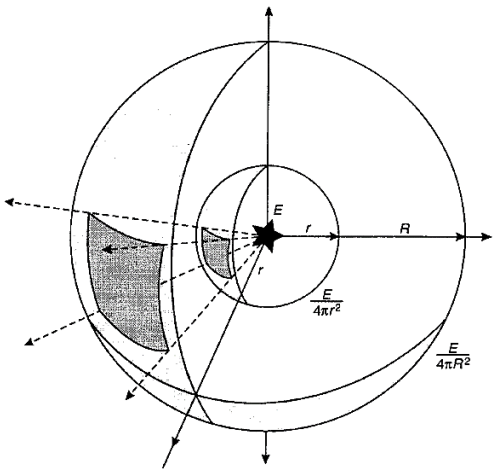

Figure 1-7, The progressive diminution of energy per unit area caused by spherical propagation from an energy source at E

Electromagnetic attenuation is a fourth and probably the most important site-specific factor in determining the GPR method's effectiveness. Radar energy is composed of both electrical and magnetic waves, which move in a conjoined fashion, the removal of either one or the other by electrically conductive or magnetically permeable ground effectively destroy the transmitted energy. It is known that this energy absorption decreases exponentially with distance travelled. It is also varies with the type of material through which the wave passes and is characterized by the attenuation coefficient α. If both spherical divergence (the 1/r term) and absorption

(exp(-αr)) are combined together, the reduction in amplitude with distance is given by the expression (1-23). For a homogeneous material

$$\frac{A}{A_0} = \frac{r_0}{r} e^{-\alpha(r-r_0)} \qquad (1\text{-}22)$$

Where A and A_0 are the amplitudes at distance (r) and (r_0) from the source respectively, and (α) is the attenuation coefficient.

A third site-specific factor is energy scattering, which can be caused when radar energy reflects in random directions from buried objects or discontinuities in the ground, redirecting some of it away from the surface receiving antenna so they are not recorded.

Limitations

The detection of buried objects becomes more difficult if the contrast with the surrounding medium, the quality of the signal, the size, the shape and the orientation related to the antenna are not favorable.

The radar is not applicable in saline water and the soil moistures limits the penetration because of the higher conductivity. It cannot be used to characterize the sea bottom or to detect mines or wrecks (magnetometry) in the sea bottom. The method is not applicable to describe the ground if the top ground layer is conductive (for example clayed soil).
Metallic objects (rails, reinforced concrete, metal bars, and reinforcements in structures, etc.) making the interpretation very difficult, even impossible. They might affect the radar section by the presence of resonance, numerous reflections, high-signal-to-noise ratio, interferences, etc.

Reflection depends on the coupling ground antenna and on the ground permittivity; therefore, there is no information about the source wave and the amplitude of the reflection cannot be compared to the source wave. In reflection mode, the amplitude of the received signal cannot be used straightway to determine the medium attenuation.

The penetration depth is an essential limitation of the GPR when the conductivity of the propagating medium increases. The penetration depth of the electromagnetic waves depends on the properties of soils and the frequency used. It could varies from less than one meter in clay soils to more than 5000 meters in polar ice. In resistive soils, which are favorable to propagation of electromagnetic waves, the penetration is about 10-20m at 100MHz. It decreases up to 1m (or less) if the conductivity is large. The detection of very deep events is limited by the used frequency and by the medium properties.

1.4. Instrumentation

Ground penetrating radar uses a variety of technologies to generate the radar signal. The technologies include impulse, stepped frequency, frequency-modulated continuous wave (FMCW). GPR instrument consist of Control unit, Antenna (T_X, R_X) and a Power supply for the unit. A trolley may also be part of the system if readings are to be taken on a time-distance method. Low frequencies antennas are appropriate for deeper depth, larger targets and give better Penetration depth while on the contrary, high frequencies antennas are suitable for shallow depth, smaller targets, e.g. concrete and they offer high Resolution images.

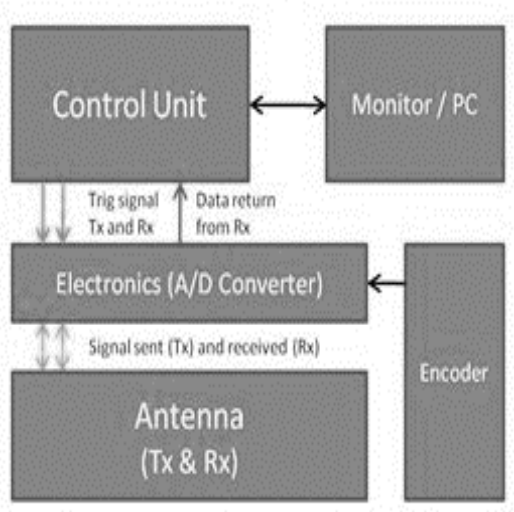

Figure 1-8, GPR Complete system

Figure 1-9, From Left: Antennas, GPR with a trolley

GPR is a relatively young geophysical technique. Over the years, there has been tremendous and rapid improvement in this field. Data acquisition, processing and inversion as well as data interpretation have significantly improved. Brands such as GSSI, Mala, Noggin and pulse EKKO, etc. have done in depth research on GPR and have produced more modern and sophisticated types to meet the challenges of the geophysical field today. These brands have post-processing software, which is compatible with modern and latest version of operating systems-windows 7.

1.5. Surveying and Acquisition

A GPR survey is carried out by displacing a GPR system through a survey line to obtain a GPR profile of the underground. This can either be done manually or by towing with a vehicle. A survey can be done in a way that it will allow the recreation of a complete block of the subsurface (in a three-dimensional model) by taking parallel measurements of the study area. The antenna frequency to be used depends on the objective of the survey and the specifics of the study area. If there is a need for a deeper penetration, a lower frequency can be more useful. The stratigraphy of the underground is also a helpful tool for the surveyor, given that GPR does not perform well in clayey soils and the penetration depths are significantly reduced.

Reflection method and common midpoint (CMP) are the two most common modes of placing the receiving and transmitting antennas with characteristic geometric settings that allow the computation of reflector depths given the travel time of the GPR pulse, or, in case there is a priori information regarding this depth, it is also possible to estimate the soil's dielectric permittivity. In the following three main methods for conducting GPR surveys were explained.

1.Reflected mode

The most used is the reflection method where, in principle, a couple of antennas, a transmitting one and a receiving one are used to collect near-vertical reflections as shown in Figure 1-10. This method is analogous to the method used for seismic reflection profiling with the difference that only one receiver is generally used due to the antenna costs. Since the transmitting and receiving antennas are moved along the profile direction by preserving their reciprocal distance, the final result is analogous to a seismic common offset experiment. Sometimes, a single antenna is used (monostatic system) for both transmitting and receiving the signal, so that the final result is a zero offset experiment. The aim of this type of survey is the production of high resolution sections that depict the reflection boundaries in the near surface structure.

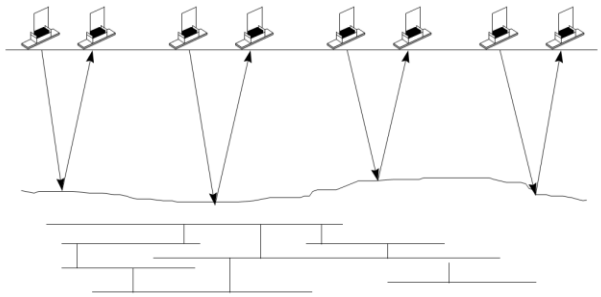

Figure 1-10, Schematic representation of a reflection survey

2.Common midpoint (CMP)

The interval between the transmitting and the receiving antennas is progressively increased by preserving the midpoint between T_X and R_X coordinates so that reflections come from the same point in depth provided that reflectors are horizontal planes. The analysis of the time-distance relation for all the observed reflectors allows to estimate the velocity variations with depth. Thus, the aim of CMP experiments is basically the collection of data suitable for velocity analysis.

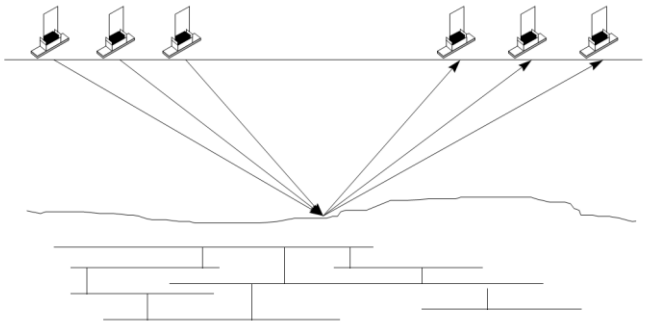

Figure 1-11, Schematic representation of a common midpoint experiment

Figure 1-11 illustrates the main wavepaths followed by EM energy travelling towards the receiving antenna whereas the corresponding time-distance relations are described in Figure 1-12. Although the antennas are generally very close to the surface because the antenna box is often in contact with the soil to maximize the energy transfer to the medium, a direct wave travelling in air is always observed and produces the fastest arrival. A direct wave travelling along the surface with the velocity of the medium may also be observed. Wavepath n.3 in Figure 1-12 corresponds to a reflection so that the travel time curve is a hyperbola that asymptotically tends to the travel time of the direct wave in the medium. Finally, wavepath n.4 indicates that energy reflected with the critical angle of the air-soil interface produces a refracted arrival with a linear move out corresponding to the free space velocity; as a result, travel time curves n.1 and n.4 present the same slope.

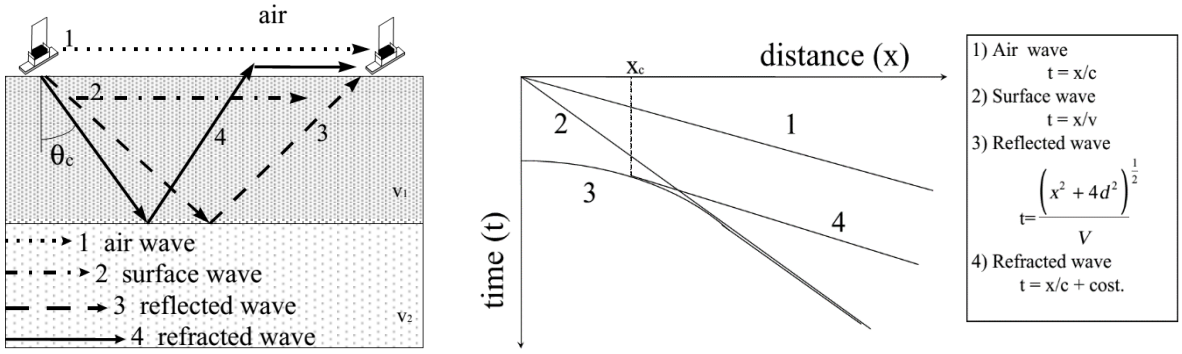

Figure 1-12, Main wavepaths followed by electromagnetic energy (θc=critical angle) (Left), Time-distance relations for the wavepaths (Right)

3.Transillumination

The third method is the transillumination experiment where transmitter and receiver are located on the opposite sides of the medium under investigation (Figure 1-13). This experiment requires a couple of boreholes and special antennas that can enter the borehole. Provided that a sufficient number of data are collected for different T_X and R_X depths, this method allows the tomographic reconstruction of the velocity field of the area within the two boreholes.

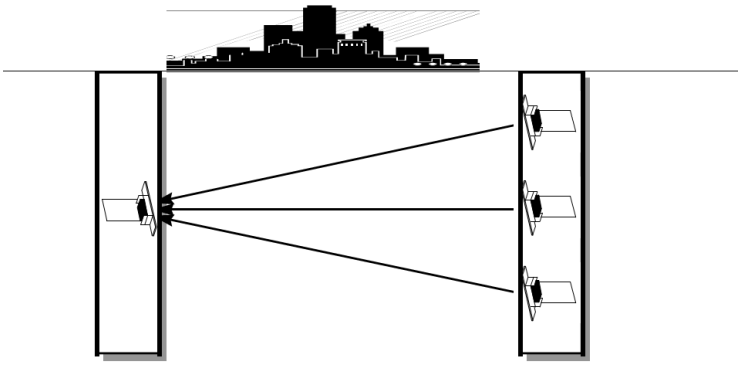

Figure 1-13, Schematic representation of a transillumination experiment

- **Antenna orientation**

In general, the antennas used for GPR are dipolar and radiate with a preferred polarity. The antennas are normally oriented so that the electric field is polarized parallel to the long axis or strike direction of the target. There is no optimal orientation for an equidimensional target. In some instances, it may be advisable to collect two data sets with orthogonal antenna orientations in order to extract target information based on coupling angle. Since most commercial systems employ polarized antennas, orientation can be important. Antenna orientation affects the subsurface footprint size. Figure 1-14 shows the shape of the radiation pattern of the GPR antenna.

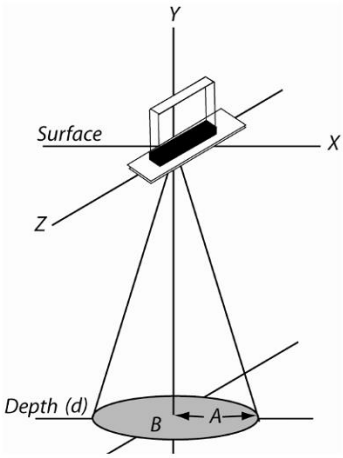

Figure 1-14, cone of transmission spreading down the subsurface

1.6. Data visualization and processing

Initially, GPR data were always displayed as reflection cross sections (essentially vertical slices through the ground along the transect surveyed). As processing and computer processing power have advanced, more and more data presentation is in the form of 3D volume (voxel) rendering and time/depth slices (plan maps). The best results are obtained when migration and some form of signal rectification or trace Hilbert transform envelope is applied.

Today, 3D presentations are common as computer power and visualization tools have advanced rapidly. Affordable access to 3D visualization tools and the rapid advance in computer technology are opening these tools to everyday GPR analysis. The power of collecting reflection survey data in a tight grid and dumping it into 3D display software is enormous. Trends and subtle hard to correlate events become very visible when displays are animated. In general, these displays lose their impact when printed in hard copy form. Generally, a great deal of experience is necessary for correct data processing and interpretation. A raw or processed GPR trace is recorded as a series of digital values equally spaced in time. It can be displayed either as a simple curve (wiggle trace), or by the variable area method in which excursions on one side of the zero line are shaded. Color is also sometimes used, either to shade excursions of one polarity in red and of the other in blue, or to shade an elongated rectangle according to signal amplitude and polarity. An ideal variable area trace would consist of a flat line punctuated by occasional "events" produced by energy arriving at the surface after reflection from points vertically below the mid-point between receiver and transmitter aerials. A GPR section is created by plotting traces side by side, producing a record on which the horizontal axis represents distance and the vertical scale is in two-way reflection time.

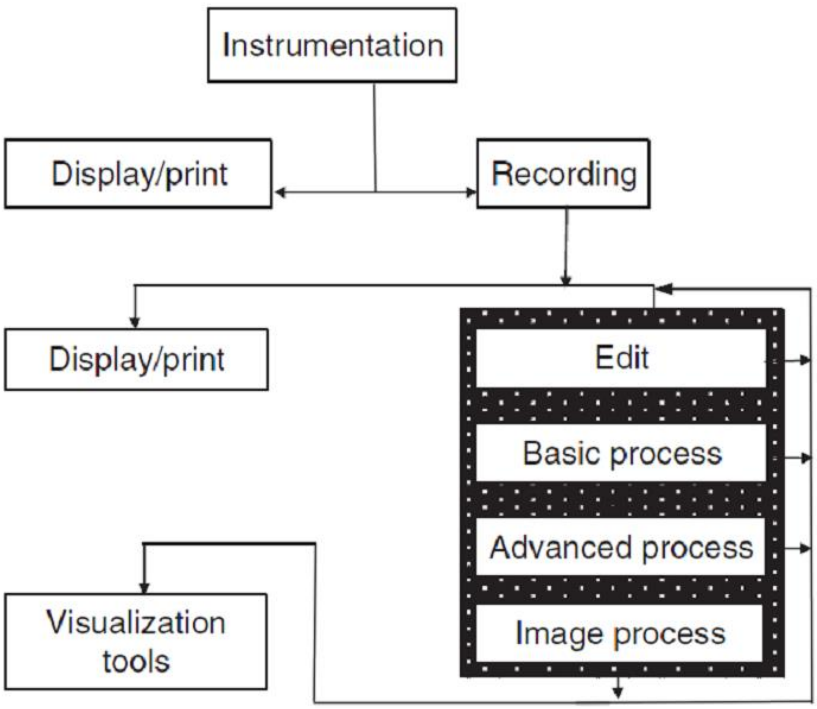

Figure 1-15, Overview of a typical ground penetrating radar (GPR) data processing flow

Processing can vary from simple editing to total transformation of GPR information. In Figure 1-15 it is shown typical processing flow of GPR data, which starts with data acquisition and real time displaying or printing of raw data. The highlighted part on the right side of the image represents typical processing sequence. In many applications, the real-time display is used for on-site interpretation and may be the end point for the radar survey. Normally data are recorded and available for post-acquisition processing and re-display. The areas of data processing have been grouped under the headings: data editing, basic processing, advanced processing, and visualization/interpretation. GPR data processing is usually a repetitive, iterative activity. A data set will flow through the processing loop several times with the data changes visually monitored by the processor. Straight through batch processing may be applied on large data sets after iterative testing on selected data samples.

Once data are recorded, the first step in processing is data editing. Field acquisition is rarely so routine that no errors, omissions or data redundancy occur. Data editing encompasses issues such as data re-organization, data file merging, data header or background information updates, repositioning and inclusion of elevation information with the data. Data editing is often thought to be the simplest operation but different authors states that is usually most time consuming operation. It is very important since it has to ensure that further data processing is done without problems, and as such, it is essential before processing takes place.

1.6.1. Basic processing

One of the main requirements for methods used in basic processing is to leave the data sets reasonably intact. In other words, the processing should not radically distort the information from that which was collected. In general, the degree of distortion is subjective and obviously excessive bandpass (or any other) filtering can drastically alter a data set. Normally minor changes to the overall data set occur if simple basic processing steps are applied intelligently.

Dewow

Due to the close proximity of receiver to transmitter the field near the transmitter contain low-frequency energy associated with signal saturation due to early wave arrivals, inductive coupling effects, and/or instrumentation dynamic range limitations. This low frequency energy often yields a slowly time-varying component to the measured field data and causes the base level of the received signal to bow up or down. This effect has become known as baseline "wow" in the GPR lexicon. Dewow (or signal saturation correction) applies a running average filter to each trace to remove the initial DC signal component and low-frequency "wow," which is highly recommended be applied to all data sets before any other processing steps are undertaken.

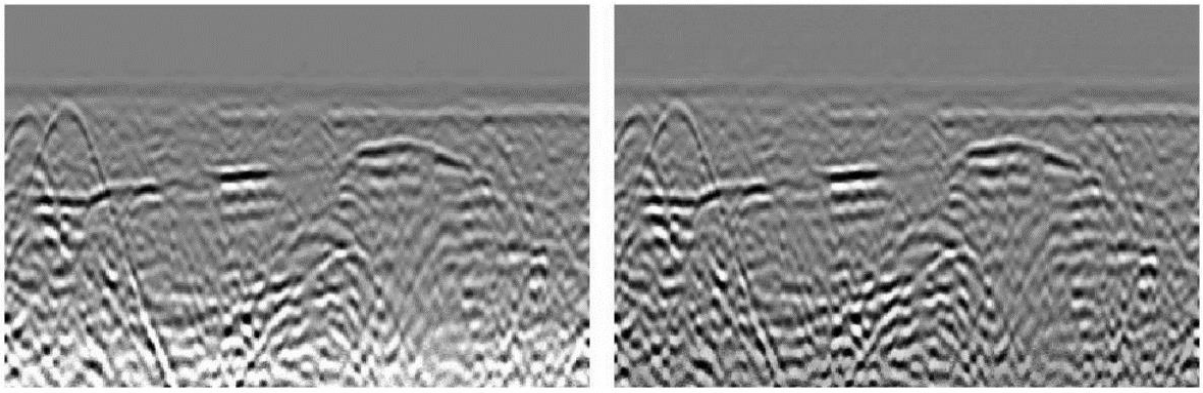

Figure 1-16, A profile before (left) and after application of dewow (right). Both profiles have gain applied

Time gain

The next step of basic processing is usually to select a time gain for the data set. Radar signals are very rapidly attenuated as they propagate into the ground. Signals from great depth are very small and display of this information at the same time as signals from shallower depths is difficult. Gains are used to boost signal strength, which generally decreases with depth, and enhance low-amplitude reflections. It is suggested in the literature to examine the average time-amplitude plots of the data before and after application of a gain to ensure the correct gain has been applied. Prior to application, the plot should show signal amplitude dropping, whereas after application of the ideal gain, signal amplitude should remain constant after its peak value.

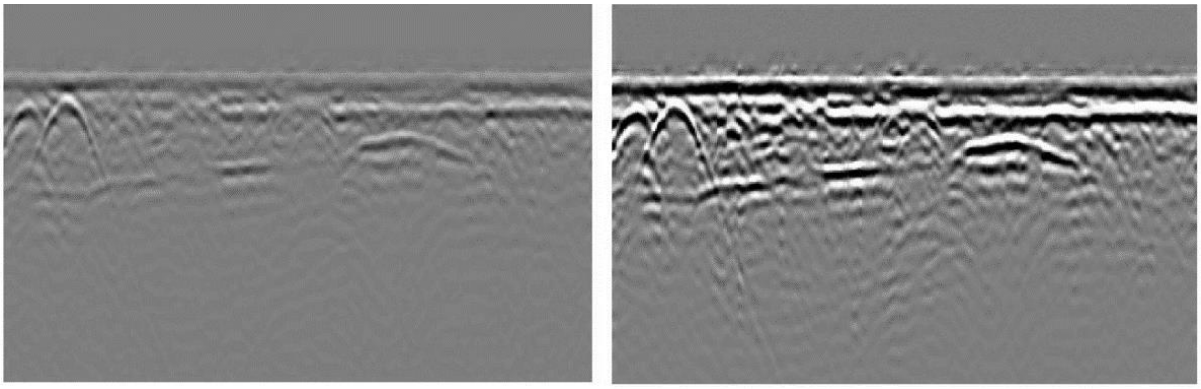

Figure 1-17, A profile after application of dynamic Automatic Gain Control – AGC. Profile has dewow applied

Time gain has historically been very subjective and also very much display device dependent. Mainly two types of gain are applied, AGC (Automatic Gain Control) and SEC (Spreading and Exponential Compensation) or energy decay. AGC applies a gain that is inversely proportional to the average signal strength, or the difference between the mean signal amplitude in a given time window and the maximum signal amplitude for the entire trace. It usually tends to over gain the upper regions of reflection profiles, to the point that subtle features of importance may be easily obscured. On the other hand, if the gain applied is not of sufficient strength, the reflections at the bottom of the profile are left relatively unaffected and without the required definition. If used carefully, however, AGC can usually provide excellent definition of local features within reflection profiles.

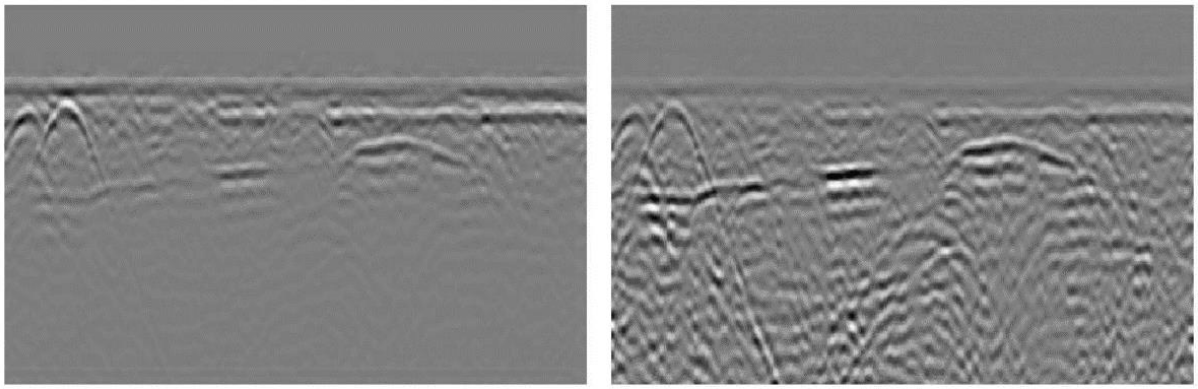

Figure 1-18, A profile before (left) and after application of manual SEC gain. Both profiles have dewow applied

SEC gain applies an exponential gain that compensates spreading and attenuation of the propagating wave front. SEC tends to produce a more balanced reflection profile. The definition of more subtle features can be compromised, but there are other methods available to bring these features to the forefront.

Velocity analysis

Another radar data processing is to analyze velocity-sounding data to extract velocity versus depth functions. This can be done by picking events and using T-2 - X-2 analysis or a variety of other methods. Figure 1-19 shows how a CMP data set has been stacked using a move out correction where the constant velocity can be applied. The resultant stacked data shows the

velocities which the data add up most coherently. Much more sophisticated versions of this algorithm are available in many of the seismic processing packages. Quite often, they are referred to as assemblance analysis routines.

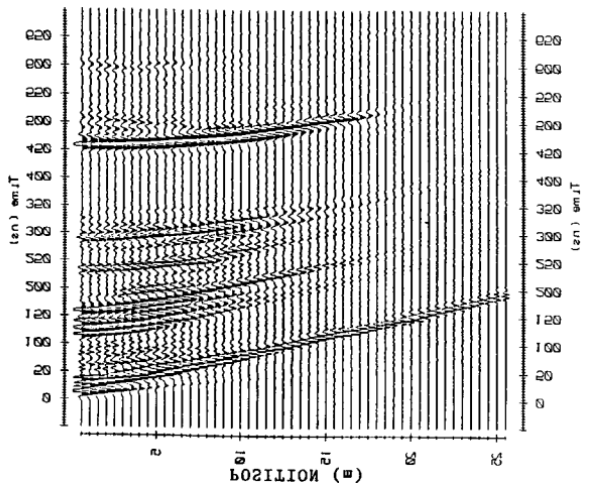

Figure 1-19, CMP Data

Temporal and spatial filtering

This is often the next stage of the processing. Filtering can be applied before or after time gain as long as the effect of the gain is understood since time gain is a non-linear process. Temporal filtering means filtering along the time axis of the data set. A whole host of different types of temporal filtering may be applied from bandpass filtering using Fast Fourier transforms (FFT) through to various types of linear and non-linear time domain convolution filter operators. In both cases, the average amplitude spectrum for the whole section has been generated. Spatial filtering is performed in the horizontal (spatial) direction to enhance or eliminate certain frequencies and features. It is suggested by the literature to examine an average amplitude spectrum plot before and after applying a filter to aid in determining filter parameters. Prior to the application, the plot should show an irregular curve representing the frequencies present in the signal. Examining the plot again after application of a filter will show which frequencies have been removed from the spectrum. Usual filters used during basic processing are bandpass, lowpass, highpass, vertical and median.

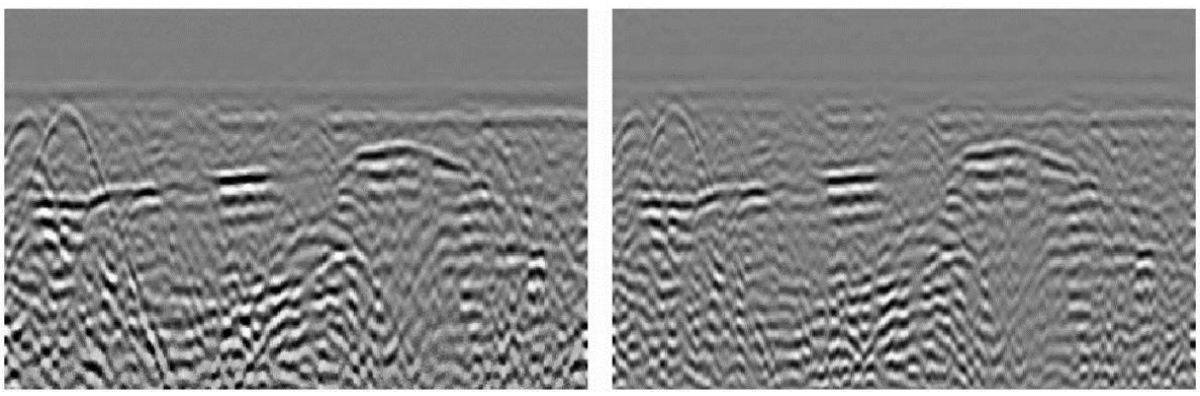

Figure 1-20, A profile before (left) and after application of a bandpass filter. Both profiles have gain and dewow applied.

Highpass filtering of the A-scan data is a useful means of improving the signal to clutter ratio in situations where clutter is caused by additional low frequency energy generated by antenna ground interactions. In addition, excessive high frequency noise can usefully be reduced by lowpass filtering. Bandpass filtering is used to isolate a limited portion of the spectrum using Fourier transform, thereby removing high and low frequency noise and solving the problems. In this way, both high and low frequency noise is removed simultaneously without significant influence on the bulk of the data. Due to this, it is at this level is usually enough to apply bandpass filter and the application of the other filters is not necessary. In addition, it is also useful for isolating a specific range of frequencies for closer analysis.

1.6.2. Advanced processing

Advanced data processing addresses the types of processing, which require a certain amount of operator bias to be applied and which will result in data, which are significantly different from the raw information, which were input to the processing. Such processes include well-known seismic processing operations such as trace attribute analysis, FK filtering, selective muting, normal move out correction, dip filtering, deconvolution, and velocity semblance analysis as well as more GPR specific operations such as background removal, multiple frequency antenna mixing and polarization mixing.

Background Subtraction

Also known as average subtraction applies a running-average background subtraction to the data, subtracting the mean trace of a specific number of traces from each trace in the defined window, with the purpose of removing horizontal banding in profiles (due to system noise, electromagnetic interference, and surface reflections), thereby enhancing dipping events and obliterating horizontal events. Average trace removal is a form of spatial filtering and it is one of the most common operations specifically applied to GPR data.

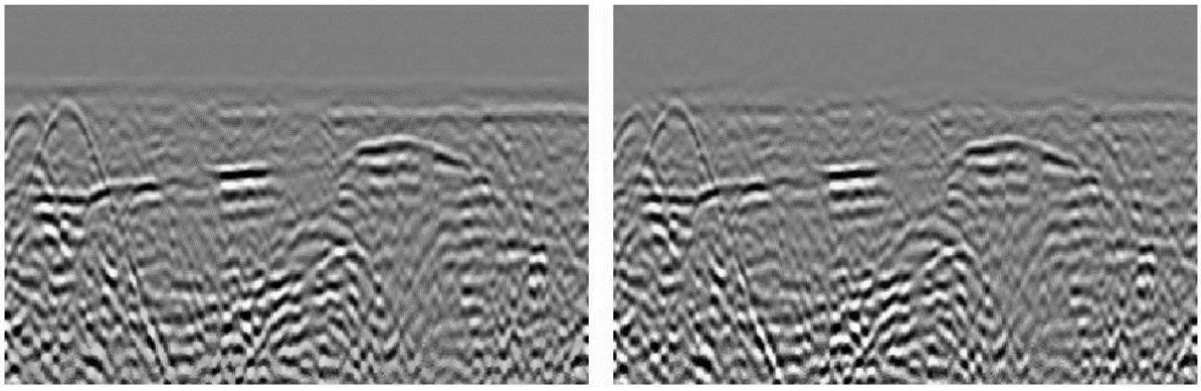

Figure 1-21, A profile before (left) and after application of background subtraction. Both profiles have gain and dewow applied.

Although being one of typical GPR data processing techniques, a number of authors recommend careful use of background subtraction in areas where there are suspected horizontal events of interest, and suggests highpass and lowpass filters as alternative options to remove horizontal banding. It is widely used and mainly always part of GPR data processing, as it helps to remove banding in the upper regions of reflection profiles. In order to ensure that,

this filter will have little effect on the bulk of the data, the maximal number of traces allowable in the running average window.

Deconvolution

It is an inverse temporal filter that compresses the recorded wavelets, thereby improving data resolution. The main purpose of deconvolution is normally to maximize bandwidth and reduce pulse dispersion to ultimately maximize resolution.

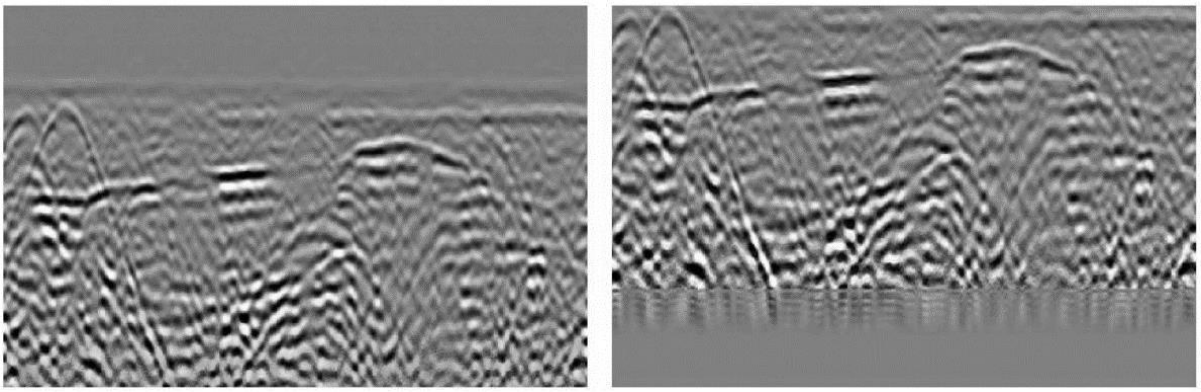

Figure 1-22, A profile before (left) and after deconvolution applied. Note both profiles have gain and dewow applied.

It can be used to remove multiples (repetitive horizontal reflections spaced at equal intervals) formed by multiple reflections between the surface and subsurface objects or layers, and convert radar wavelets to spikes. The deconvolution algorithm relies on the assumptions that subsurface layering is horizontal with uniform intra-layer velocities, and that reflected waveforms have regular signals that do not scatter energy. By many authors has been noted however that much of this processing technique remains obscure and that it rarely has achieved great deal of benefit. Part of the reason for this is that the normal GPR pulse is the shortest and the most compressed that can be achieved for the given bandwidth and signal-to-noise conditions. Instances where deconvolution has proven beneficial when extraneous reverberation or system reverberation is present. Most of the practitioners recommend against its use.

Migration

It applies a synthetic aperture image reconstruction process to focus scattered signals, collapse hyperbolas to their apices, and reposition dipping reflections. Migration requires an accurate radar velocity and knowledge of the origin of the distorted reflections and wave travel paths before it can be applied to the data. It operates on a number of assumptions, including constant laterally invariant velocity layers; spatially uniform and spherically propagating source; no antenna separation; and no dispersion or attenuation.

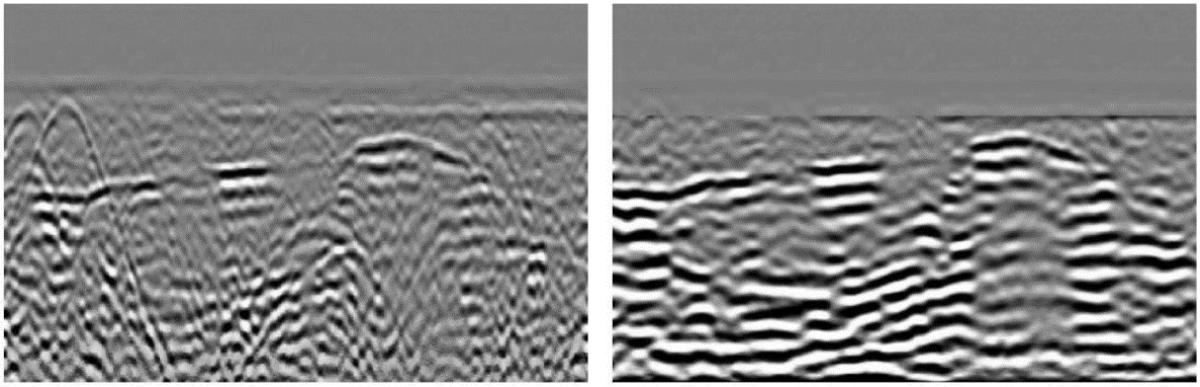

Figure 1-23, A profile before (left) and after migration. Note both profiles have gain and dewow applied.

A number of authors warns that migration may introduce false reflectors, and that it may distort reflections incorrectly. One benefit to migration is increased image resolution. It is suggested that it is only when migration is applied that exact structural dimensions can be determined. It is recommended to analyze data prior to migration, as the presence of hyperbolas may aid in detecting important subsurface features. Correct velocity can be determined with the help of migration, as it is only at the correct velocity when inverse of the hyperbola appear. The conclusion could be made that migration might be dangerous in the hands of a novice but powerful in the hands of a processor who has acquired the ability to use it effectively and recognizes the limitations. Migration is often an iterative process as background velocity is adjusted to optimize the migrated result.

1.7. Applications

The method has been successfully applied in wide-ranging fields. In the areas of hydrology, geology, civil engineering, archaeology and mining engineering for the detection of voids, cracks and fractures.

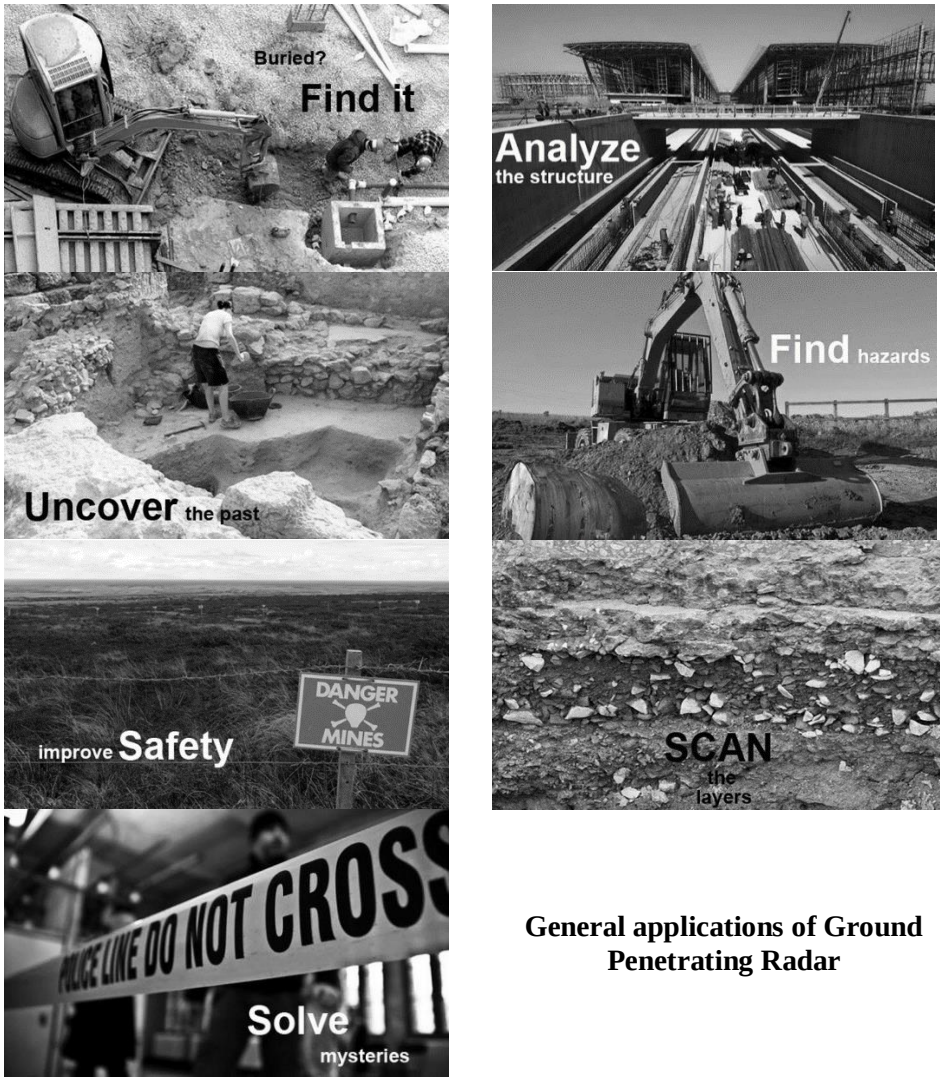

General applications of Ground Penetrating Radar

Figure 1-24, General applications of GPR

GPR has widespread applications in the field of engineering. For example, it can be used in concrete engineering to provide information concerning rebar spacing, placement, depth of coverage and concrete thickness. Historically, this work was performed using X -ray, and involved working outside regular hours. It also involved evacuating large areas, arranging for special security and safety precautions and then dealing with radioactive material. GPR has been used in doing the same work; for example in active hospitals, schools, and shopping centers with no need to evacuate, during crowded open hours. In addition to, GPR can be used in void detection. GPR can distinguish between slab-on-grade and suspended slabs. Therefore, we can locate voids beneath concrete pads. These voids may be the results of inadequate compaction during construction, washouts or erosions. The information can then be

tied into site plans and additional analysis and corrective actions can be performed. The detection of discontinuities (fractures, faults, beds …) is very important in mining applications. The NDT characteristic of GPR is very valued in archaeology or in a survey concerning historical building. GPR is used in archaeological investigations for the mapping of buried sites. Preservation of historical buildings requires particular care, as any intervention must not alter or damage the style, structure or contents of the edifice. In order to properly plan the restoration of a building, non-destructive techniques can be used extensively to detect structural elements and weaknesses. Ground-penetrating radar (GPR) is particularly well adapted to this type of work, as the method is non-invasive, rapid and provides high resolution images of contrasting subsurface materials.

1.7.1. GPR and fractures within rock masses

One of the most important features of rock masses are fractures. They have a major influence on the behavior of the rock masses. In order to have a better understanding of fluid transport in rock masses and to estimate the stability of the rock formation a quantitative description of fracture patterns is necessary. These properties are very essential for many fields of sciences and engineering (e.g. seismology, structural geology, volcanology, mining, petroleum engineering, aquifer protection, nuclear waste repositories, geothermal sites, etc.). The fracture scale ranges from µm for micro cracks to km for large faults.

The formation of fractures in rocks can be due to different occurrences like geologic phenomena or a modification of the in situ stresses by the human activity. Joints and faults are geologic structures, produced by the deformation of the rock under tectonic forces. Human activities such as rock excavation, mining activity, tunneling, boreholes or use of explosives in mines cause a redistribution of the stresses in the rock formation resulting in a growing of pre-existing fractures or inducing new fractures.

In the process of analyzing structures as tunnels, dams, foundations, railways etc. the fracture properties are very important for determining the stability of rock formation. This importance come from the fact that structures produce a change of the in situ stresses, and the pore pressure depending on the geo-mechanical properties of the formation. A mapping of the pre-existing fractures and of the induced fractures is important to ensure the stability.

The fractures dominate the groundwater flow in rock masses. In rocks, the groundwater flows mostly in the fractures, faults and joints and not through the matrix pores. The fractures provide also the preferential path for the flow of contaminants. They are the place of geochemical reactions between the rocks and the water. The safety of an underground repository of highly radioactive waste depends on the characteristics of the rock formation. The mapping of the fractures in the subsurface is very important in the geothermal industry. The problem of the fractures is very similar in the mining sector than in the civil engineering sector. The excavation of shafts, galleries, and the extraction of the rock induces a redistribution of the stresses in the surrounding rock.

Detection of fractures within resistive rock masses is at present a very common application of Ground Penetrating Radar (GPR) technique. GPR investigations have been performed in several mines and quarries, as well as over unstable rock slopes. The detection and location of

fractures is obviously of great importance for safety reasons but can also be used, for instance by the quarrying industry, to improve the production of ornamental rock slabs. Extraction of rock for building stone requires the selection of sound and workable rock. The ability of ground penetrating radar to detect structure integrity and undesired jointing and cracking prior to extraction deliver major economic benefit. Marble, granite and limestone quarrying operations worldwide use GPR for critical development decisions. According to the desired trade-off between resolution and penetration depth, the full frequency range of commercial GPR systems (from tens of MHz to few GHz) has been employed in these investigations.

In most cases rock fractures can be considered as beds whose thickness is smaller than the resolution limit (i.e., a Thin beds) *[1.8. Thin beds],* and can be envisaged as layers embedded in a homogeneous formation, giving rise to reflected signals from the top and the bottom of the bed having opposite polarities. Studies on reflections from thin beds have been carried out by the seismic industry for nearly sixty years now and new developments are still underway. In the last decade, the GPR community has focused on thin beds response to determine rock fracture features (aperture and filling material).

1.8. Thin beds

1.8.1. Resolution

A definition of the term "thin bed" involves the concept of resolution. Resolution is the ability to separate two features that are very close together; the minimum separation of two bodies before their individual identities are lost" (SEG Encyclopedic Dictionary of Exploration Geophysics, 1991). If we consider two similar features (Figure 1-25), the measurable anomalies that they produce may show as separate, distinguishable anomalies when the two features are well separated. We call this condition "resolved". We call a condition unresolved when they are close together, however, their effects merge and it is impossible (or at least difficult) to tell that two rather than just one feature is present. The problems of resolution are to determine how (and where) to separate resolved from unresolved domains. To quantize the separation of resolved from unresolved domains, mathematical criteria have to be set and different criteria in the literature lead to different definitions of "resolvable limit".

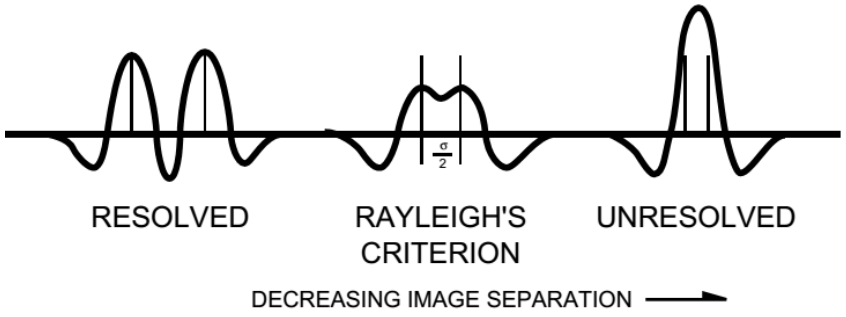

Figure 1-25, Rayleigh's criterion

In seismic work, usually separates between vertical and horizontal resolution. Vertical resolution concerns the minimum thickness of a bed so that reflections from the bed's top and base can be distinguished. The resolution increases with increasing frequency.

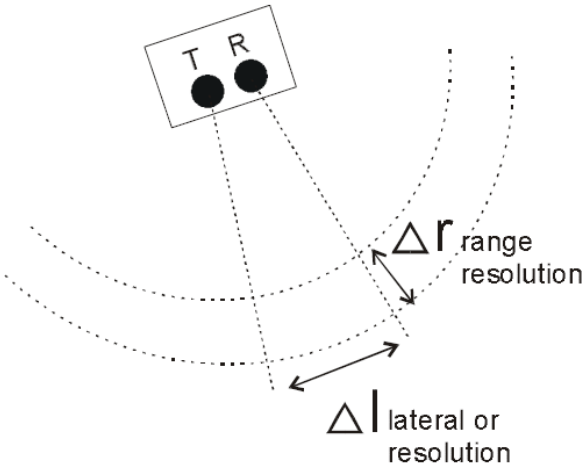

Figure 1-26, Range or depth resolution

The acceptable threshold for vertical resolution generally is a quarter of the dominant wavelength. This is subjective and depends on the noise level in the data. Sometimes the quarter-wavelength criterion is too generous, particularly when the reflection coefficient is small and no reflection event is discernable. To improve the vertical resolution one must shorten the wavelet shape, which requires higher frequencies or shorter wavelength. In passing through the earth a seismic wavelet becomes longer and broader, the shorter wavelengths being attenuated more than the longer ones. Deconvolution is the seismic processing operation that is designed to remove some of the effects of the natural filtering and to produce a shorter wavelet with a waveshape that is easier to interpret. By creating shorter wavelengths, it follows that it improves resolution.

Resolution as defined here and in the geophysical literature implies that reflections from the top and bottom of a thin bed are seen as separate events or wavelet lobes. Using this definition, resolution does not consider amplitude effects. The thickness and areal extent of beds below the resolution limit often can be mapped on the basis of amplitude changes. Sometimes frequency filtering to remove low frequency components can help, and occasionally one removes the high-frequency components so that one can determine thickness from amplitude measurements.

1.8.2. Useful definitions

- **Thin, thick layers**

A layer is regarded as "thin" when its thickness is less than 1/4 of the dominant wavelength. The definition of a Thin-bed may follow different paths:

- Evaluates the time separation of the signals reflected back from the bed (i.e., are solution point of view).
- Investigates the amplitude characteristics of the composite reflection (quasi-linear relation between amplitude and bed thickness).
- Considers the shape of the reflected wavelet (time derivative of the incident wavelet).

Whereas the thickness of a thick layer is determined mainly from time difference measurements.

- **Resolvable limit**

For discrete seismic reflectors, the minimum separation so that one can ascertain that more than one interface is involved. The value depends on the criteria for ascertaining. The Rayleigh resolution limit is $\lambda/4$, where λ is the dominant wavelength. The Widess limit is $\lambda/8$.

- **Rayleigh resolution limit**

The minimum distance between successive reflections such that their individual entities can be recognized is $\lambda/4$ where λ=wavelength. Usually λ is taken as that of the dominant frequency component.

- **Wavelet**

A seismic pulse usually consisting of only a few cycles. An embedded wavelet, basic wavelet, or equivalent wavelet is the time-domain reflection shape from a single positive reflector at normal incidence.

- **Ricker wavelet**

A zero-phase wavelet, the second derivative of the Gaussian function or the third derivative of the normal-probability density function. A Ricker wavelet is often used as a zero-phase embedded wavelet in modeling and synthetic seismogram manufacture.

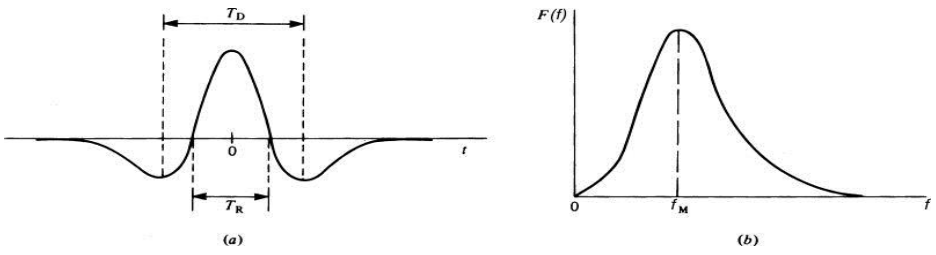

Ricker wavelet. (a) Time-domain and (b) frequency-domain representations.

- **Dominant wavelength**

The wavelength associated with the dominant frequency.

- **Detectable limit**

The minimum thickness for a bed to give a reflection that stands out above the background. Often of the order of 1/25 of the dominant wavelength. Also called the limit of visibility.

- **Dominant frequency**

The dominant frequency is usually determined by measuring the time between successive peaks or troughs and taking the reciprocal. The dominant frequency of wavelets refers to an approximate repetition (the reciprocal of the peak-to-peak time interval) even though the entire wavelet does not repeat.

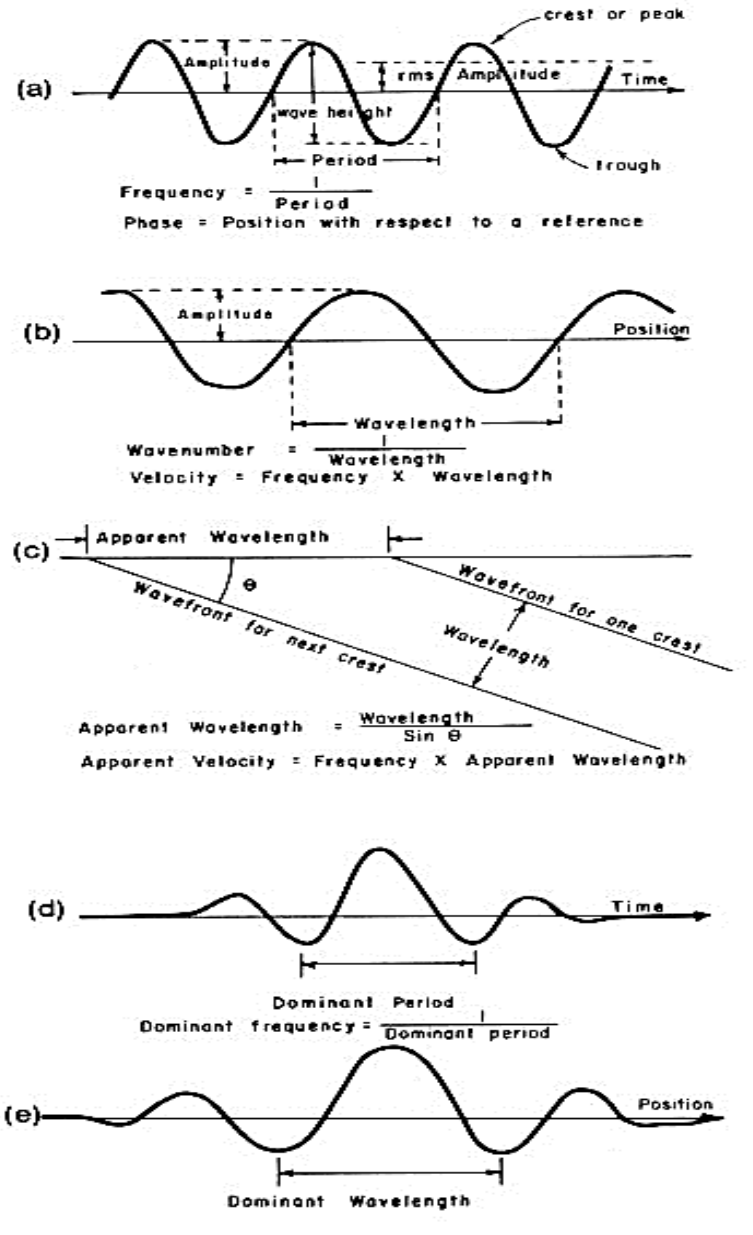

Figure 1-27, Wave definitions. For sinusoids, (a) how displacement at one point varies with time; (b) how wave looks at different places at a given instant. (c) If wave front approaches at an angle, the apparent wavelength differs from the true wavelength. For non-periodic waves, (d) dominant period is based on the time between principal adjacent troughs (or peaks); (e) dominant wavelength is measured similarly.

- **Tuning effect**

Constructive or destructive interference resulting from two or more reflectors spaced closer than a quarter of the dominant wavelength. The composite wavelet exhibits amplitude and phase effects that depend on the time delays between the successive reflection events and the magnitude and polarity of their associated reflection coefficients, and also on the shape of the embedded wavelet. The tuning effect illustrated for a wedge (Figure 1-28); the material above and below it is the same, but the wedge has different acoustic impedance. When the wedge is a quarter-wavelength (1/4) thick, the second half-cycle of the reflection from the top interferes constructively with the first half-cycle from the bottom, resulting in an increase in amplitude. How many amplitude maxima there are and the magnitude of the increase depend on the shape of the embedded wavelet.

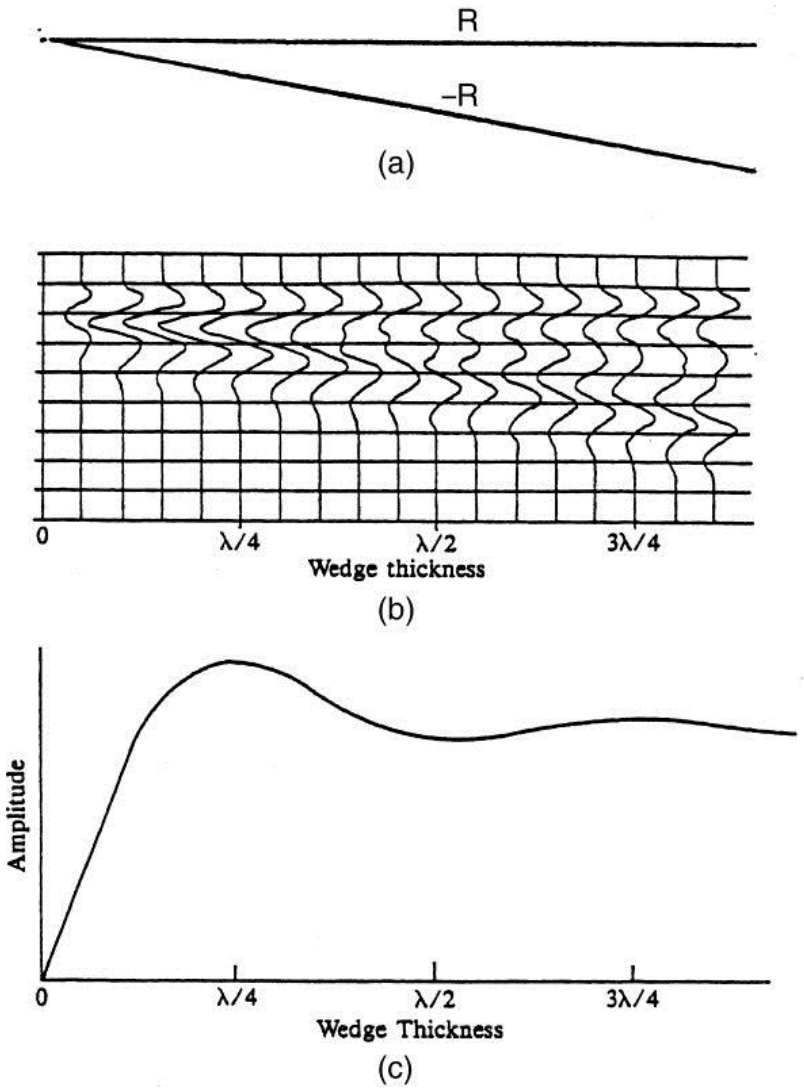

Figure 1-28, (a) The wedge; (b) seismic section across a linear wedge that has lower acoustic impedance than the surrounding sediments for a minimum-phase wavelet; (c) amplitude versus thickness graph.

1.8.3. Summary of previous works on thin-beds

Researchers of the seismic industry directed early studies on thin-bed response. In the following, previous works on thin-bed response will be reviewed.

1878	Rayleigh
1953	Ricker
1973	Widess
1980	Koefoed and de Voogd
1982	Kallweit and Wood
1983	Voogd and den Rooijen
1995	Chung and Lawton
1988	Annan
2010	Sambuelli and Calzoni

Table 1-3, Summary of previous works on Thin-bed

Rayleigh (1878)

The first definition by Lord Rayleigh with respect to optical resolution is also the most useful and does not differ by very much from other definitions. Lord Rayleigh in 1878 pointed out that the diffraction image remains almost unchanged if the converging wavefront deviates from a perfect sphere by less than approximately one-quarter of wavelength. In other word, The Rayleigh limit of resolution is that the bed thickness must be 1/4 of the dominant wavelength, which is also the thickness where interpretation criteria change.

Ricker (1953)

Ricker (1953) examined the overlapping of two reflections of equal amplitude and polarity from the opposite edges of a thin bed. He set the resolvable limit as the separation where in the composite reflection the maxima of the distinct wavelets merge into a single peak (Figure 1-29). This limit is known as the zero-curvature criterion since it can be determined by differentiating the incident wavelet twice. Using a zero-phase 3-loop Ricker wavelet, the resolution limit is 0.214 the dominant wavelength within the thin layer. Considering two reflections with equal amplitude and opposite polarities (i.e., a thin layer embedded in a homogeneous material). Ricker also observed that, as the bed gets thinner, the composite reflection becomes the derivative of the incident wavelet and the thinning of the bed can be followed through a study of the decrease in amplitude. In other words, in the thickness range below the resolution limit, the information on the bed is encoded in the amplitude of the composite reflection.

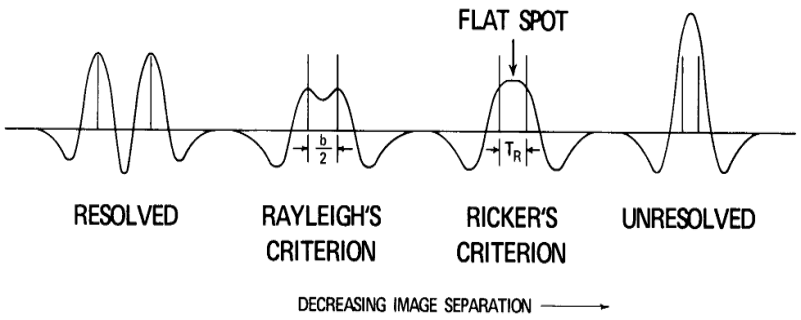

Figure 1-29, Rayleigh's limit of resolution occurs when images are separated by the peak-to-trough time interval, whereas Ricker's limit occurs when they are separated by a time interval equal to the separation between inflection points.

Widess (1973)

The problem of vertical resolution was posed in a classic paper entitled "How thin is thin bed?" by Widess (1973). Widess described a study of the composite waveform obtained by convolving a zero-phase wavelet with two spikes of equal amplitudes and opposite polarities. A fundamental observation is that as spike separations decrease, the effect of convolving a wavelet with two spikes of opposite polarities is one of differentiation. Widess observed that as separations decrease, there is a point where the composite wavelet stabilizes into a good replica of the derivative waveform such that, for all practical purposes, there is no change in the peak-to-trough time but rather only a change in amplitude of the composite waveform. Widess concluded by inspection that the limiting separation for wavelet stabilization occurs when the bed thickness (i.e., spike separation) is equal to l/8 of a wavelength of the predominant frequency of the propagating wavelet. He remarked (1973, p.1180) that beds thinner than 1/8 of a wavelength can be resolved in principle by measuring changes in amplitude of the composite reflection. By means of a sinusoidal approximation, Widess also determined a linear relation between the maximum amplitude of the composite reflection (A_r) and (bed thickness/wavelength) ratio.

$$A_r \cong 4\pi A_m r \frac{d}{\lambda_d} \qquad (1\text{-}23)$$

Koefoed and de Voogd (1980)

Koefoed and de Voogd (1980) investigated the quasi-linearity between thickness and reflection amplitude. They also observed that neglecting transmission losses and internal multiples within the bed, as Widess did, results in a decrease of the thin-layer response and in an increase of the linearity limit to unacceptably large values of the thickness/wavelength ratio. Within the linearity limit and for sinusoidal excitation, they modified Widess's amplitude relation in

$$A_r \cong 4\pi A_i r \frac{d}{\lambda_d} \frac{1}{1-r^2} \qquad (1\text{-}24)$$

Where A_i is the maximum amplitude of the incident signal and r is the reflection coefficient of an individual interface of the thin layer. Therefore, the factor $(1-r^2)$ in the denominator takes account of transmission losses and internal multiples. Unsurprisingly, the contribution of multiples becomes more important for increasing values of the reflection coefficient.

Kallweit and Wood (1982)

Using a wedge model and a zero-phase 3-loop Ricker wavelet, Kallweit and Wood (1982) showed that Rayleigh's criterion determines the practical resolution limit. The quarter-wavelength thickness is called tuning thickness and is where the apparent thickness (peak-to-peak time of composite reflection) equals true thickness. Above tuning thickness peak-to-peak time measurements are good approximation of bed thickness, while below tuning thickness amplitude information can be used to retrieve layer thickness provided that an amplitude calibration procedure is possible. They also noted that there is no thickness below which the composite reflection stabilizes into the derivative of the incident wavelet and thus rejected Widess's criterion.

Voogd and den Rooijen (1983)

Voogd and den Rooijen developed the observations of Widess using an integral representation of the source wavelet, although they did not provide any limiting value for the thickness of a thin bed.

Chung and Lawton (1995)

They found the Widess's equation agrees well with modeling results for bed whose thickness is below $\lambda_d/8$, this implying that the thin-bed assumption is no longer valid above that thickness. They verified the sinusoidal approximation of Widess for the amplitude of the composite reflection and showed that, considering a Ricker wavelet, Widess's equation is modified in

$$A_r = 0.75\left(4\pi A_i r \frac{d}{\lambda_d}\right) \qquad (1\text{-}25)$$

Annan (1988)

The maximum amplitude reflected from a thin bed, which is exactly the same expression of Koefoed and de Voogd (1980). This is not surprising since both relationships are obtained considering sinusoidal excitation, transmission losses and internal multiples.

$$A_r \cong 4\pi A_i R_{12} \frac{d}{\lambda_d} \frac{1}{1-R_{12}^2} \qquad (1\text{-}26)$$

Sambuelli and Calzoni (2010)

They tested Annan's relationship on GPR measurements performed on an artificially fractured marble block and found that agreement between real and theoretical values of the reflection coefficient is achieved for fracture apertures between 1/10 and 1/5 of the signal wavelength (although they considered the nominal signal wavelength instead of the dominant one).

CHAPTER 2

ANALYSIS OF REAL AND SYNTHETIC DATASETS

2.1. Sandstone blocks

At first measurement session was performed on Pietra Giuggiolena (Noto sandstone, Sicily). Experimental set up and acquisition procedure are explained in the following.

2.1.1. Experimental set up and acquisition procedure

GPR measurements were performed in the laboratory to test the behavior of the electromagnetic signal when impinging on a thin bed. The GPR measurements were carried out with a K2 IDS system and a dual-polarized antenna with a nominal frequency of 2GHz. Radar traces were collected setting a time triggering mode with a stacking factor of 8, a 10ns acquisition window and a sampling frequency of about 25GHz. To simulate the presence of thin fractures in rock, 0.41m x 0.30m x 0.25m sandstone blocks were employed, quarried in southern Italy, which are believed to be completely dry.

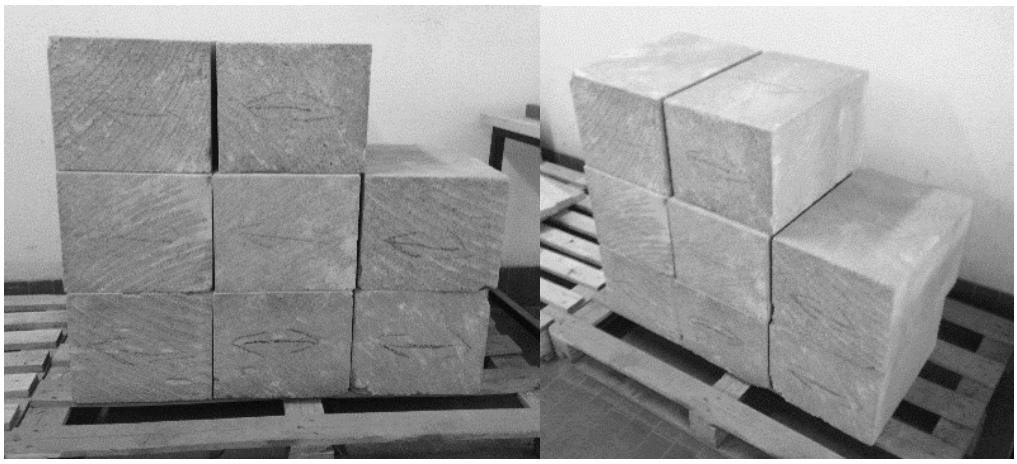

Figure 2-1, Pietra Giuggiolena (Noto sandstone, Sicily) blocks

Acquisitions carried out using just two sandstone blocks, one in front of the other to simulate an air thin bed were unsuccessful because of disturbing sidewall reflections. Instead, the acquisition configuration depicted in Figure 2-2 was preferred.

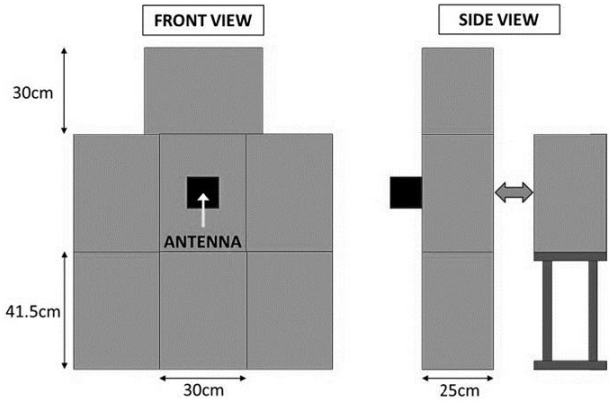

Figure 2-2, Sketch of GPR test performed in the laboratory

At first, radar measurements were performed to determine the velocity of the electromagnetic signal within the sandstone that was estimated to be 13.15cm/ns, thus giving a relative permittivity of about 5.2. Afterwards a reference reflection collected by placing a metal screen on the opposite side of the block where the antenna was placed. By comparing amplitudes of the signals reflected by the *sandstone/air* and the *sandstone/metal* interfaces the sandstone/air reflection coefficient computed to be 0.38±0.01, giving a range of the relative dielectric permittivity from 4.7 to 5.2. Then an additional block in front of the central one was placed to simulate an air-filled fracture. The thicknesses of the air thin bed to be tested were computed using the dominant wavelength of the signal reflected at the sandstone/air interface. Though this procedure is not correct theoretically (the wavelength should be determined considering the signal transmitted into the thin bed), we considered it to be a good approximation assuming there is little or no frequency dependent attenuation during signal propagation in the sandstone block. The dominant wavelength was computed to be 0.176m, corresponding to a dominant frequency of about 1.70GHz. Radar traces were collected for different apertures of the air gap.

A list of acquisition parameters are mentioned in Table 2-1.

Acquisition system	K2 IDS system, Nominal frequency of 2GHz
Antenna polarization	Dual-polarized antenna
Block material	Sandstone blocks, quarried in southern Italy
Single block dimensions	0.41m x 0.30m x 0.25m
Fracture filling material	Air
Stacking factor of Time triggered acquisitions	8
Time window	10 ns
Samples per scan	256
Sampling frequency	25.6 GHZ
Sampling interval	0.39 ns

Table 2-1, Acquisition parameters

2.1.2. Collected data

The list of measurements and their description are provided in Table 2-2.

FILE	DESCRIPTION
1	Single block on the ground; thickness 25cm
2	Single block on the ground; thickness 25cm with metal screen
3	Single block on the ground; thickness 41,5cm
4	Single block on the ground; thickness 41,5cm with metal screen
6	3 blocks laid horizontally on the ground; thickness 25cm with screen
7	3 blocks laid vertically on the ground; thickness 25cm with screen
8	7 blocks on the ground; thickness 25cm with screen
9	7 blocks with fracture λ/2: 8.82cm (aperture not reliable)
10	7 blocks with fracture λ/4: 4.41cm (aperture not reliable)
11	7 blocks with fracture λ/8: 2.21cm (aperture not reliable)
12	7 blocks with fracture λ/12: 1.47cm (aperture not reliable)
13	7 blocks with fracture λ/16: 1.10cm (aperture not reliable)
14	7 blocks with fracture λ/32: 0.55cm
15	7 blocks with fracture λ/16: 1.10cm
16	7 blocks with fracture λ/12: 1.47cm
17	7 blocks with fracture λ/8: 2.21cm
18	7 blocks with fracture λ/4: 4.41cm
19	7 blocks with fracture λ/2: 8.82cm
20	7 blocks with fracture 3λ/32: 1.65cm
21	7 blocks with fracture 6λ/32: 3.31cm
22	7 blocks with fracture 3λ/8: 6.62cm

Table 2-2, Collected data for Sandstone blocks

Note:

- Aperture not reliable: the procedure initially used to create the aperture of the fracture generated a fracture with an aperture larger at the bottom.
- Dominant wavelength calculated considering File 8.

2.1.3. Data analysis

2.1.3.1. Real data

Raw data obtained from GPR measurements are in **.dt* format. In order to analyze data in MATLAB environment, the code RADARPOLI2D developed at POLITECNICO DI MILANO was used. Thanks to this code, raw data changed to **.mat* format and further analysis was done in the MATLAB environment. Figure 2-3 and Figure 2-4 show raw data for files LID20001 and LID20002. Presence of metal screen is visible in the file LID20002.

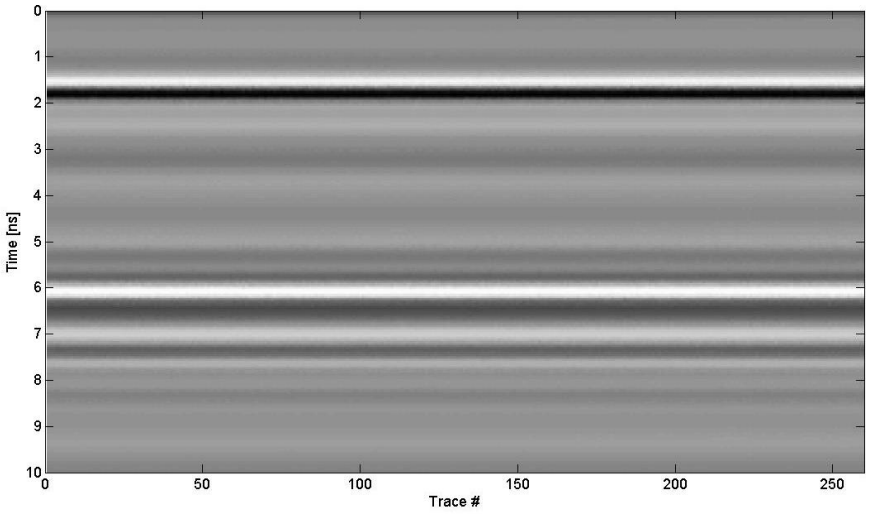

Figure 2-3, File LID20001 (Single block on the ground; thickness 25cm)

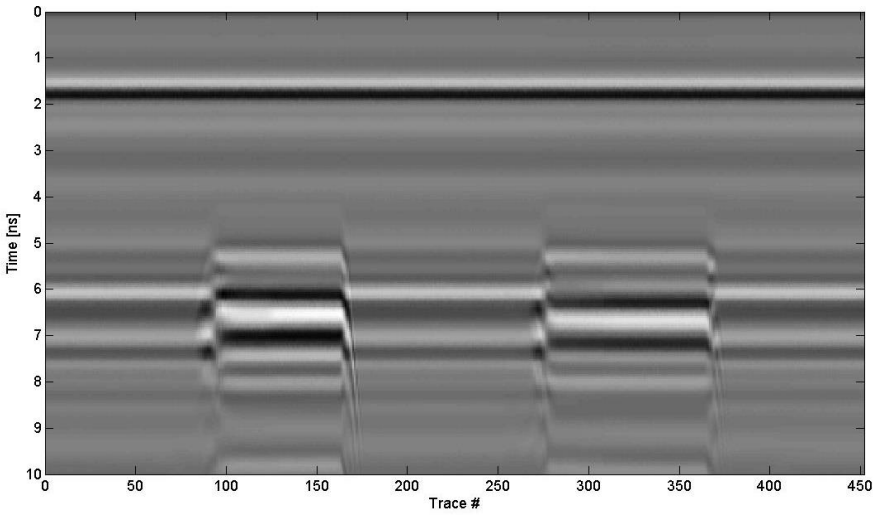

Figure 2-4, File LID20002 (Single block on the ground; thickness 25cm with metal screen)

After that, traces for each aperture were obtained individually. In Figure 2-5 all traces are shown as a function of fracture thickness.

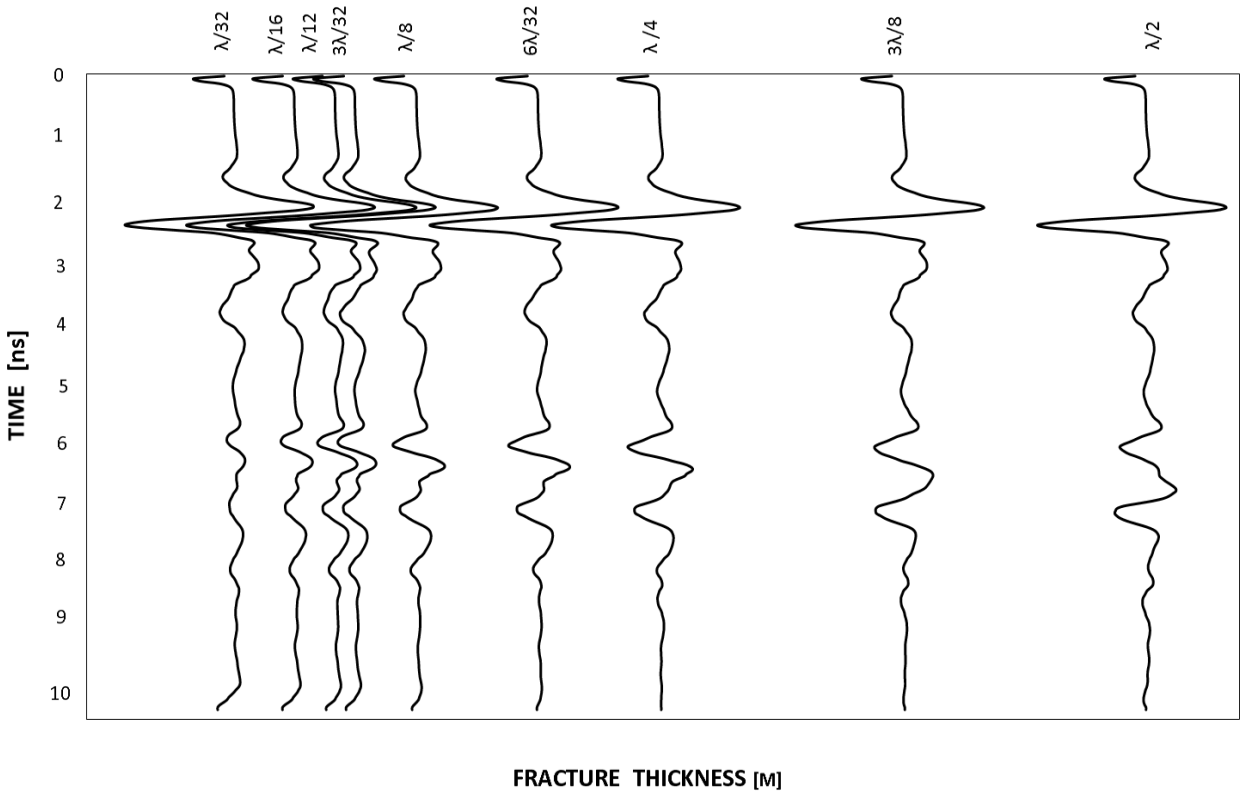

Figure 2-5, Traces of real data as a function of bed thickness

Subsequently, reflection coefficient for each aperture was calculated. In Table 2-3, reflection coefficient for each aperture are listed. Files are sorted by thickness of fractures.

Bed Thickness (Cm)		**File name**	**Reflection Coefficient**
λ/32	0.55	LID20014	0.15
λ/16	1.10	LID20015	0.25
λ/12	1.47	LID20016	0.31
3λ/32	1.65	LID20020	0.30
λ/8	2.21	LID20017	0.41
6λ/32	3.31	LID20021	0.48
λ/4	4.41	LID20018	0.51
3λ/8	6.62	LID20022	0.46
λ/2	8.82	LID20019	0.44
λ	17.64	LID20008	0.36

Table 2-3, Reflection coefficients of real data

In Figure 2-6, reflection coefficients are illustrate as a function of bed thickness.

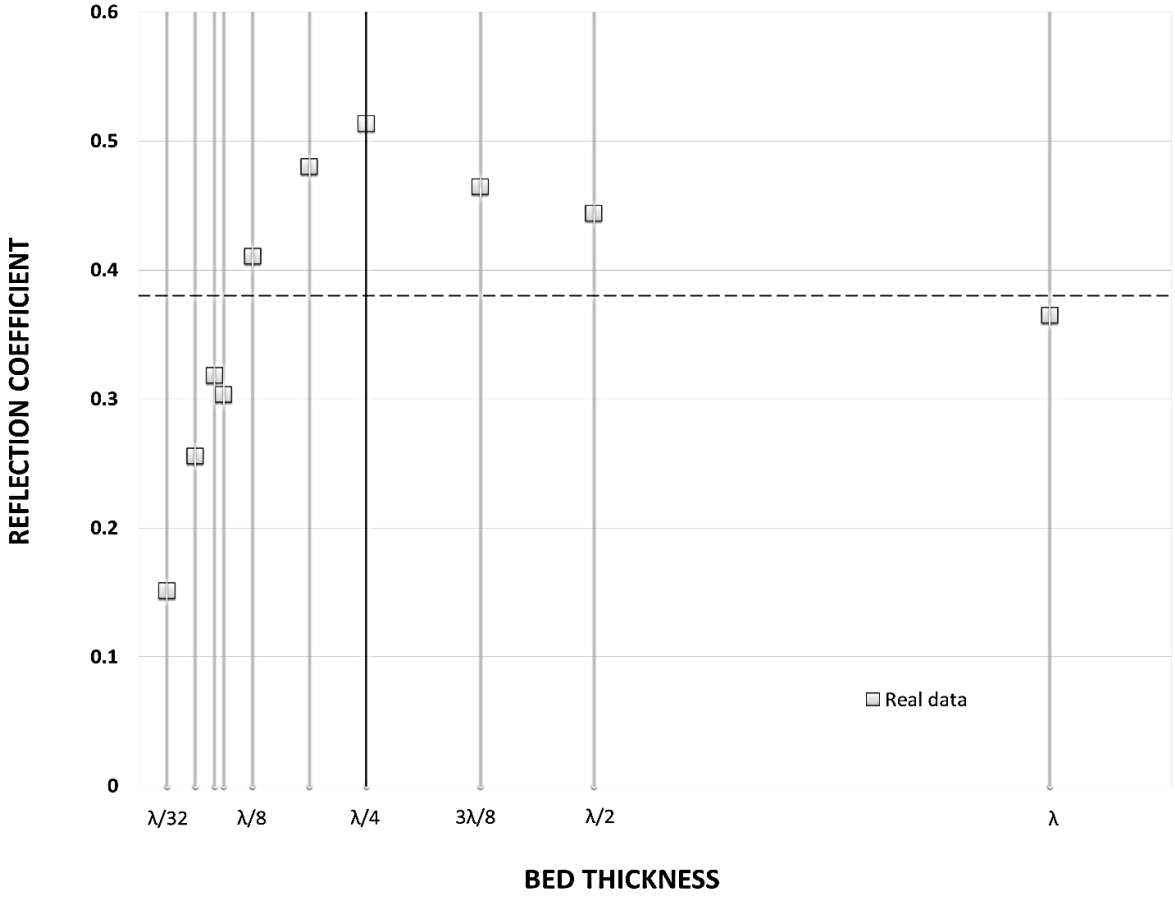

Figure 2-6, Reflection coefficient as a function of bed thickness, Dashed horizontal line is the value for the sandstone/air interface (0.38)

Figure 2-6 shows that the maximum reflection coefficient was occurred at 4.41 cm. It is consistent with the theoretical value of $\lambda_d/4$. (See section 1.8.2, Tuning effect)

2.1.3.2. Synthetic data

2.1.3.2.1. FDTD-analysis

FDTD (finite difference time domain) simulations were carried out to study the electromagnetic wave behavior propagating in presence of thin bed. The FDTD technique implements finite-difference approximations of Maxwell's equations in the time domain. The grid technique of Yee (1966) is used to sample the fields the grid space. This method permits the modelling of many electromagnetic phenomena. Many articles have been published describing the use of the technique to model radiation from antenna. Wang and Tripp (1996) have developed an algorithm for simulating electromagnetic wave propagation in 3-D media. Roberts and Daniels (1997) have used the FDTD-technique to model near-field GPR in 3-D because of the flexibility of the method. Kunz and Luebbers (1993) give a complete overview of the FDTD method. The shape of the antenna, the radar pulse, and the dielectric properties of the media can be defined in the FDTD technique. The fields are calculated in the time-domain in the near and in the far field at any time.

GprMax is an electromagnetic wave simulator for Ground Penetrating Radar modelling which is developed in two versions of 2D and 3D (Giannopoulos, 1996). It is based on the Finite-Difference Time-Domain numerical method. This software tool is available free of charge for both academic and commercial use and has been successfully employed in situations, where a deeper understanding of the operation and detection mechanism of GPR was required. In this work, the version 2.0 of GprMax 2D/3D was used in order to model synthetic data.

All electromagnetic phenomena, on a macroscopic scale, are described by the well known Maxwell's equations. These are first order partial differential equations, which express the relations between the fundamental electromagnetic field quantities and their dependence on their sources.

$$\begin{aligned} \nabla \times \mathbf{E} &= -\frac{\partial \mathbf{B}}{\partial t} \\ \nabla \times \mathbf{H} &= \frac{\partial \mathbf{D}}{\partial t} + \mathbf{J_c} + \mathbf{J_s} \\ \nabla \cdot \mathbf{B} &= 0 \\ \nabla \cdot \mathbf{D} &= q_v \end{aligned} \qquad (2\text{-}1)$$

Where (t) is time (seconds) and qv is the volume electric charge density (coulombs/ cubic meter). In Maxwell's equations, the field vectors are assumed to be single-valued, bounded, continuous functions of position and time. In order to simulate the GPR response from a particular target or set of targets the 2-1 have to be solved subject to the geometry of the problem and the initial conditions.

The nature of the GPR forward problem classifies it as an *initial value – open boundary* problem. This means that in order to obtain a solution one has to define an initial condition (i.e. excitation of the GPR transmitting antenna) and allow the resulting fields to propagate through space reaching a zero value at infinity since, there is no specific boundary, which limits the problem's geometry and where the electromagnetic fields can take a predetermined value.

Although the first part is easy to accommodate (i.e. specification of the source), the second part cannot be easily tackled using a finite computational space.

The FDTD approach to the numerical solution of Maxwell's equations is to discretize both the space and time continua. Thus, the discretization spatial Δx, Δy, Δz, and temporal Δt steps play a very significant role – since the smaller they are, the closer the FDTD model is to a real representation of the problem. However, the values of the discretization steps always have to be finite, since computers have a limited amount of storage and finite processing speed.

Hence, the FDTD model represents a discretized version of the real problem and of limited size. The building block of this discretized FDTD grid is the Yee cell named after Kane Yee who pioneered the FDTD method. This is illustrated for the 3D case in Figure 2-7.

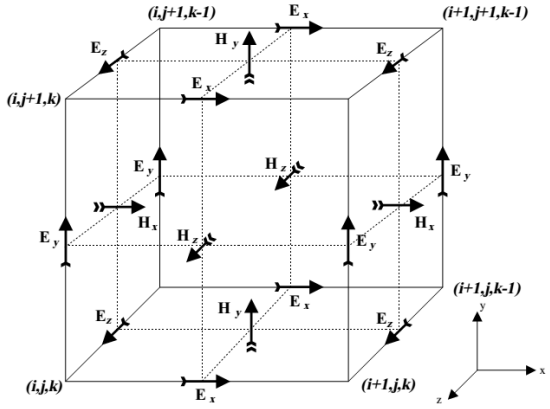

Figure 2-7, 3D FDTD Yee cell

The 2D FDTD cell is a simplification of the 3D one and is depicted in Figure 2-8.

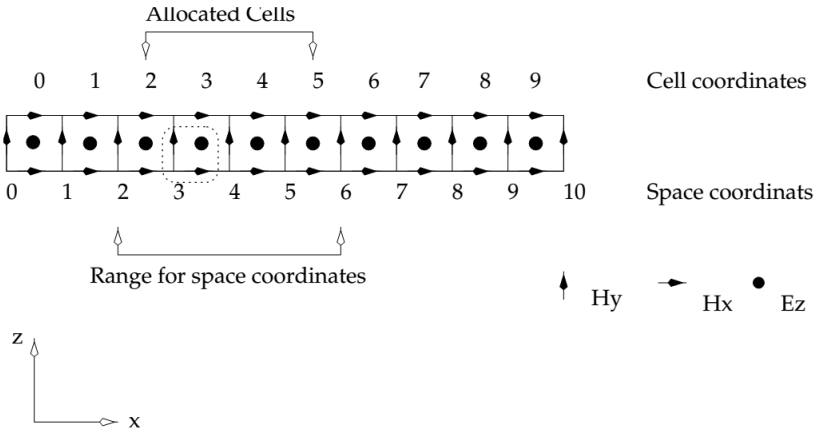

Figure 2-8, Schematic of the GprMax3D coordinate system and conventions. The depicted field components are the ones, which correspond to space, coordinate 1. (Δx = Δy = Δz = 1 meter)

By assigning appropriate constitutive parameters to the locations of the electromagnetic field components complex shaped targets can be included easily in the models. However, objects with curved boundaries are represented using a staircase approximation.

The numerical solution is obtained directly in the time domain by using a discretized version of Maxwell's curl equations which are applied in each FDTD cell. Since these equations are discretized in both space and time, the solution is obtained in an iterative fashion. In each iteration the electromagnetic fields advance (propagate) in the FDTD grid and each iteration corresponds to an elapsed simulated time of one Δt. Hence by specifying the number of iterations one can instruct the FDTD solver to simulate the fields for a given time window.

The price one has to pay for obtaining a solution directly in the time domain using the FDTD method is that the values of Δx, Δy, Δz and Δt can not be assigned independently. FDTD is a conditionally stable numerical process. The stability condition is known as the CFL condition after the initials of Courant, Freidrichs and Lewy and is:

$$\Delta t \leq \frac{1}{c\sqrt{\frac{1}{(\Delta x)^2}+\frac{1}{(\Delta y)^2}+\frac{1}{(\Delta z)^2}}} \qquad (2\text{-}2)$$

Where c is the speed of light. Hence, Δt is bounded by the values of Δx, Δy and Δz. The stability condition for the 2D case is easily obtained by letting $\Delta z - \rightarrow \infty$.

One of the most challenging issues in modelling open boundary problems as the GPR one is the truncation of the computational domain at a finite distance from sources and targets where the values of the electromagnetic fields cannot be calculated directly by the numerical method applied inside the model. Hence, an approximate condition known as *absorbing boundary condition* (ABC) is applied at a sufficient distance from the source to truncate and therefore limit the computational space. The role of this ABC is to absorb any waves impinging on it, hence simulating an unbounded space. The computational space (i.e the model) limited by the ABCs should contain all important features of the model such as sources and output points and targets.

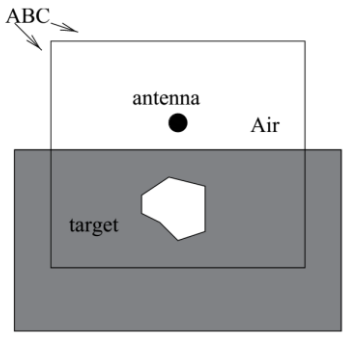

Figure 2-9, 2D GPR forward problem and its GprMax2D domain bounded by ABCs

Figure 2-9 illustrates this basic difference between the problem to be modelled and the actual FDTD modelled space. Figure 2-9, it is assumed that the half-space that contains the target(s) is of infinite extent. Therefore, the only reflected waves will be the ones originating from the target. In cases where the host medium is not of infinite extent (e.g. a finite concrete slab) the assumption of infinite extent can be made as far as the actual reflections from the slab termination are not of interest or its actual size is large enough that any reflected waves which will originate at its termination will not affect the solution for the required time window. In general, any objects that span the size of the computational domain (i.e. model) are assumed to extend to infinity. The only reflections, which will originate from their termination at the truncation boundaries of the model are due to imperfections of the ABCs and in general are of a very small amplitude compared with the reflections from target(s) inside the model. All other boundary conditions which apply at interfaces between different media in the FDTD model are automatically enforced in GprMax2D/3D.

In constructing a GPR model in two and three dimensions, some assumptions are necessary. These mainly result from the need to keep the amount of computational resources, required by the model, to a manageable level and to facilitate the study of the important features of the GPR response to a target, without cluttering the solution with details, which will obscure the fundamental response. However, GprMax2D/3D can easily handle more "complicated" GPR modelling scenarios if required. The assumptions made for both GprMax2D and GprMax3D models are:

- All media are considered to be linear and isotropic.
- In GprMax3D if the physical structure of the GPR antenna is not included in the model then the antenna is modelled as an ideal Hertz dipole (i.e. a small current source). In GprMax2D the transmitting antenna is modelled as a line source. Using a Hertz dipole in GprMax3D results in reducing the computational resources required to run a 3D model in reasonable time, whereas in the GprMax2D case the use of a line source is a consequence of the assumption of the invariance of the problem in one direction.
- The constitutive parameters are, in most cases, assumed not to vary with frequency. This assumption simplifies a time domain model. However, a formulation able to handle a Drude (i.e. Debye plus a constant conductivity) relaxation model for the complex permittivity is included in both GprMax2D and GprMax3D.

Therefore, for the 2D case the governing equations reduce to the ones describing the propagation of T M mode electromagnetic waves (relative to the invariance direction (z) of the model).

In general, GprMax2D/3D solve numerically Maxwell's equations in two and three dimensions. Any linear, isotropic media with constant constitutive parameters can be included in the model. In addition they can model dielectrics with frequency depended permittivity described by the Debye formula

$$\epsilon = \epsilon_\infty + \frac{\epsilon_s - \epsilon_\infty}{1 + \jmath\omega\tau} \qquad (2\text{-}3)$$

Where ε_∞ is the permittivity at light frequencies, ε_s is the DC permittivity and ω is the angular frequency. Is the DC permittivity and ω is the angular frequency. The computational domain of both GprMax2D/3D could be truncated either using a third order Higdon local absorbing boundary condition (ABC) or by introducing Perfectly Matched Layers (PML) in the model. The default is the Higdon ABC however; the performance of the PML is superior especially if more than six (6) layers are used. The parameters of the Higdon ABC can be altered if required using simple commands. In the case of PML only the number of layers of the PML is adjustable by the user.

The ABCs employed in GprMax2D/3D will, in general, perform well (i.e. without introducing significant artificial reflections) if all sources and targets are kept at least 15 cells away from them. The formulation of the type of ABCs employed in GprMax2D/3D does not take into account any near-field effects, which dominate close to radiation centers (i.e. sources and targets).

Perfectly Matched Layer (PML) layers which have a user adjustable thickness absorb very efficiently most waves that propagate in them. Although, source and output points can be specified inside these layers it is wrong to do so from the point of view of correct modelling. The fields inside these layers are not of interest to GPR modelling. Placing sources inside these layers could have effects that have not been studied and will certainly provide erroneous results from a GPR modeler's point of view.

The above requirements have to be taken into account when the size of the model is to be decided. Further, for the same reason, free space (i.e. air) should be always included above a source for at least 15 to 20 cells in both GprMax2D and GprMax3D GPR models. Obviously, the more cells there are between observation points, sources, targets and the absorbing boundaries the better the results will be.

Excitation of a model in GprMax2D is achieved by specifying the current of a line source. In GprMax3D - when a Hertzian dipole is used - excitation is achieved by specifying the current and polarization of the small Hertzian dipole. More than one sources can be active at a given time thus making simulation of GPR arrays simple. There is a choice of excitation waveforms for GprMax2D/3D. In addition, the user can specify its own excitation function. The discretization of the GprMax2D/3D models can be different in the direction of each coordinate axis but cannot vary along this direction. The smallest element in GprMax2D which can be allocated with user defined characteristics is an area of $\Delta x \times \Delta y$ and in GprMax3D a volume of $\Delta x \times \Delta y \times \Delta z$.

There is no specific guideline for choosing the right discretization for a given problem. In general, it depends on the required accuracy, the frequency content of the source's pulse and the size of the targets. Obviously, all targets present in a model must be adequately resolved. This means, for example, that a cylinder with radius equal to one or two spatial steps does not really look like a cylinder. Another important factor, which influences the discretization, is the errors associated with numerical induced dispersion. This means that contrary to the real world where electromagnetic waves propagate with the same velocity irrespectively of their direction and frequency (assuming no dispersive media and far-field conditions) in the discrete one this

is not the case. This error can be kept in a minimum if the following rule of thumb is satisfied: the discretization step should be at least ten times smaller than the smallest wavelength of the propagating electromagnetic fields. Note that in general low-loss media wavelengths are much smaller compared to free space. The above rule is described by the equation:

$$\Delta l = \frac{\lambda}{10} \qquad (2\text{-}4)$$

The input file, which has to be supplied to GprMax2D/3D, contains all the necessary information to run a GPR model. The general structure of an input file is the same in both programs. The input file is a plain ASCII text file, which can be prepared with any editor or word-processing program. In the input file, the hash character (#) is reserved and is used to denote the beginning of a command, which should be passed to the programs. The general syntax of all available commands is:

#command_name: parameter1 parameter2 parameter3...

The essential commands, which represent the minimum set of commands required to run our GprMax2D/3D simulation, are listed in Table 2-4.

	Syntax of the commands
1	#title:
2	#medium: f1 f2 f3 f4 f5 f6 str1
3	#domain: f1 f2 f3
4	#dx_dy_dz: f1 f2 f3
5	#time window:
6	#box: f1 f2 f3 f4 f5 f6 str1
7	#bowtie: c1 c2 f1 f2 f3 f4 f5 str1
8	#tx: c1 f1 f2 f3 str1 f4 f5 and #rx: f1 f2 f3
9	#geometry_file: file1
10	#abc_type: pml
11	#hertzian_dipole: f1 f2 str1 str2
12	#analysis: i1 file1 c1
13	#end_analysis:

Table 2-4, Syntax of commands

The commands #medium and #hertzian_dipole are of a great importance for this work. Through these commands, dielectric constant, conductivity of medium and input current frequency, which are the main parameters of some series of our analysis, were described. Position of Transmitter and Receivers which are the other parameters that considered in this work were specified by the #tx and #rx Commands. Finally, the command of #bowtie was used to examine the influence of bowtie antenna in the simulation. In the following, commands and specifications of them in this work were explained.

1. #title:
With the command #title you can include a title for your model. This title is saved in the output file(s).

2. #medium:
With the #medium: command you can introduce into the model a set of constitutive parameters describing a given medium.
The syntax of the command: #medium: f1 f2 f3 f4 f5 f6 str1
The parameters of the command are the relative permittivity of the medium ε_{rs} (f1), the relative permittivity at theoretically infinite frequency $\varepsilon_{r\infty}$ (f2), the relaxation time of the medium τ (f3), the conductivity of the medium σ (f4), the relative permeability of the medium μ_r (f5) and the magnetic conductivity of the medium σ^* (f6). str1 is a string characterizing the medium (medium identifier)

In this work, we do not want a Debye medium therefore; we can set the relaxation time of the medium (i.e. τ) to zero. In such a case, GprMax will use only the values specified in the relative permittivity of the medium and the conductivity of the medium to describe the dielectric properties. In addition, as we know a medium is non-magnetic, we can set the relative permeability of the medium to 1.0 and the magnetic conductivity of the medium to zero. Consequently, the only parameters, which are taken into account, are *Dielectric constant* and *Conductivity* of the medium. The effect of these parameters were examined during analysis.

3. #domain:
The command #domain: is used to specify the size in meters of the model.
The syntax of the command: #domain: f1 f2 f3
The parameters f1, f2 and f3 are the size in meters your model in the x, y and z direction respectively.

4. #dx_dy_dz:
The syntax of the command: #dx_dy_dz: f1 f2 f3
The command #dx_dy_dz: is used to specify the discretization of space in the x (f1), y (f2) and z (f3) directions respectively (i.e. Δx, Δy and Δz).
The spatial discretization controls the maximum permissible time step Δt with which the solution advances in time in order to reach the required simulated time window. The relation between Δt and Δx, Δy and Δz is

$$\Delta t \leq \frac{1}{c\sqrt{\frac{1}{(\Delta x)^2}+\frac{1}{(\Delta y)^2}+\frac{1}{(\Delta z)^2}}} \qquad (2\text{-}5)$$

Where c is the speed of light. In GprMax3D, the equality is used to determine Δt from Δx, Δy and Δz. As is evident from 4.1 small values of Δx, Δy and Δz result in small values for Δt which means more iterations in order to reach a given simulated time. However, it is important to note that the smaller the values of Δx, Δy, Δz and Δt are the more accurate the model will be.

5. #time window:

The command #time_window: should be used to specify the total required simulated time in seconds.

The syntax of the command: #time_window:

6. #box:

With the command #box: you can introduce a rectangle of specific properties in the model.

The syntax of the command: #box: f1 f2 f3 f4 f5 f6 str1

The parameters f1 f2 f3 are the lower left (x, y, z) coordinates of the parallelepiped in meters. Similarly, the f4 f5 f6 are the upper right (x, y, z) coordinates of the parallelepiped. The parameter str1 is a medium identifier defined either with a #medium: command or in a media file currently in use. Further, the identifiers free_space or pec can be used if the parallelepiped is to represent a free space region or a perfect conductor.

7. #bowtie:

With the command #bowtie: we introduced a bowtie antenna with specific properties in the model. Two triangular patches make up the antenna by application of this command.

The syntax of the command: #bowtie: c1 c2 f1 f2 f3 f4 f5 str1

The parameter c1 is the direction (i.e. polarization) of the bowtie antenna and can be x, y or z. Similarly, the parameter c2 denotes the remaining direction to define a plane where the antenna lies. The parameters f1, f2 and f3 are the spatial x, y, z coordinates of the antenna's feed point. The parameter f4 is the length of the antenna's elements (half the total length of the complete bowtie) and the parameter f5 is the flare angle in degrees. The parameter str1 is a medium identifier defined either with a #medium: command or in a media file currently in use. Further, the identifiers free_space or pec can be used if the bowtie is to represent a free space region or a perfect conductor.

8. #hertzian dipole:

The command #hertzian_dipole: is used to define the simplest excitation in GprMax3D which is to specify a current density term at an electric field location. This will simulate an infinitesimal dipole (it does have a length of Δl).

The syntax of the command: #hertzian_dipole: f1 f2 str1 str2

The parameters f1 and f2 are the amplitude and frequency of the source's waveform. The parameter str1 is a waveform type identifier and could be any of the ones available in GprMax2D or the keyword user when a User specified waveform is to be employed using an #excitation_file: command. The parameter str2 is a source identifier that will be used in a #tx: command to relate this type of source to a location in the model.

9. #tx: and #rx:

The commands #tx: and #rx: used together in order to introduce a source position (#tx:) and output points (#rx:). Any number of #tx: commands could be specified in the model as well as any number of #rx: and/or #rx_box: commands. The parameter c1 defines the polarization of the source and could be one of x, y or z.

The syntax of the commands: #tx: c1 f1 f2 f3 str1 f4 f5

#rx: f1 f2 f3

The parameters f1, f2 and f3 are the (x,y,z) coordinates in metres of the source in the model. The parameter str1 is the source ID that has been specified before using a source description command (i.e. #hertzian_dipole:, #voltage_source:, etc.). The parameter f4 is a delay in the source's initiation.

10. #geometry file:

With the command #geometry_file: you can specify a file in which information about the model's geometry is stored in binary format. This information can be used to create an image of the model and check if it is properly constructed.

The syntax of the command is: #geometry_file: file1

The parameter file1 is the filename of the geometry file.

11. #abc_type:

In order to use the PML boundary condition the command #abc_type: has to be used.

The syntax of the command: #abc_type: pml

12. #analysis:

When source types were introduced and placing sources and output points were accomplished a pair of new commands #analysis: and #end_analysis: were used. The source command #tx: and receiver commands #rx: and are to be placed between these two commands.

The syntax of the command: #analysis: i1 file1 c1

The parameter i1 is the number of new runs of the model. This is similar to what the number of scans was in the old #scan command and it means that the model will run again – after resetting all arrays and time to zero - for every single i1. The parameter file1 is the name of the file where all the results for this #analysis: are going to be stored and the parameter c1 is a single character either (a) or (b) denoting that the format of the output file (file1) will be ASCII or BINARY, respectively. It is important that an #analysis: command is followed (after other source and output controlling commands have been inserted) by the command #end_analysis:

13. #end analysis:

Which denotes the end of an analysis section that was started using an #analysis: command. The #end_analysis: command has no parameters. In the input file, there can be any number of #analysis: and #end_analysis: pair of commands.

The syntax of the command: #end_analysis:

2.1.3.2.2. 2D Simulations with GprMax

For each aperture, 2D simulation was done with GprMax2D. The name of each analysis is representative of the parameters used in modeling; for example, *STI-32* is regarding to simulation of *Sandstone* with *Two* blocks where antennas are *In contact* with surface of block and the aperture is *λ/32* (This method of naming will use also for the following models). Figure 2-10 is an example of model with air-bed thickness of (1/8) wavelength.

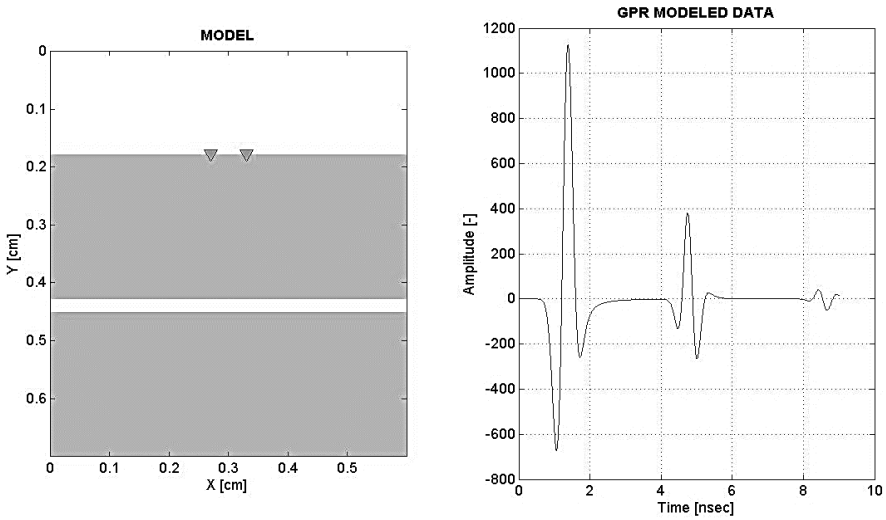

Figure 2-10, Example of model with air-bed thickness of (1/8) wavelength

The modeled radar traces were calculated individually. These traces are provided in Figure 2-11 as a function of fracture thickness.

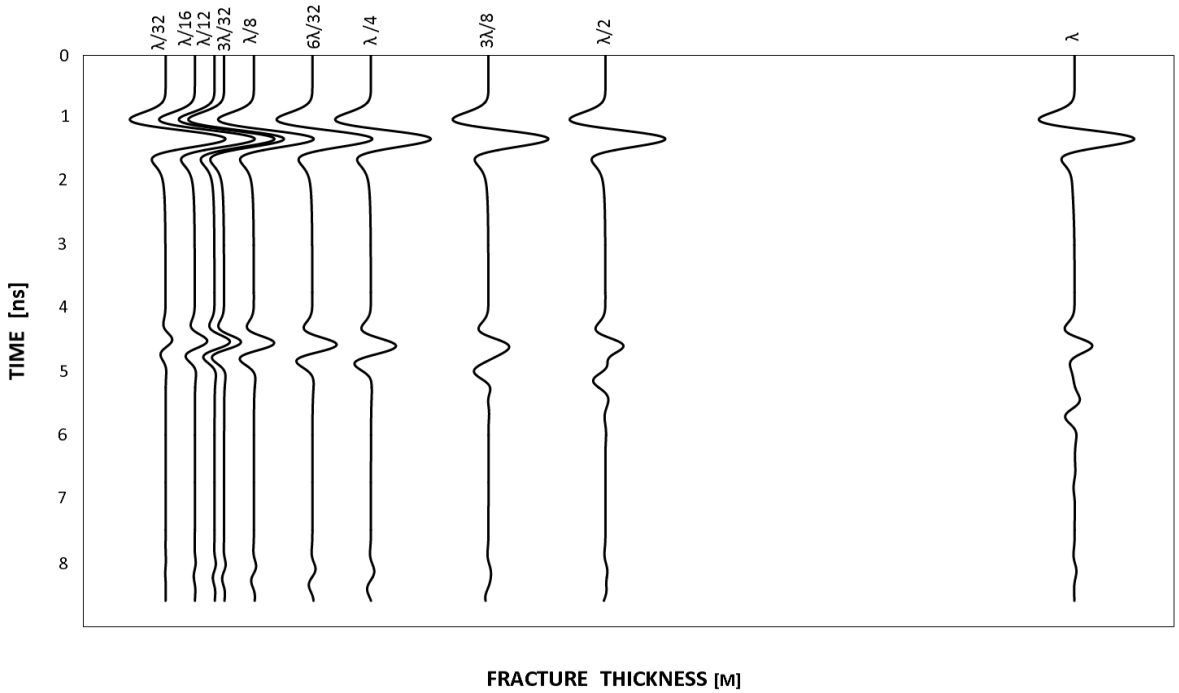

Figure 2-11, Modeled radar traces as a function of bed thickness

Reflection coefficients of FDTD GPR simulations, which were calculated for each aperture, are listed in Table 2-5.

Bed Thickness (Cm)		**File name**	**Reflection Coefficient**
λ/32	0.55	**STI-32**	0.14
λ/16	1.10	**STI-16**	0.27
λ/12	1.47	**STI-12**	0.34
3λ/32	1.65	**STI-3-32**	0.38
λ/8	2.21	**STI-8**	0.45
6λ/32	3.31	**STI-6-32**	0.54
λ/4	4.41	**STI-4**	0.56
3λ/8	6.62	**STI-3-8**	0.46
λ/2	8.82	**STI-2**	0.40
λ	17.64	**STI-1**	0.39

Table 2-5, Reflection coefficients of FDTD GPR simulation

2.1.3.3. Comparison of reflection coefficients for real and synthetic data

In Figure 2-12, reflection coefficients for both real data and FDTD GPR simulation are compared.

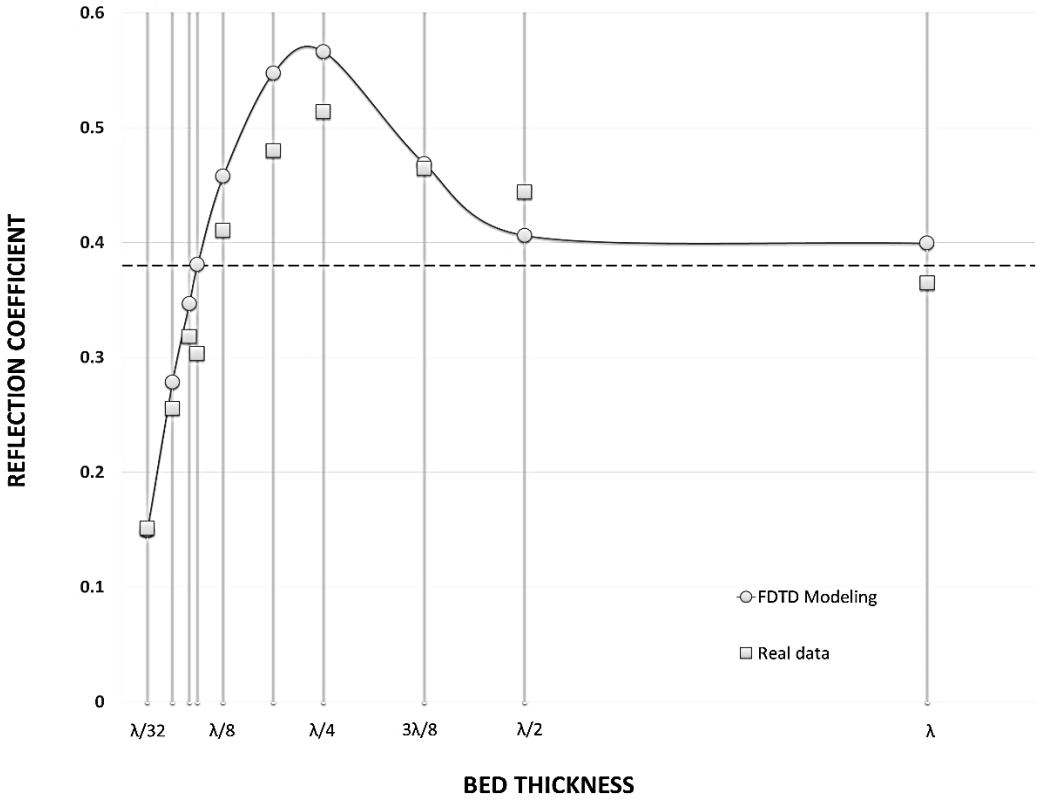

Figure 2-12, Comparison of reflection coefficient between Real data and FDTD modeling, Dashed horizontal line is the value for the sandstone/air interface (0.38)

According to this graph, there is a linear relationship between reflection coefficient and bed thickness. This linear relationship is valid for bed whose thickness is below $\lambda_d/8$. As mentioned previously in section 1.8.3, Chung and Lawton (1995) verified the sinusoidal approximation of Widess for the amplitude of the composite reflection and showed that, Widess's equation agrees well with modeling results for bed whose thickness is below $\lambda_d/8$, this implying that the thin-bed assumption is no longer valid above that thickness. They modified Widess's equation considering a Ricker wavelet in

$$A_r = 0.75\left(4\pi A_i r \frac{d}{\lambda_d}\right) \qquad (2\text{-}6)$$

Ar	maximum amplitude of the composite reflection
Ai	the maximum amplitude of the incident signal
r	the magnitude of the reflection coefficients
d	the thin-bed thickness
λd	the dominant wavelength in the thin bed

Chung and Lawton (1995) equation was compared with results of in this work (Figure 2-13).

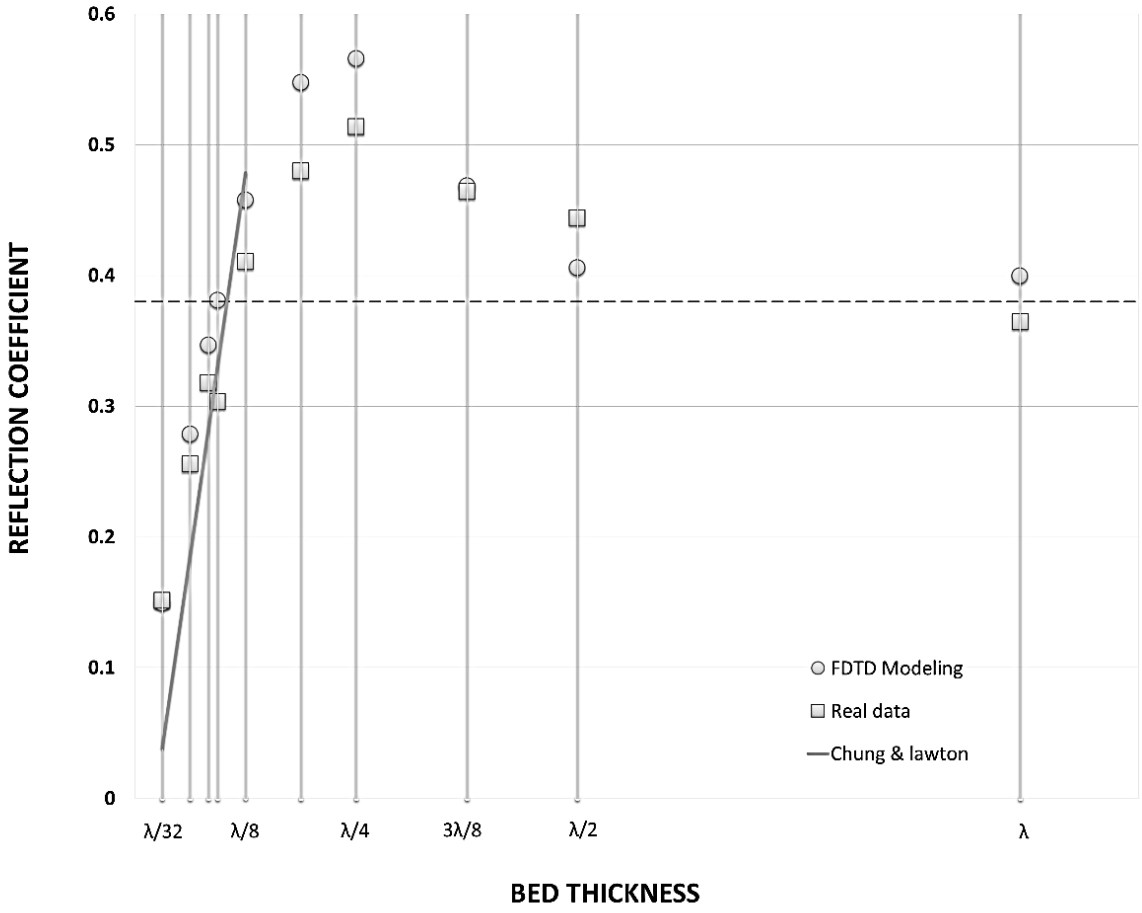

Figure 2-13, Comparison of FDTD Modeling, real data and Chung and Lawton (1995) equation

2.2. Marble blocks

The GPR test was done to investigate thin-bed response into detail and to compare the new outcomes with the results from sandstone blocks. There are some considerations, which were employed in this series of tests. One of them is employing bigger rock blocks to discard annoying sidewall reflections as well as to better simulate the normal incidence condition. For achieving this goal two marble blocks with bigger size compare to sandstone blocks were employed. The 3D FDTD modeling were accomplished with GprMax3D to take into account 3D effects.

2.2.1. Experimental set up and acquisition procedure

GPR measurements were carried out in laboratory of Politecnico di Milano. Acquisitions performed using two marble blocks of 0.74m x 0.60m x 0.21m (Figure 2-14).

Figure 2-14, Marble blocks

Marble blocks were located one in front of the other in order to simulate the presence of thin fracture (an air thin bed) embedded in rock. Because of the weight of marble blocks, lift truck was used to move and arrange them (Figure 2-15).

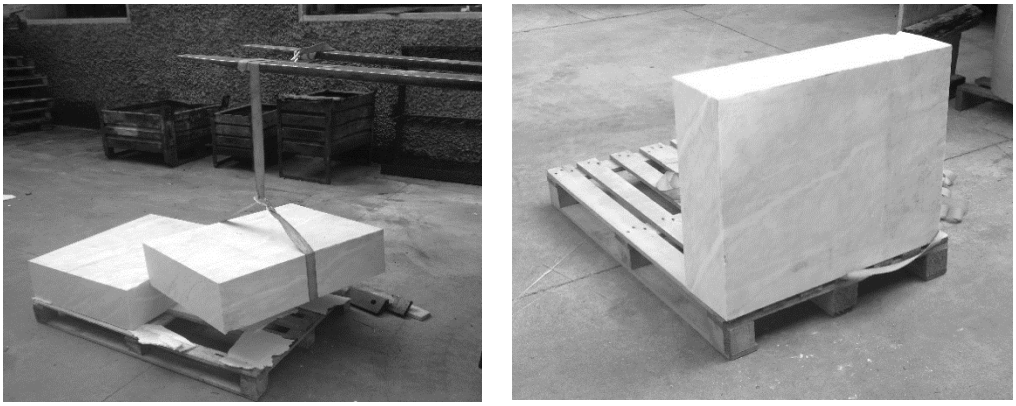

Figure 2-15, Process of arrangement of marble blocks

Different fracture apertures were employed by moving one block towards the other one. Apertures are from 0.674cm (λ/32) to 21.58cm (λ) (Figure 2-16).

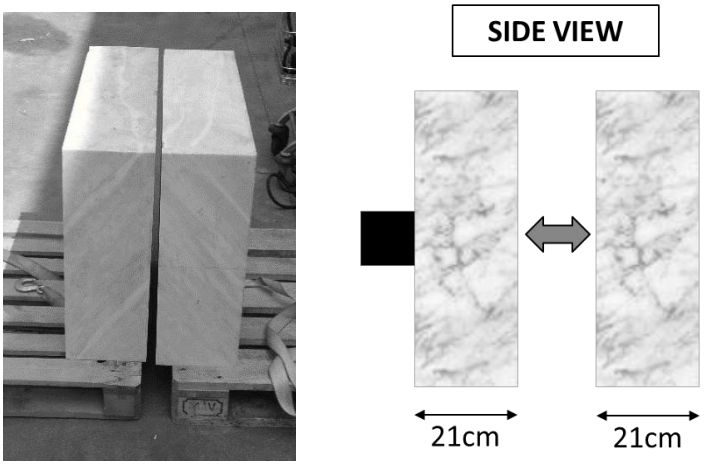

Figure 2-16, simulate the presence of thin fracture (an air thin bed) embedded in rock.

The GPR instrument was IDS system called "Aladdin". This instrument is equipped with two 2GHz antennas polarized perpendicular to each other (Figure 2-17). It should be mentioned that the GPR system used in this test is the same of experiment on the Sandstone blocks.

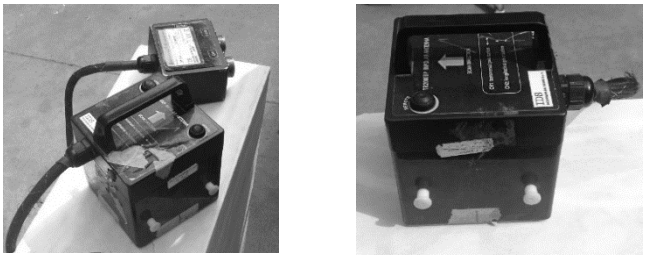

Figure 2-17, Aladdin GPR instrument

Center point of the marble block on one side of biggest face was found and the GPR was placed there to discard annoying sidewall reflections.

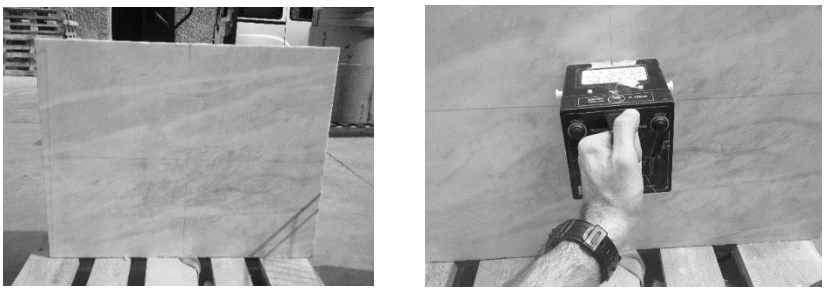

Figure 2-18, the GPR was placed on the center of marble block to discard annoying sidewall reflections

A reference reflection was collected by placing a metal screen (Figure 2-19) on the opposite side of the block where the antenna was placed.

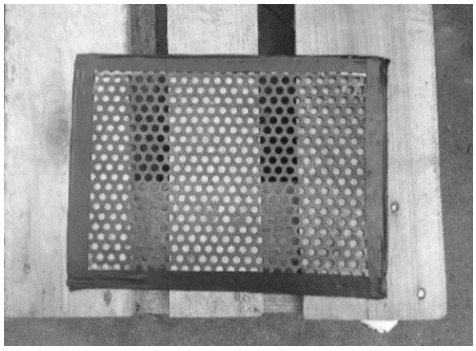

Figure 2-19, Metal screen

Channel 2 should be less disturbed by the block edges because of the shape of its radiation pattern, therefore measurements with this channel were employed (Figure 2-20). (See section 1.3, Antenna orientation)

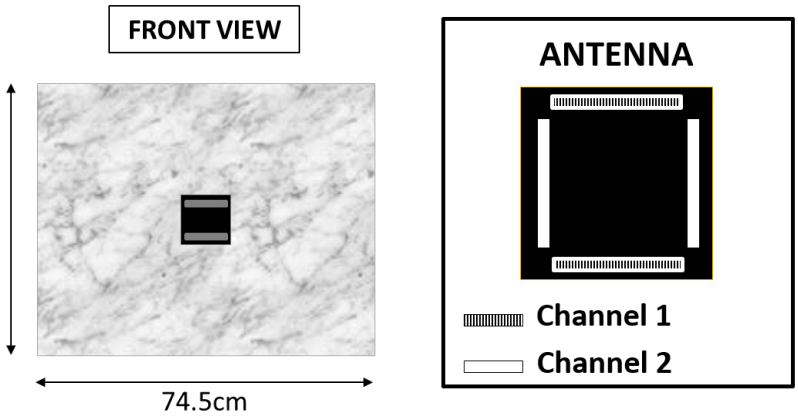

Figure 2-20, Measurement were employed with channel 2

Radar traces were collected setting a time triggering mode with a stacking factor of 4, and a 30ns acquisition window. In the beginning radar measurements to determine the velocity of the electromagnetic signal within the marble block were performed. A reference reflection was collected by placing a metal screen on the opposite side of the block where the antenna was placed. By comparing amplitudes of the signals reflected by the marble/air and the marble/metal interfaces the reflection coefficient of marble/air was computed.

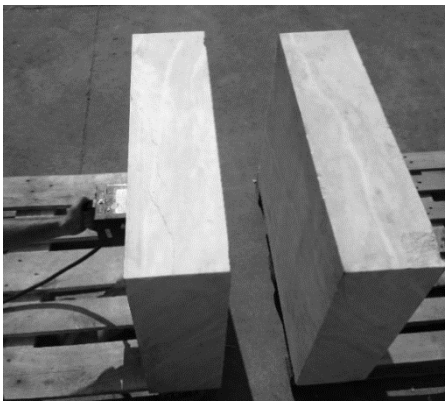

Figure 2-21, GPR data acquisition

A list of acquisition parameters are listed in Table 2-6.

Acquisition system	IDS Aladdin 2GHz
Antenna polarization	HH, VV
Block material	White Marble (Carrara, Massa-Carrara, Italy)
Single block dimensions	74.5 x 60 x 21cm
Fracture filling material	Air
Stacking factor of time triggered acquisitions	4
Time window	30 nsec
Samples per scan	2048
Sampling frequency	68.26 GHZ
Sampling interval	0.015 ns

Table 2-6, Acquisition parameters for marble block

2.2.2. Collected data

Twenty-two measurements were accomplished during field tests. The first three ones were collected with single marble block in order to compute velocity, dielectric constant and reflection coefficient of marble/air.

Other measurements were collected with two marble blocks in front of each other in order to simulate the presence of thin fracture (an air thin bed) embedded in rock. At first, two marble blocks were placed in contact to each other and then progressively moved apart from each other; beginning from 0.67 cm until 21.58 cm (one dominant wavelength). List of measurements and their description are provided in Table 2-7.

FILE	DESCRIPTION
1	Single block; thickness 21cm
2	Single block; thickness 21cm; metal screen
3	Single block; thickness 74.5cm; metal screen
4	Two blocks in contact; thickness 21+21cm; metal screen
5	Two blocks; fracture aperture λ/32: 0.67cm; metal screen
6	Two blocks; fracture aperture 2λ/32= λ/16: 1.34cm; metal screen
7	Two blocks; fracture aperture 3λ/32: 2.02cm; metal screen
8	Two blocks; fracture aperture 4λ/32= λ/8: 2.69cm; metal screen
9	Two blocks; fracture aperture 5λ/32: 3.37cm; metal screen
10	Two blocks; fracture aperture 6λ/32: 4.04cm; metal screen
11	Two blocks; fracture aperture 7λ/32: 4.72cm; metal screen
12	Two blocks; fracture aperture 8λ/32= λ/4: 5.39cm; metal screen
13	Two blocks; fracture aperture 9λ/32: 6.07cm; metal screen
14	Two blocks; fracture aperture 10λ/32: 6.74cm; metal screen
15	Two blocks; fracture aperture 11λ/32: 7.42cm; metal screen
16	Two blocks; fracture aperture 12λ/32=3 λ/8: 8.09cm; metal screen
17	Two blocks; fracture aperture 13λ/32: 8.77cm; metal screen
18	Two blocks; fracture aperture 14λ/32: 9.44cm; metal screen
19	Two blocks; fracture aperture 15λ/32: 10.11cm; metal screen
20	Two blocks; fracture aperture 16λ/32= λ/2: 10.79cm; metal screen
21	Two blocks; fracture aperture 24λ/32= 3λ/4: 16.18cm; metal screen
22	Two blocks; fracture aperture 32λ/32= λ: 21.58cm; metal screen

Table 2-7, Collected data for Marble blocks

2.2.3. Data analysis

2.2.3.1. Real data

The procedures which were done on raw data are similar to the case of sandstone (See section 2.1.3.1. Real data). Traces for each aperture were obtained individually. In Figure 2-22 all traces are shown as a function of fracture thickness. Reflection coefficient as a function of bed thickness are illustrated in the section (2.2.3.1.3.Thin bed analysis).

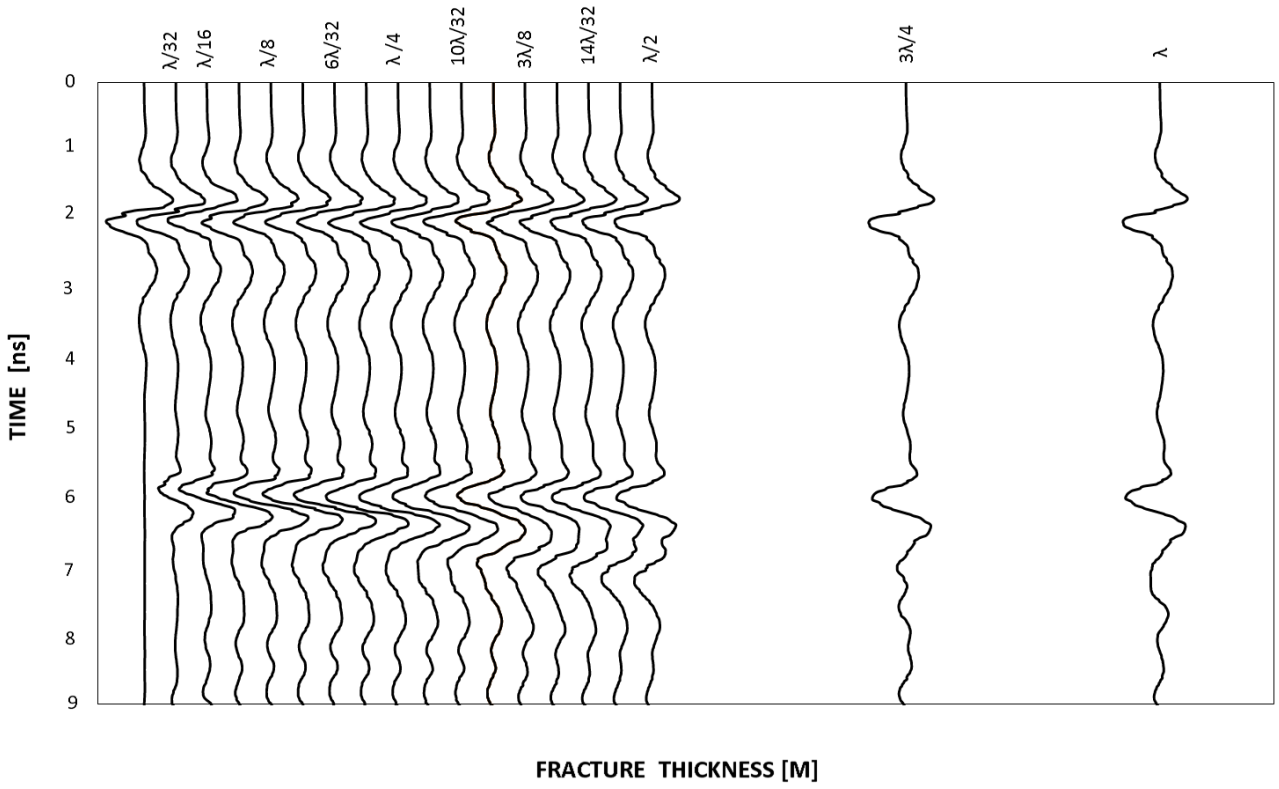

Figure 2-22, Traces of real data as a function of bed thickness

2.2.3.1.1. Field test parameters

Fracture apertures are related to the dominant wavelength of the radiated signal in the fracture material (i.e., air). The dominant wavelength is, by definition, related to the dominant period, which has been calculated considering the first two positive peaks wavelet reflected from the bottom of the marble block (in principle the dominant period should be measured on the signal travelling into the fracture material but this would require separable transmitter and receiver). Here are the parameters, which were obtained in the field.

Velocity in the marble was calculated by placing a metal screen on the other side of marble block (Figure 2-23), and measuring the travel distance (2d) of reflected signal divided by the travel time:

$$v_m = \frac{2d}{t} = \frac{2(21)}{4.37} = 9.59\ cm/nsec \qquad (2\text{-}7)$$

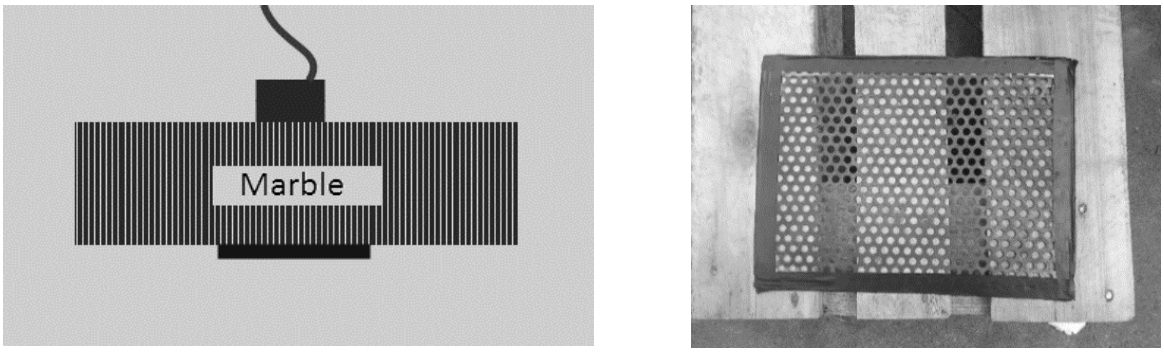

Figure 2-23, Metal screen

Dominant period was calculated by considering the first two positive peaks wavelet reflected from the bottom of the marble block:

$$\Delta_t = 4.743 - 4.025 = 0.71\ ns \qquad (2\text{-}8)$$

Dominant frequency is:

$$f_d = \frac{1}{\Delta_t} = \frac{1}{0.718} = 1.39\ GHz \qquad (2\text{-}9)$$

Dominant wavelength in the marble:

$$\lambda_{d_m} = \frac{v}{f_d} = \frac{9.59}{1.39} = 6.89\ cm \qquad (2\text{-}10)$$

Dominant wavelength in the thin bed (i.e. in air):

$$\lambda_{d_A} = \frac{v}{f_d} = \frac{30}{1.39} = 21.54\ cm \qquad (2\text{-}11)$$

Summary of field test parameters are provided in Table 2-8.

Average velocity	9.60 cm ⁄ nsec
Dominant period	0.71 ns
Dominant frequency	1.39 GHz
Dominant wavelength in the marble	6.89 ≅ 6.9 cm
Dominant wavelength in the thin bed	21.54cm

Table 2-8, In the field test parameters

2.2.3.1.2. Reference parameters

In the following, data were analyzed in order to obtain meaningful parameters for the analysis of the reflections from the thin bed according to its aperture. For each collected file, average traces were extracted and only channel 2 was considered because of its more favorable radiation patters. Reflection by the bottom of the marble block was isolated by means of a Tukey window, which is flat in its central part (Figure 2-24). This does not change the peak amplitude of the reflect signal. Both raw and filtered data were considered. Filtering was performed with an IIR zero phase lowpass Butterworth filter with 1dB ripple in pass-band, -40dB in stop-band, high-cut frequency 5GHz and high-trunk frequency 7GHz (See section 1.6). Calculated reference parameters are as follow (For detailed results see Appendix, Reference parameters).

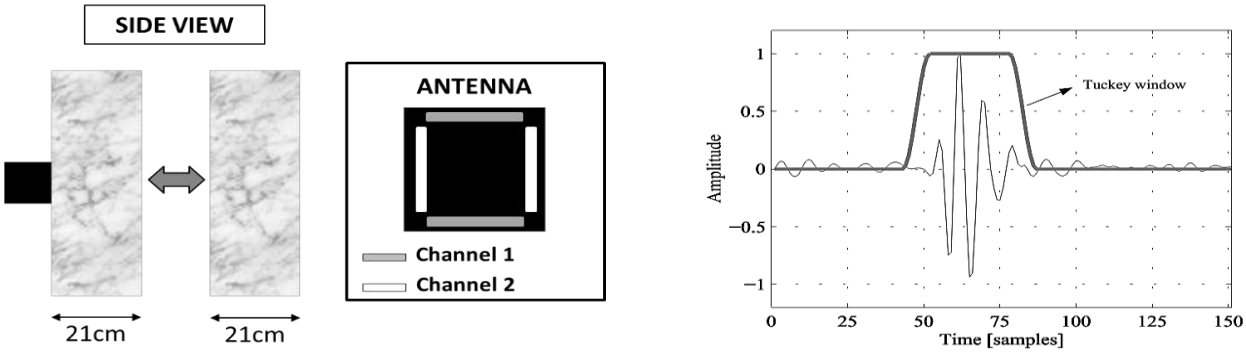

Figure 2-24, Only channel 2 is considered because of its favorable radiation patters (Left), Tukey window used to select the signal (Right)

Average velocity in the marble is:

$$v_m = 9.67\ cm/nsec \qquad (2\text{-}12)$$

Average value of the dominant frequency (f_d). Only signal reflected by marble/air interface and travelling in a single block (raw and LP-filtered):

$$f_d = 1.38\ GHz \qquad (2\text{-}13)$$

Dominant wavelength in the thin bed (i.e. in air):

$$\lambda_{d_A} = \frac{v}{f_d} = \frac{30}{1.38} = 21.69cm \qquad (2\text{-}14)$$

Average attenuation was computed from one block to two blocks (21cm to 42cm). As we know spherical divergence for distance doubled ($r_2=2r_1$) is equal to 6dB ($20log_{10}\left(\frac{2r_1}{r_1}\right)=6dB$). Therefore, attenuation of nearly 6dB for distance doubled means there is just spherical divergence and no absorption (See section 1.3, Attenuation).

$$A = 5.96\ dB \qquad (2\text{-}15)$$

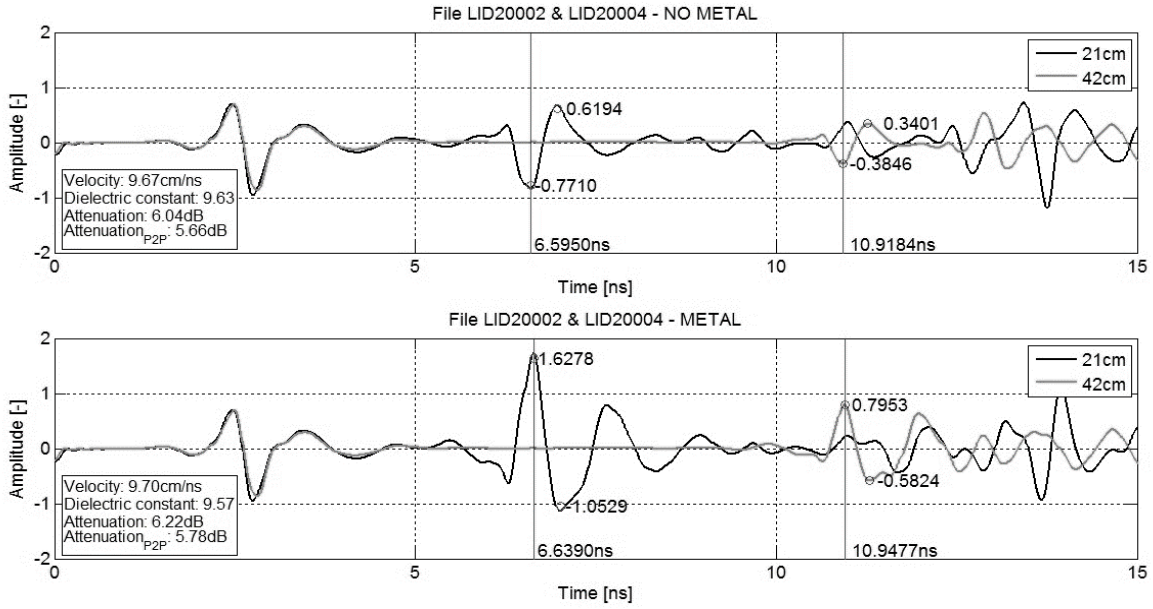

Figure 2-25, Velocity and attenuation analysis- Low-Passed filter (5GHz, zero-phase)

Marble relative dielectric constant is computed using low-loss approximation, (See section 1.2, Loss factor).

$$\varepsilon_{r_m} = \left(\frac{C}{V}\right)^2 = \left(\frac{30}{9.67}\right)^2 = 9.76\ cm/nsec \qquad (2\text{-}16)$$

Reflection coefficient marble/air (It is reasonable to use the low-loss approximation because there is just spherical divergence and no absorption):

$$R_{Marble/Air} = \frac{\sqrt{\varepsilon_{r_m}} - 1}{\sqrt{\varepsilon_{r_m}} + 1} = 0.51 \qquad (2\text{-}17)$$

Summary of calculated reference parameters are provided in Table 2-9.

Average velocity	9.60 cm/nsec
Average dominant frequency	1.38 GHz
Dominant wavelength	21.69 cm
Average attenuation	5.96 dB
Relative dielectric constant	9.76 cm/nsec
Reflection coefficient marble/air	0.51

Table 2-9, Reference parameters

2.2.3.1.3. Thin bed analysis

In the following, measurements related to the reflection from thin bed with different apertures were analyzed. For each measurement, the average trace were extracted. In addition, background signal amplitude and timing were evaluated, and amplitude and jitter corrections were performed if necessary. To compute reflection coefficients associated to each aperture of thin bed, reflection from the metal screen was taken as reference (if background signals of the reference trace and of the thin bed trace are different, amplitude correction was performed again). Figure 2-26 shows relation between reflection coefficient and bed thickness.

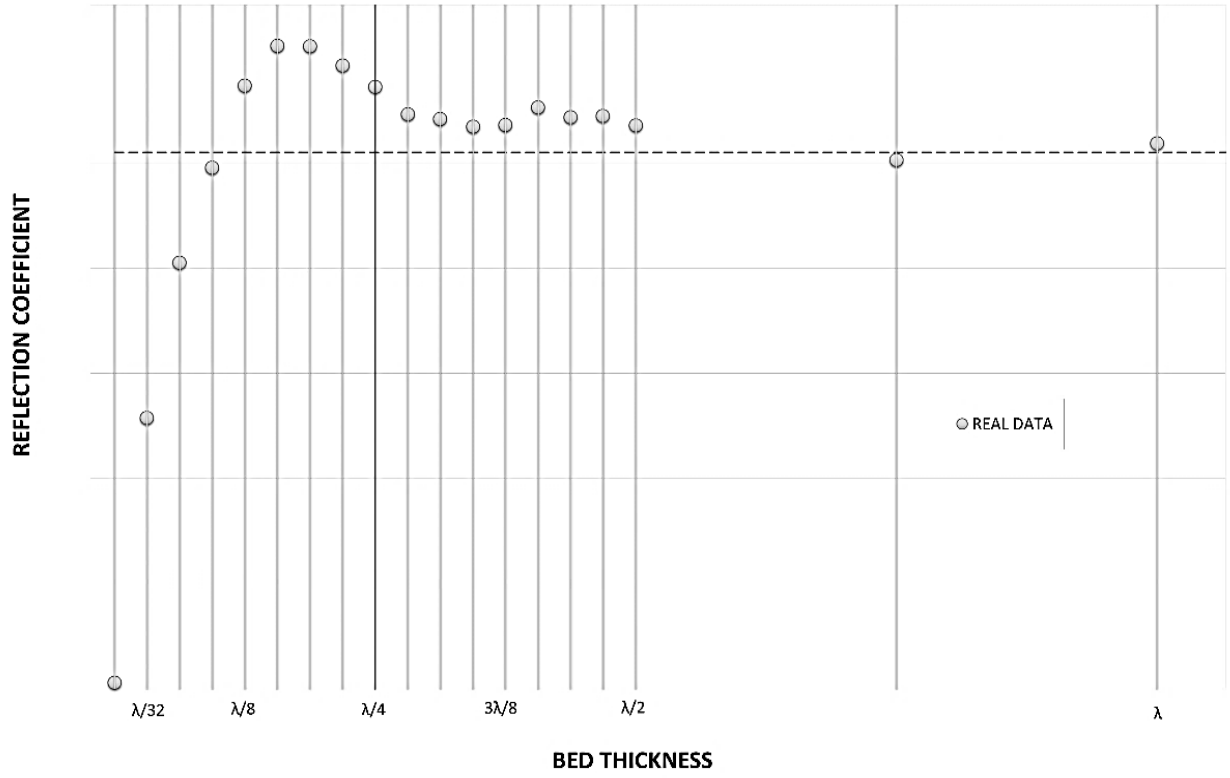

Figure 2-26, Reflection coefficient as a function of bed thickness

Figure 2-26 shows that the maximum reflection coefficient occurs at $5.5\lambda_d/32$ (3.71cm). It is different from the theoretical value of $\lambda_d/4$ (See section 1.8.2, Tuning effect). It seems that the dominant wavelength has been overestimated in the field. Considering the discrepancy with theory, the wavelength should be nearly 15cm instead of 21.58cm. Convolutional models also indicate the similar value for wavelength (See section 1.2, Convolutional model). The comparison between real data and convolutional models (transmission losses, No amplitude decay, No internal multiples) according to different dominant frequency of the source 3-loop Ricker wavelet is provided in Figure 2-27. The best fitting convolutional model implies a dominant frequency of 1.96 GHz and an associated dominant wavelength of 15.3 cm. It should be mentioned that, in the case of Sandstone block the maximum reflection coefficient was occurred at $\lambda_d/4$ and it was consistent with the theory.

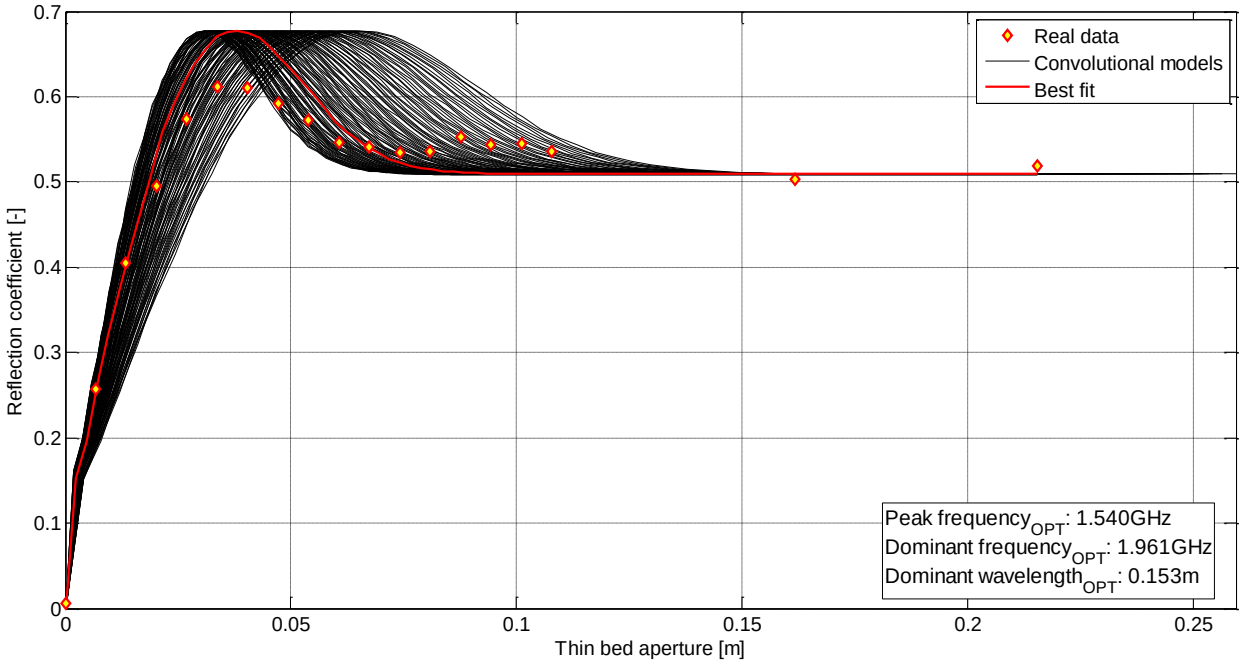

Figure 2-27, The comparison between real data and convolutional models

Considering a wavelength of 15cm, the corresponding dominant frequency is:

$$f_d = \frac{v}{\lambda_d} = \frac{30}{15} = 2\ GHz \qquad (2\text{-}18)$$

And the associated dominant period is:

$$T_d = \frac{1}{f_d} = 0.5\ ns \qquad (2\text{-}19)$$

Therefore, there is a 0.21ns deference in picking of the dominant period of 0.71ns, which was performed during field acquisition (Table 2-8). Considering sampling interval of 1.5e-2 ns (Table 2-6), this would correspond to an error of about 15 samples. This error is unlikely. The first assumption for this error was the frequency dependent attenuation of reflected signal, because we considered the signal collected by receiver antenna and not the signal traveled in the thin bed (Figure 2-28). Accordingly signal with higher dominant period T_d, and larger dominant wavelength λ_d might be collected by receiver antenna.

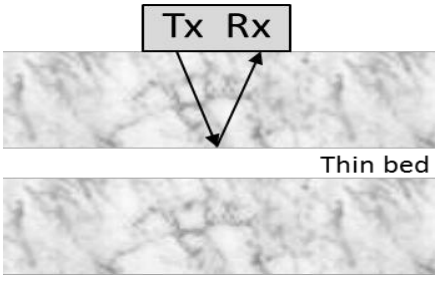

Figure 2-28, The dominant wavelength has been computed considering the signal reflected by the bottom of the block and collected by the receiving antenna

In the case of frequency dependent attenuation, we should have lower frequency content (Peak and dominant frequency) when traveled distance of reflected signal is longer. Considering this fact frequency content of file 1 (One block) and File 4 (Two blocks in contact) are compared. See specification of these files in Table 2-7.

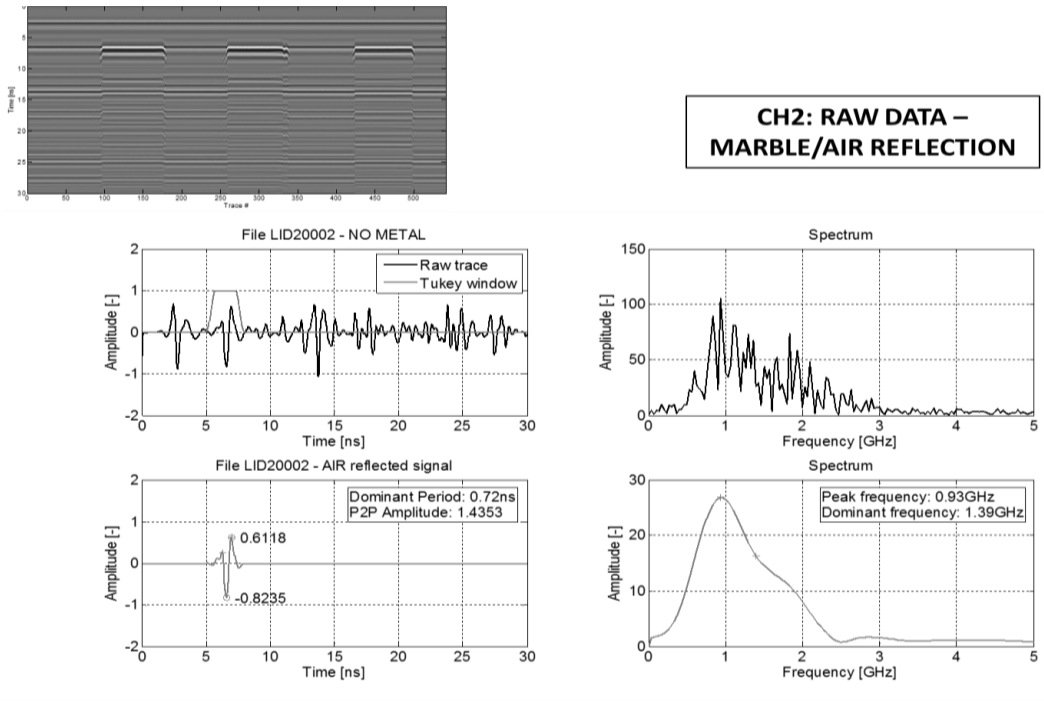

Figure 2-29, File 2 (Single block with metal screen)

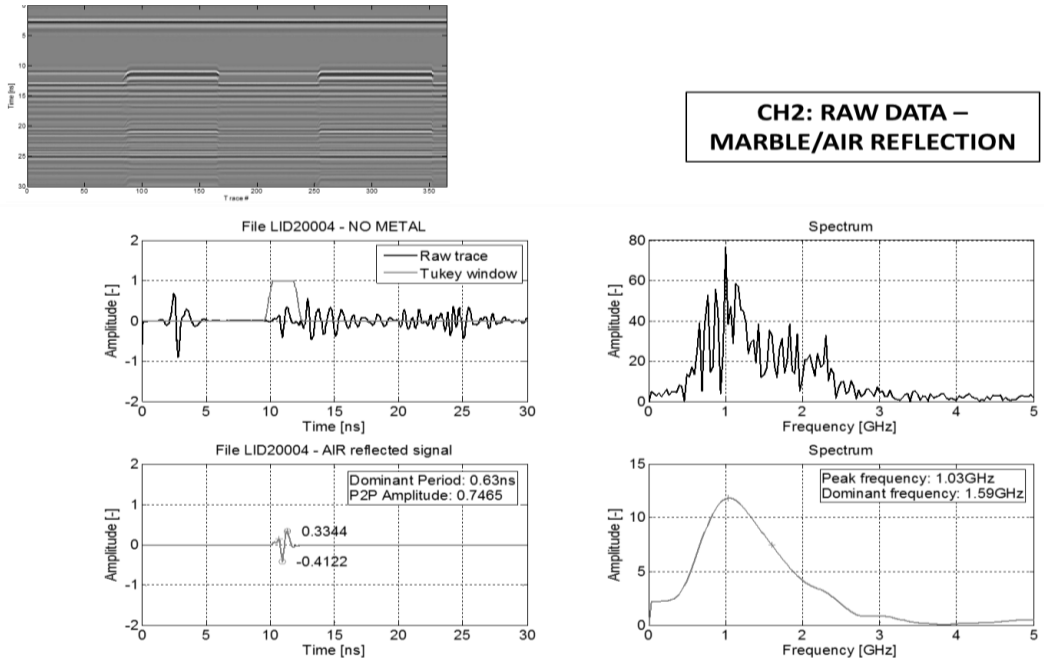

Figure 2-30, File 4 (Two blocks with metal screen)

According to Figure 2-29 and Figure 2-30 the frequency content of file 4 with two blocks in contact is higher than the frequency content of file 1 with only one block. For that reason, the assumption of the frequency dependent attenuation of reflected signal is ignored. The other assumption could be regarding to the shape of wavelet. The source wavelet should be Ricker wavelet (See section 1.8.2, Ricker wavelet) which may not what is exactly happened in the reality and in the acquisitions with GPR instrument.

2.2.4.1. Synthetic data

2.2.4.1.1. Comparison criteria

The aim of following simulations is finding a received signal with similar shape (time and frequency characteristics) and amplitude ratio (Equation (2-20)) to the one obtained in the real tests. In order to compare synthetic and real data, File1 (Table 2-7) is taken into account. This file is related to the test on a single block with thickness of 21cm.

The amplitude ratio for real tests and namely for the File1 is equal to 1.06; its time and frequency characteristics are provided in Table 2-10. Simulations with GprMax should tune by considering different parameters to find shape and amplitude ratio similar to this file.

$$\frac{\text{peak} - \text{to} - \text{peak amplitude of the background signal}}{\text{peak} - \text{to} - \text{peak amplitude of the reflected signal}} = 1.06 \qquad (2\text{-}20)$$

SINGLE BLOCK (FILE LID20001)	
Time and frequency characteristics	
Dominant Period	0.69 ns
Peak Frequency	1.00 GHz
Dominant Frequency	1.45 GHz

Table 2-10, Time and frequency characteristics (FILE LID20001)

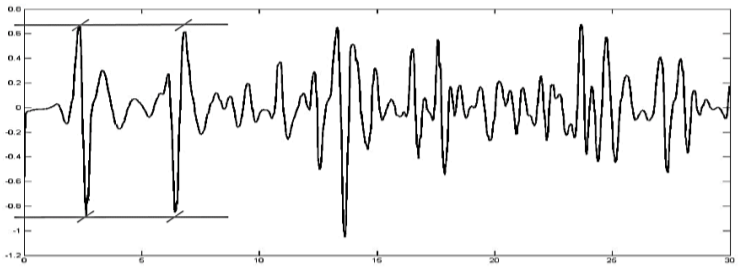

Figure 2-31, Ratio of background signal to reflected signal (FILE LID20001)

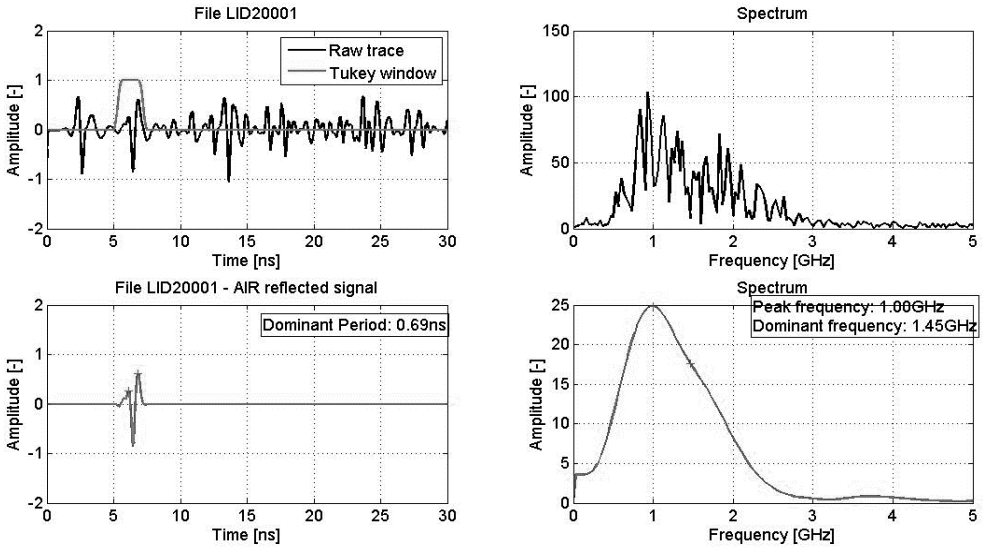

Figure 2-32, Time and frequency characteristics (FILE LID20001)

2.2.4.1.2. 3D Simulations with GprMax

2.2.4.1.2.1. Current frequency

Several simulations were performed in order to find a received signal with similar shape (time and frequency characteristics) to the File 1 (See section 2.2.4.1.1). Simulations were performed with a single block; transmitter and receiver antennas are located on the same side and in contact with the marble block (Figure 2-33). Table 2-11 shows that the best match is found when current frequency is equal to 0.85e9 GHz (Figure 2-34). From now on, this current frequency was used for 3D simulations with GprMax.

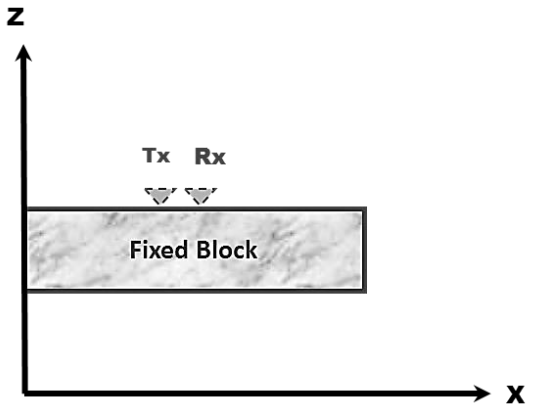

Figure 2-33, Illustration of the simulation in GprMax

	MSI (Marble – Single block – In contact)			
	Current Frequency GHz	**Time and frequency characteristics**		
1	0.79e9	Dominant Period	0.72 ns	
		Peak Frequency	1.12 GHz	
		Dominant Frequency	1.38 GHz	
2	From 0.85e9	Dominant Period	0.69 ns	Best fit
		Peak Frequency	1.22 GHz	
		Dominant Frequency	1.44 GHz	
3	Till 851.47e6	Dominant Period	0.69 ns	
		Peak Frequency	1.22 GHz	
		Dominant Frequency	1.44 GHz	
4	851.48e6	Dominant Period	0.68 ns	
		Peak Frequency	1.22 GHz	
		Dominant Frequency	1.46 GHz	

Table 2-11, Time and frequency characteristics of different current frequencies

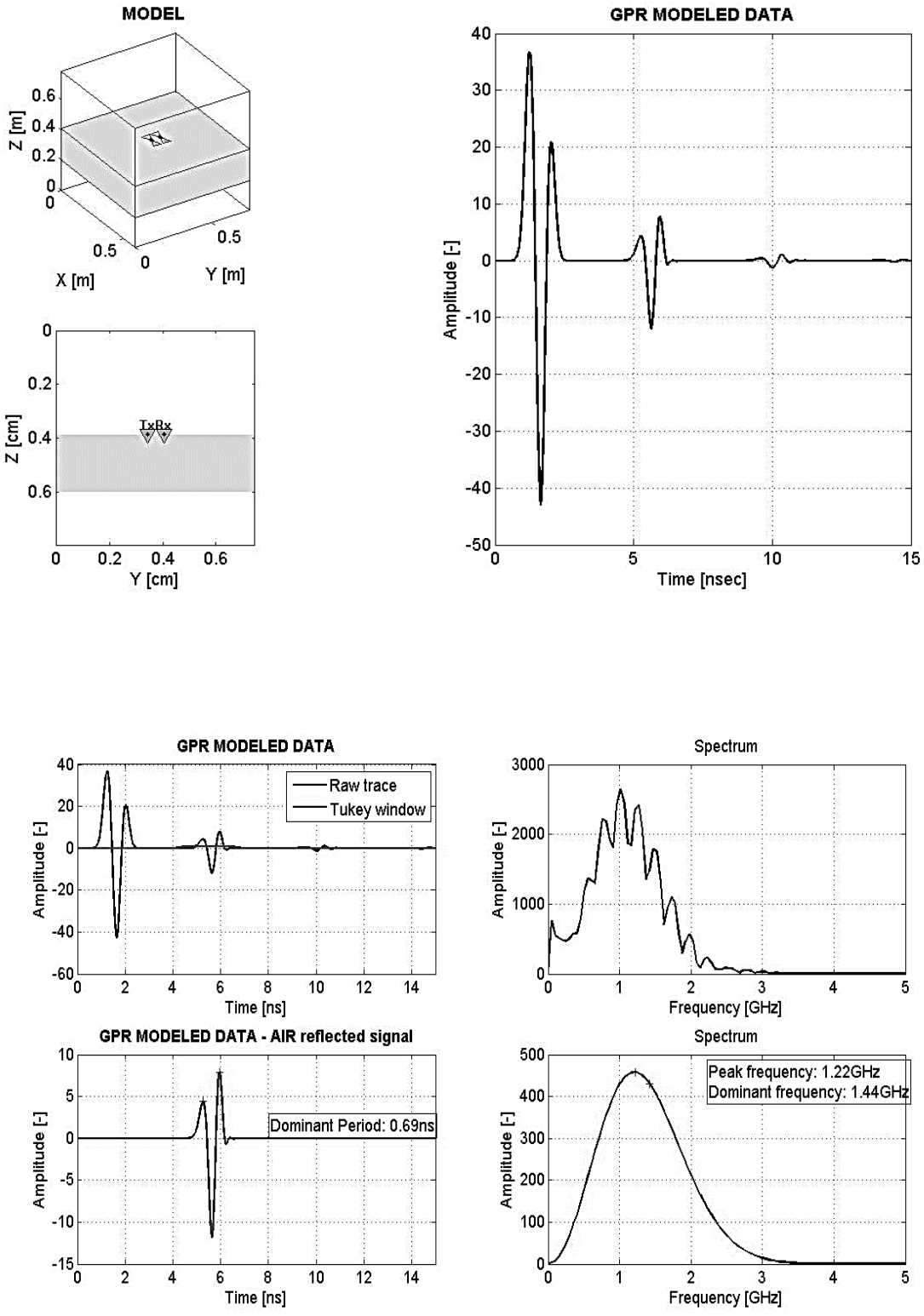

Figure 2-34, GPR 3D Simulation for 0.85 GHz current frequency

2.2.4.1.2.2. Conductivity and Dielectric constant

A received signal with similar shape (time and frequency characteristics) was found in the previous section. In this part of simulations, conductivity (σ) and dielectric constant (εr) of the marble block were adjusted in order to find the amplitude ratio (Equation (2-20)) similar to the real tests. For modeling the source wavelet, reflected wavelet by the bottom of the block in the single block experiment was considered.

Due to the fact that the velocity in air is known and the velocity in the marble was computed by placing metal screen on the other side of the marble block and dividing travel distance by travel time (See section 2.2.3.1.1), possible error in computing dielectric constant is very low (Equation (2-16)). Therefore, the only parameter which was taken into account in this section is the conductivity of the marble.

The cases, which are taken into account, are listed in Table 2-12. In all models, current frequency is equal to 0.85e9 GHz (See section 2.2.4.1.2).

	File Name	Blocks	Detachment	Conductivity (s/m)
1	**MSI-C0**	Single Block	In contact	0
2	**MSI-C0.01**	Single Block	In contact	0.001

Table 2-12, Different conductivity

Figure 2-35 shows that compare to the real tests, the amplitude ratio is high in both cases and the value of conductivity is not change this fact.

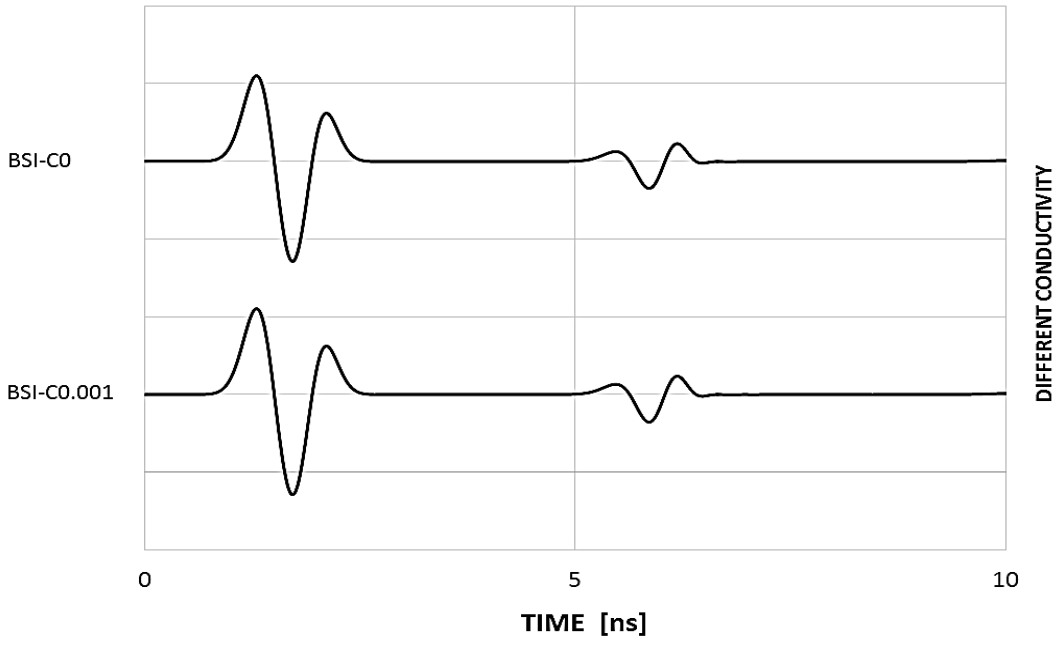

Figure 2-35, Different conductivities

2.2.4.1.2.3. Position of antennas

Simulations with two positions for antennas (1 cm and 2 cm above the marble block) in combination with two different values for conductivity (0 s/m and 0.001 s/m) were designed (Figure 2-36). The aim is again to find amplitude ratio similar to the real tests. Simulations with their specifications are listed in Table 2-13.

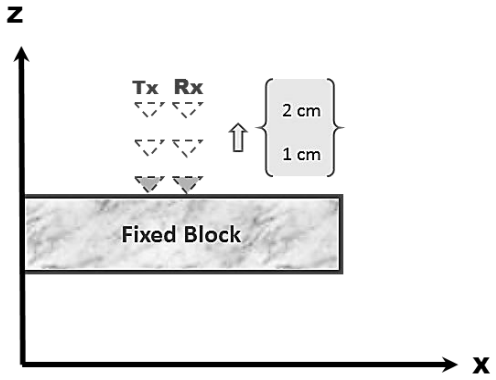

Figure 2-36, Different T_x and R_x positions above the marble block in combination with different aperture thicknesses

	File Name	Blocks	Detachment	Conductivity (s/m)
1	**MS1-0**	Single Block	1 Cm	0
2	**MS1-0.001**	Single Block	1 Cm	0.001
3	**MS2-0**	Single Block	2 Cm	0
4	**MS2-0.001**	Single Block	2 Cm	0.001

Table 2-13, Different T_x and R_x positions above the marble block

As it is visible in Figure 2-37, in all models the amplitude ratio is higher than real tests.

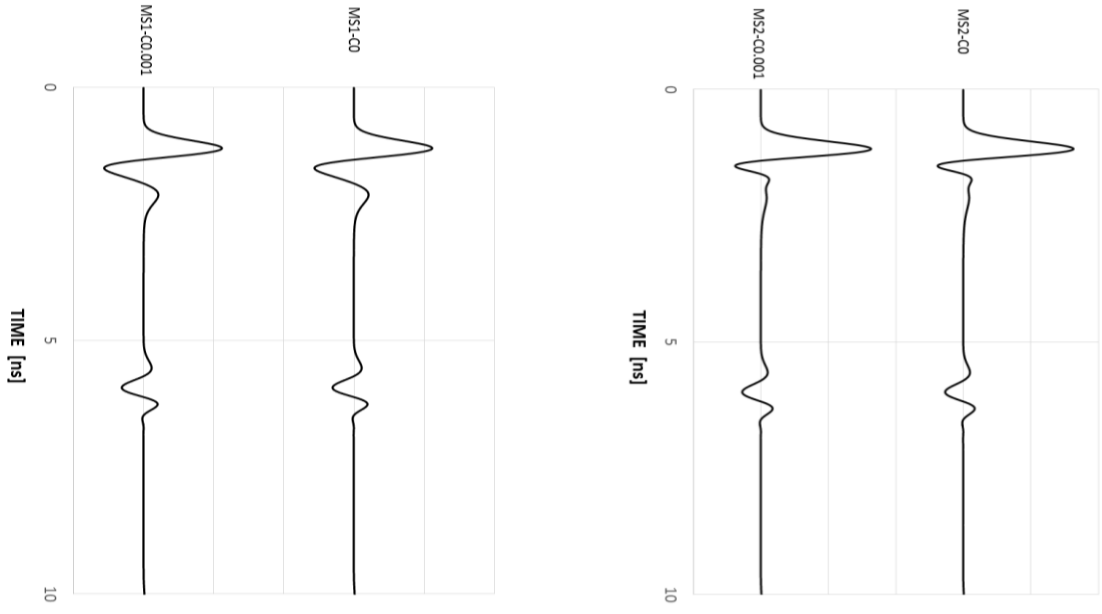

Figure 2-37, Different positions of antenna

2.2.4.1.2.4. Type of antenna

The effect of bowtie antenna was examined in this part. Bowtie antenna was used as a source combined with a Ricker wavelet input current. The cases, which were taken into account, are:

	File Name	Blocks	Detachment	Conductivity (s/m)
1	**MSBI-0**	Single Block	In contact	0
2	**MSBI-0.001**	Single Block	In contact	0.001
3	**MSB1-0**	Single Block	1 Cm	0
4	**MSB1-0.001**	Single Block	1 Cm	0.001
5	**MSB2-0**	Single Block	2 Cm	0
6	**MSB2-0.001**	Single Block	2 Cm	0.001

Table 2-14, Use the bowtie antenna as sources

Figure 2-38, indicates that, similar amplitude ratio to the real tests was not found.

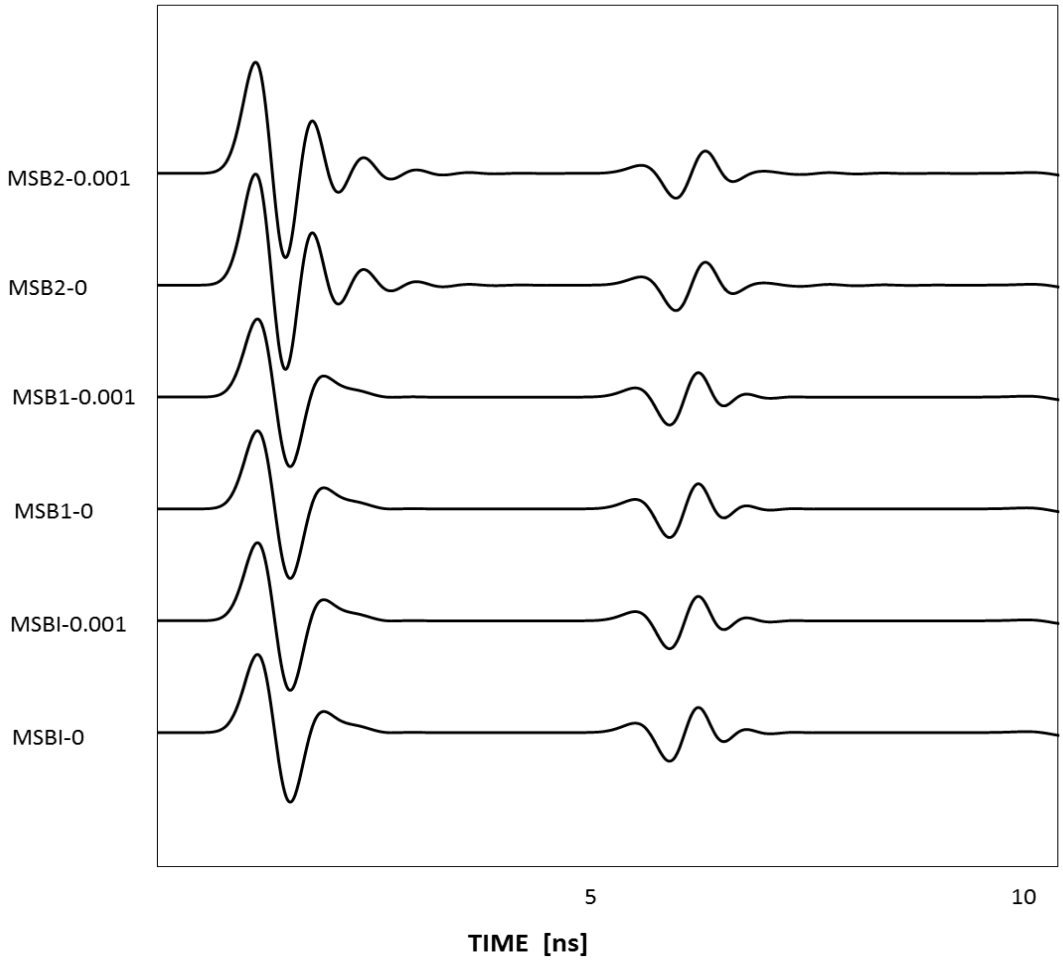

Figure 2-38, Bowtie antenna in combination with different conductivities and detachments

2.3. Conclusion

With regard to sandstone blocks, processing of data were done and trend of reflection coefficients as a function of bed thickness were obtained. The results suggest that for apertures smaller than one eighth of dominant wavelength (λd/8), a quasi-linear relationship exists between thickness and reflection amplitude. It was found that below this thickness, the information encoded in the amplitude of the thin-bed response and may be used to determine bed thickness according to this linear relationship. The trend of reflection coefficients as a function of bed thickness was compared with Chung and Lawton (1995) equation, and a good consistency was observed for the thickness below λd/8.

Considering the marble blocks, after data processing the obtained trends of amplitude versus bed thickness was different from what expected. It was found that the dominant wavelength seems to be overestimated in the field. As a possible reason of this error, frequency dependent attenuation of reflected signal was examined. However, this assumption was not proved since in the case of reflected signal with a longer travel distance, lower frequency content was not observed. It is argued that the unexpected amplitude trend may come from difference between shape of source wavelet and the Ricker wavelet.

3D simulations were accomplished in order to find a received signal with similar shape (time and frequency characteristic) and similar amplitude ratio (i.e. the peak-to-peak amplitude of background signal to the peak-to-peak amplitude of reflected signal) between real and synthetic data. This goal was completed by tuning different parameters of modeling. When current frequency was adjusted to 0.85 GHz, a received signal with similar shape to the real data was found. After that, in order to find similar amplitude ratio with real data, different conductivities of marble and different detachments of antennas from the surface of marble block, and also combination of them were examined. In addition, the effect of bowtie antenna in combination with different conductivities and different detachments were studied. However all accomplished simulations with GprMax3D, show higher amplitude ratio in comparison with real data. This difference could come from the fact that, it is not possible to take into account all physical phenomena in the model (e.g. absorbing materials within GPR instrument).

References

1. Annan, A. P., 2001, Ground Penetrating Radar workshop notes, Sensor and software Inc.
2. Annan, A. P., Davis, J. L., Gendzwill, D., 1988, Radar sounding in Saskatchewan, Canada. Geophysics, 53, 1556-64
3. Arosio et Al., 2013, GPR Investigations of rock fractures: considerations on thin beds. SAGEEP
4. Campana, S., Piro, S., 2009, Seeing the Unseen: Geophysics and landscape archeology. CRC Press
5. Chung, H., Lawton, D. C., 1995a, Amplitude response of thin beds: sinusoidal approximation versus Ricker approximation. Geophysics, 60, 223-30
6. Chung, H., Lawton, D. C., 1995b, Frequency characteristics of seismic reflections from thin beds. Canadian Journal of Exploration Geophysics, 31, 32-37
7. Daniels, D., J., 2004, Ground Penetrating Radar 2nd Edition, Volume 1. IET
8. de Voogd, N., den Rooijen, H., 1983, Thin-layer response and spectral bandwidth. Geophysics, 48, 12-18
9. Dojack, L., 2012, Ground Penetrating Radar Theory, Data Collection, Processing, and Interpretation: A Guide for Archaeologists.
10. Giannopoulos, A., 2005, GprMax2D/3D user's manual
11. Giannopoulos, A., 2005, Modeling Ground Penetrating Radar by GprMax. Construction and building materials, 19, 755-762
12. Giannopoulos, A., 2005, Numerical modeling of Ground Penetrating Radar using GprMax. Proc. 3rd International Workshop on Advanced Ground Penetrating Radar, 10–15
13. Gochioco, L., M., Modeling studies of interference reflections in thin-layered media bounded by coal seams, Geophysics, 57, 1209-1216
14. Gregoire, C., 2001, Fracture characterization by ground penetrating radar. Ph.D. Thesis, Katholieke Universiteit Leuven
15. Harry, M., Jol., 2008, Ground Penetrating Radar theory and applications. Elsevier
16. Kallweit, R. S., Wood, L. C., 1977, Seismic resolution of zero-phase wavelets. Amoco Houston Division
17. Kallweit, R. S., Wood, L. C., 1982, The limits of resolution of zero-phase wavelets. Geophysics, 47, 1035-46
18. Koefoed, O., de Voogd, N., 1980, The linear properties of thin layers, with an application to synthetic seismograms over coal seams. Geophysics, 45, 1254-68
19. Malacara hernández, D., Malacara hernández, Z., 2013, Handbook of optical design, Third edition. CRC Press
20. Milson, J., 2003, Field geophysics. University College London, John Wiley & Sons
21. Reynolds, J. M., 1997, An Introduction to applied and environmental geophysics. John Wiley & Sons
22. Ricker N., 1953, Wavelet contraction, wavelet expansion, and the control of seismic resolution. Geophysics, 18, 769-92
23. Sambuelli, L., Calzoni, C., 2010, Estimation of thin fracture aperture in a marble block by GPR sounding. Bollettino di Geofisica Teorica e Applicata, 51, 239-52
24. Sheriff, R. E., 1997, Seismic resolution a key element. Geophysical corner
25. Widess, M. B., 1973, How thin is a thin-bed?. Geophysics, 38, 1176-80
26. Zanzi, L., Notes on Ground Penetrating Radar. Dip. di Ingegneria Strutturale Politecnico di Milano

Appendix

In the following, detailed results regarding section (2.2.3.1.2. Reference parameters**)** are provided.

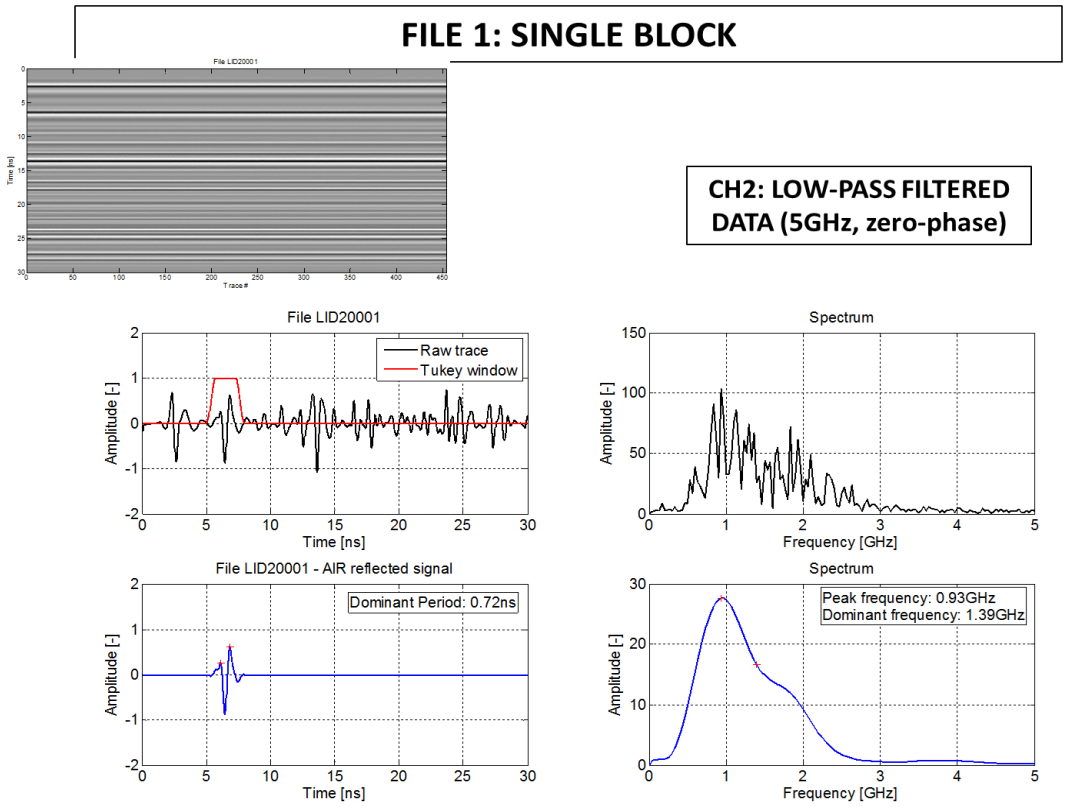

Figure A-1, File 1 (Single block_Low-pass filtered data)

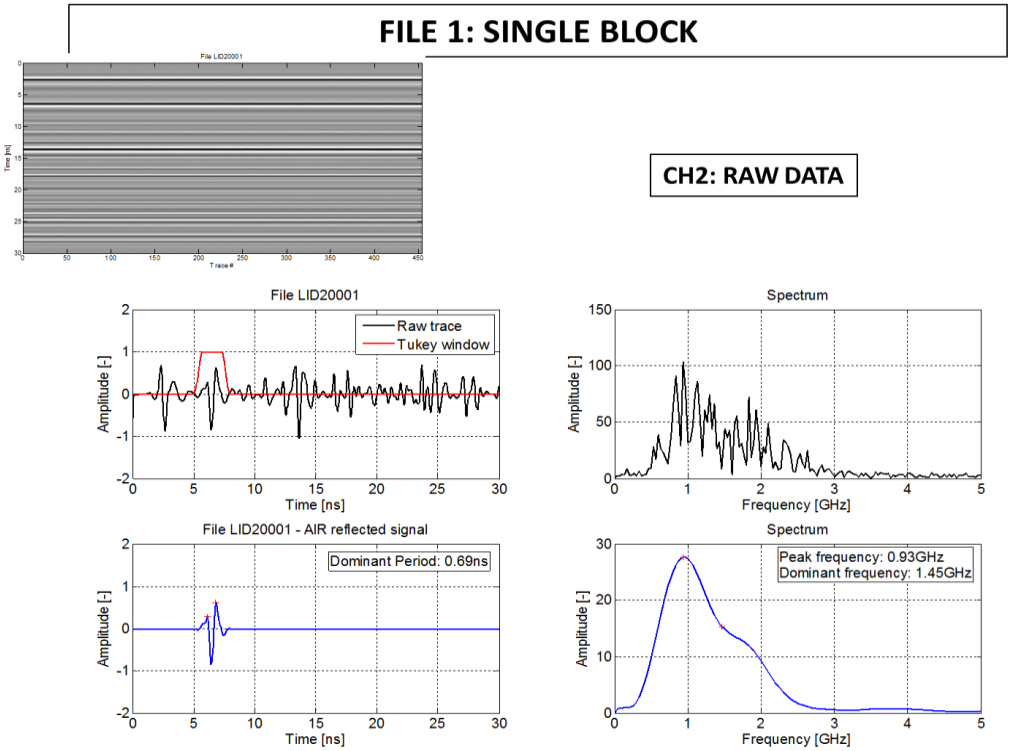

Figure A-2, File 1 (Single block_Raw data)

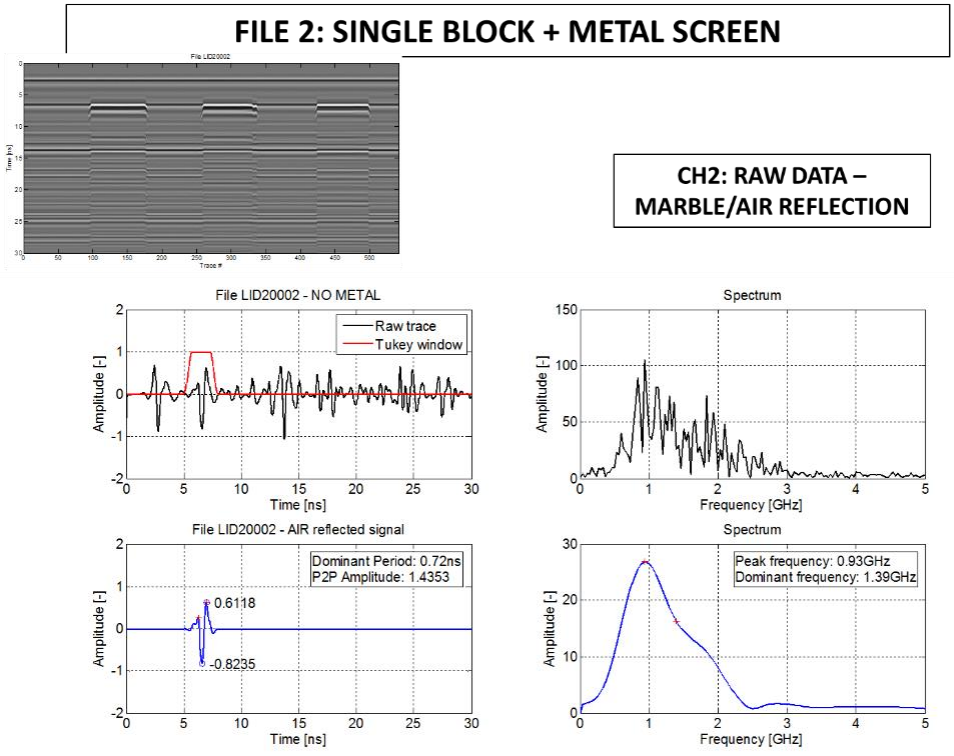

Figure A-3, File 2 (Single block_Metal screen_Raw data)

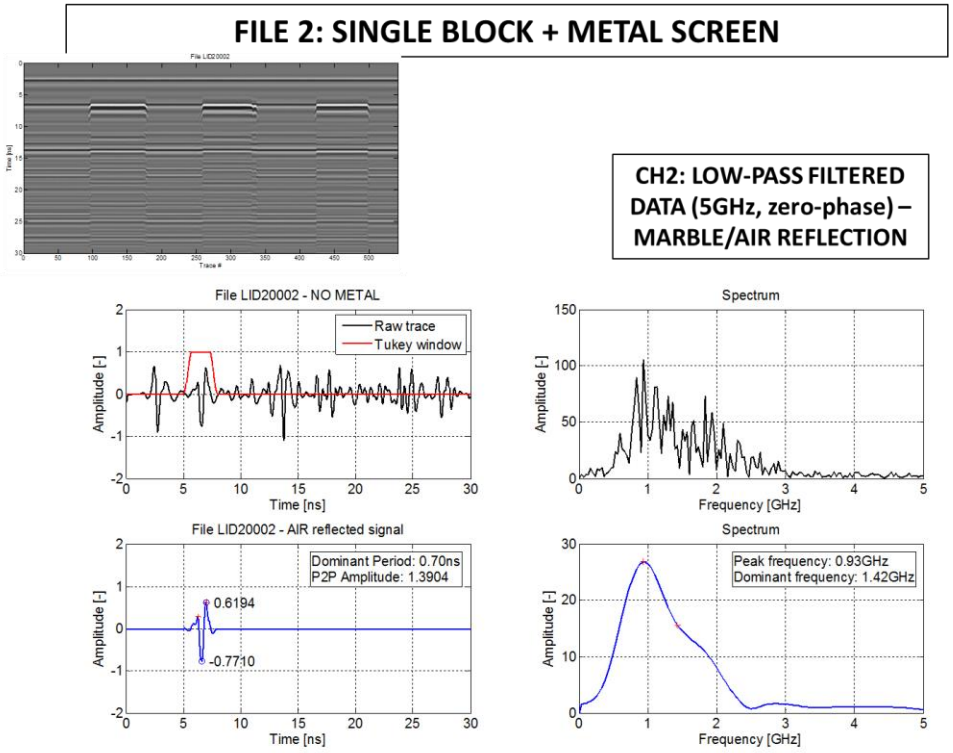

Figure A-4, File 2 (Single block_Metal screen_Low-pass filtered data)

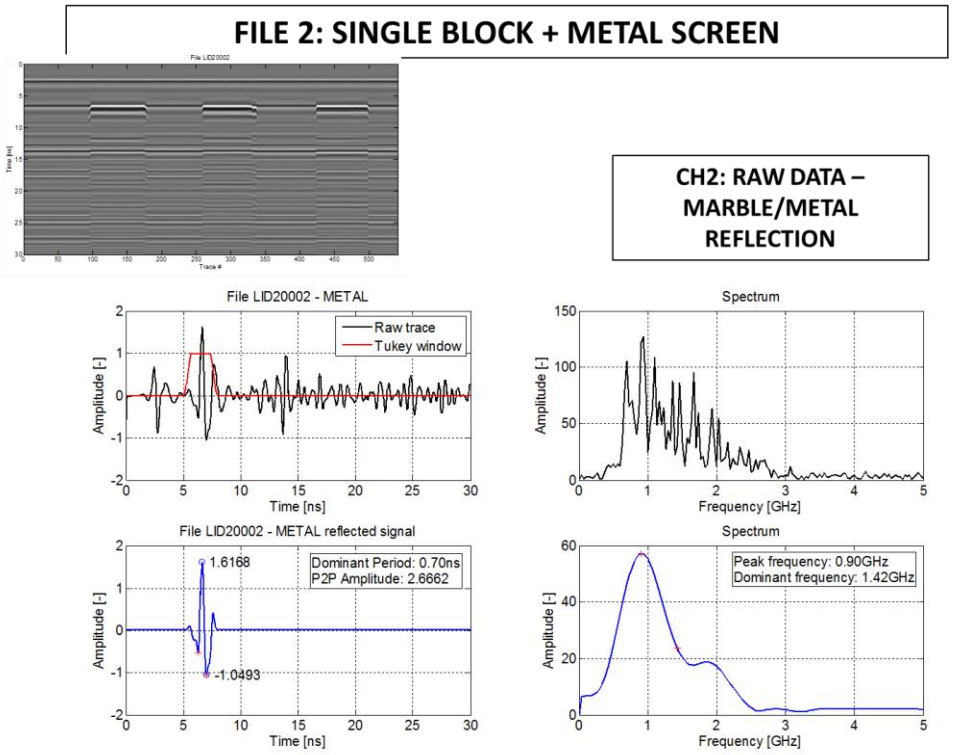

Figure A-5, File 2 (Single block_Metal screen_Raw data)

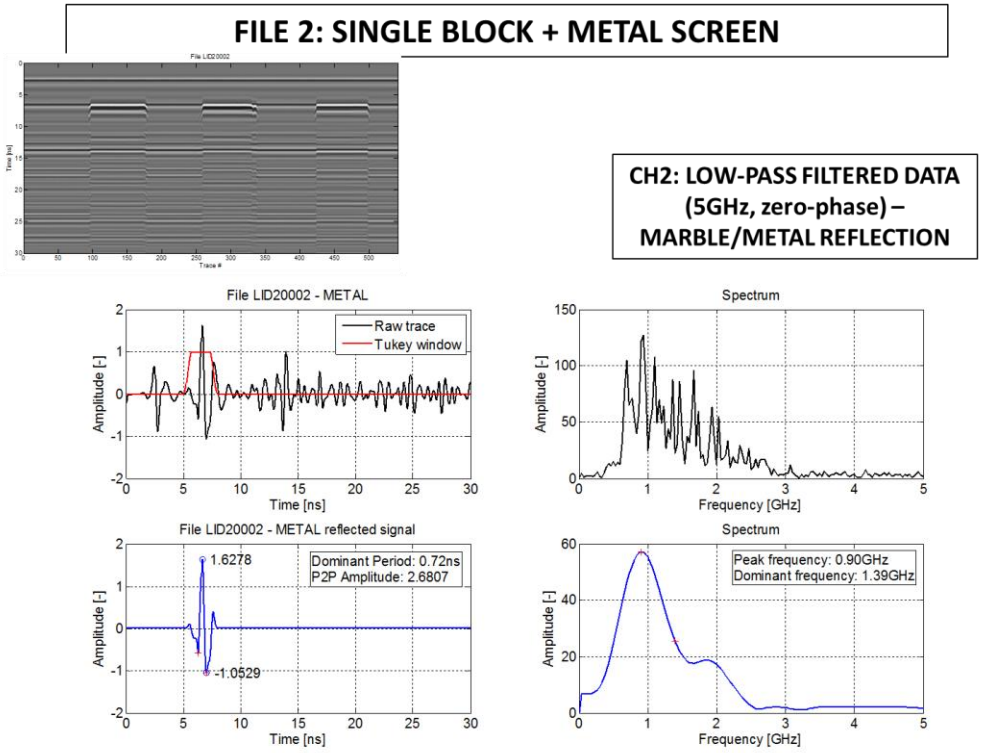

Figure A-6, File 2 (Single block_Metal screen_Low-pass filtered data)

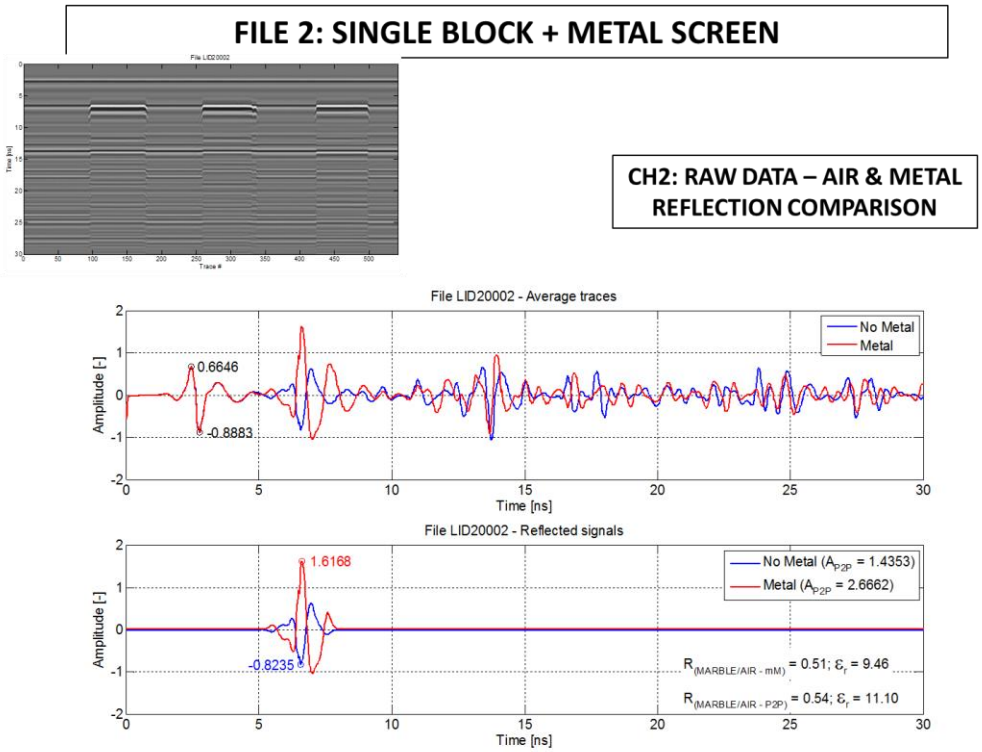

Figure A-7, File 2 (Single block_Metal screen_Raw data)

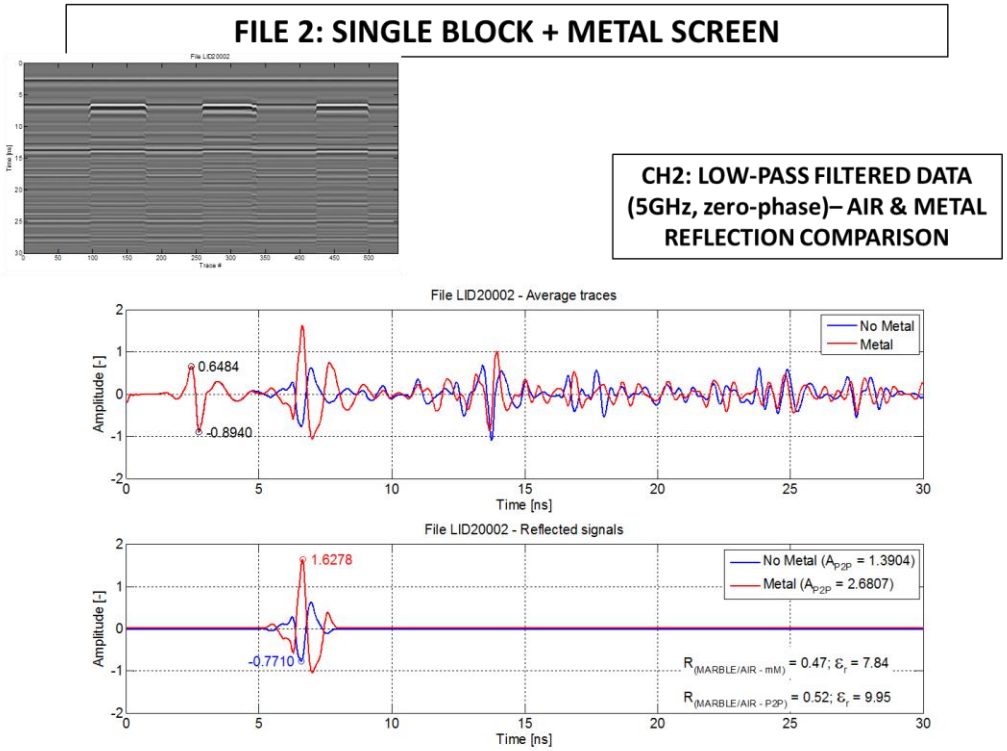

Figure A-8, File 2 (Single block_Metal screen_Low-pass filtered data)

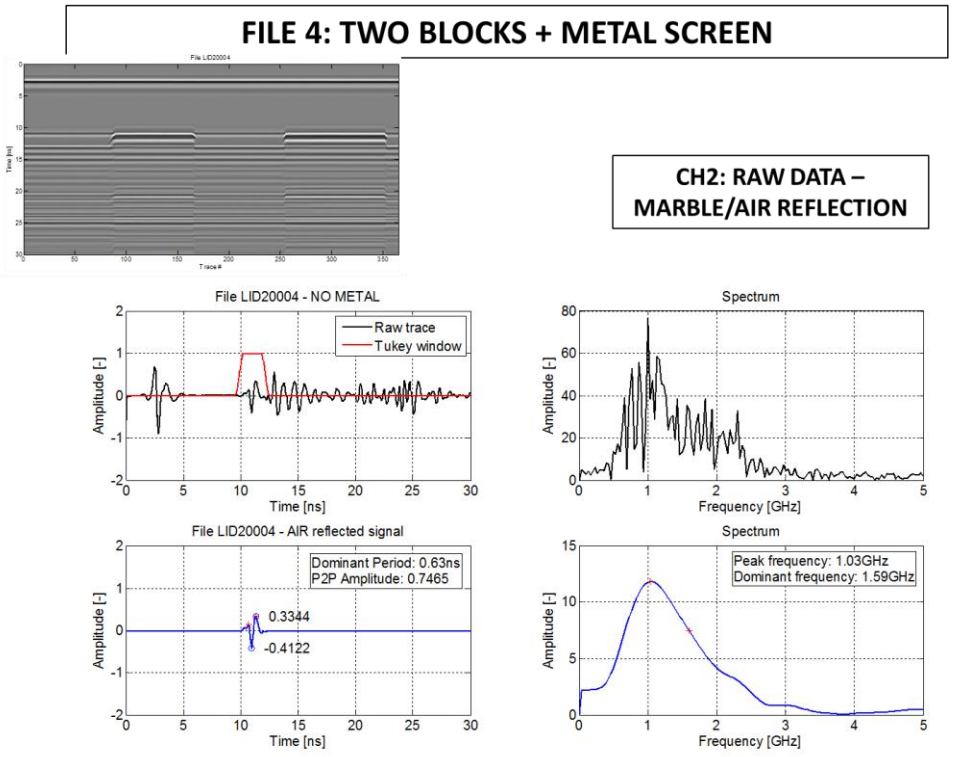

Figure A-9, File 4 (Two blocks_Metal screen_Raw data)

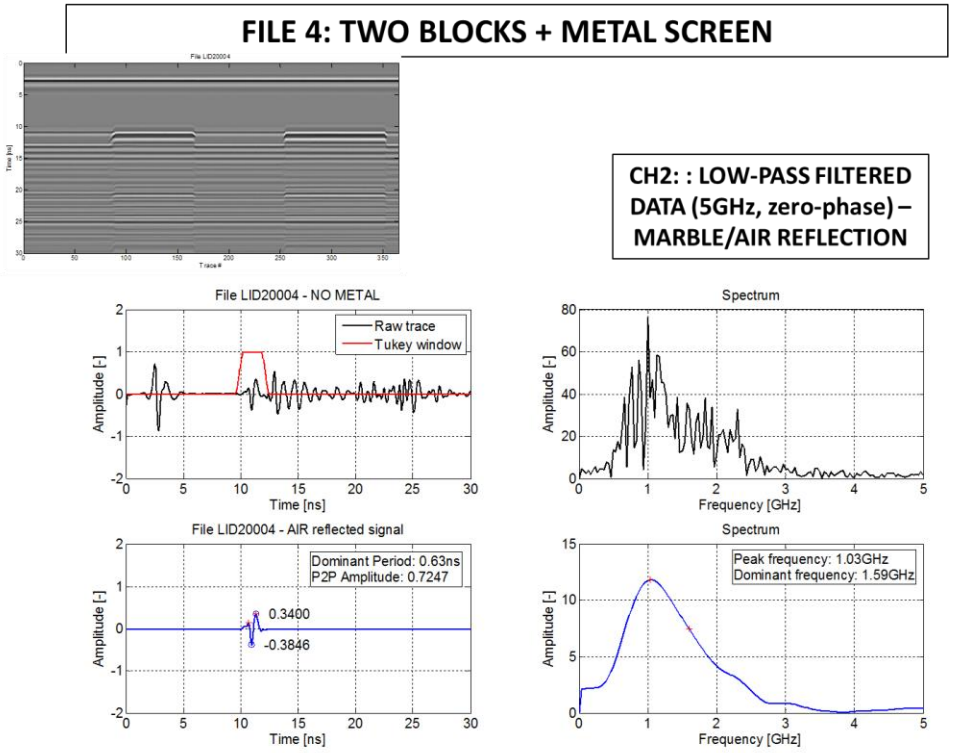

Figure A-10, File 4 (Two blocks_Metal screen_Low-pass filtered data)

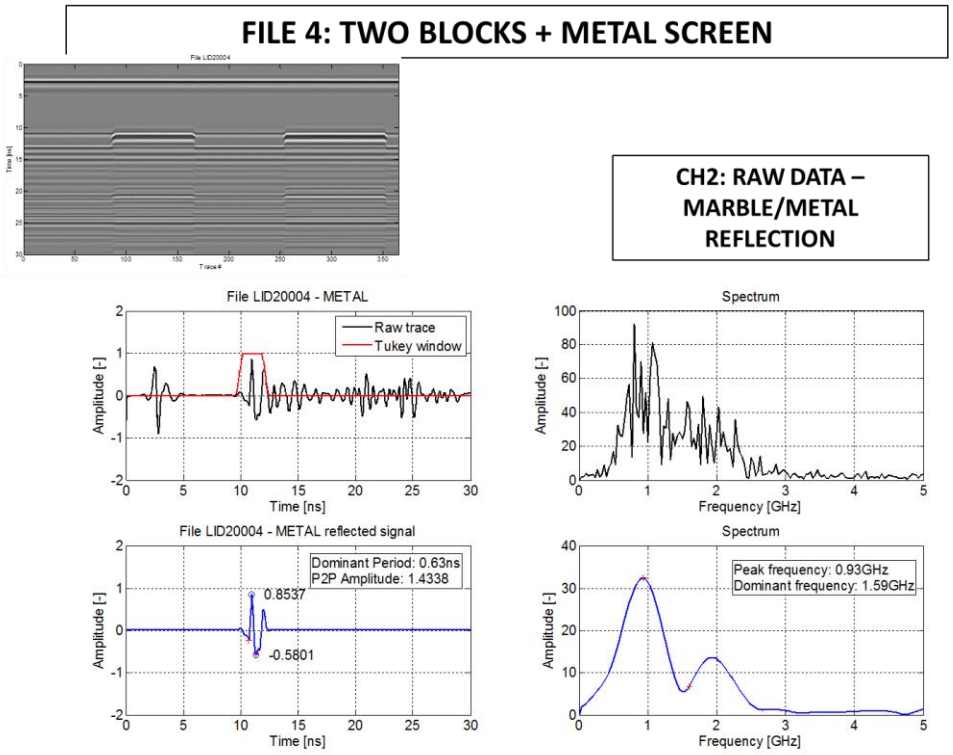

Figure A-11, File 4 (Two blocks_Metal screen_Raw data)

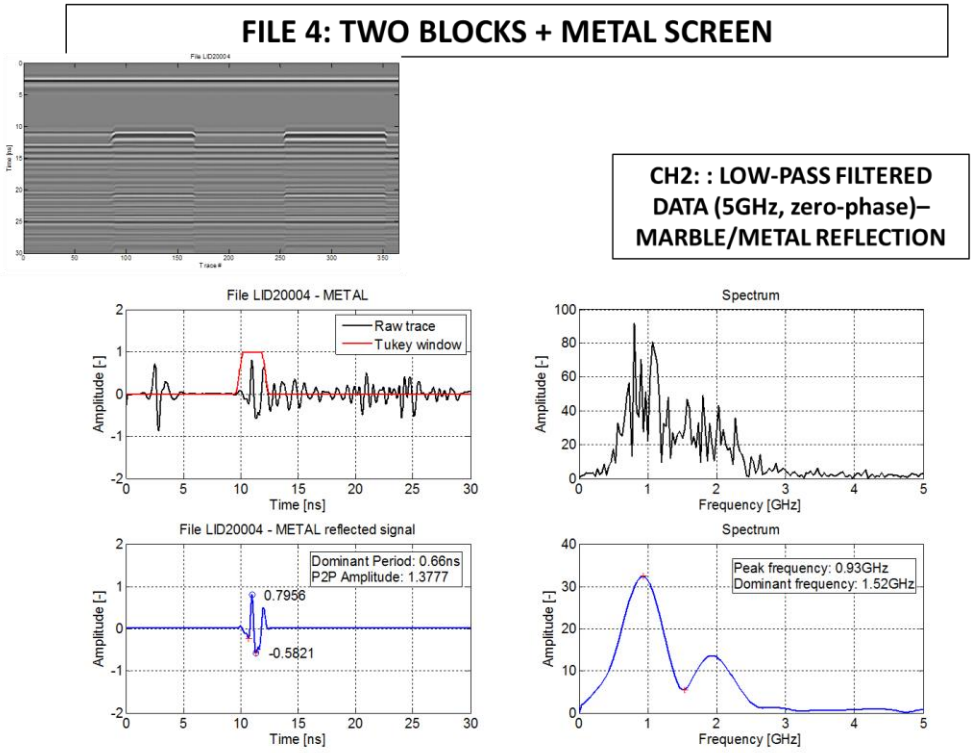

Figure A-12, File 4 (Two blocks_Metal screen_Low-pass filtered data)

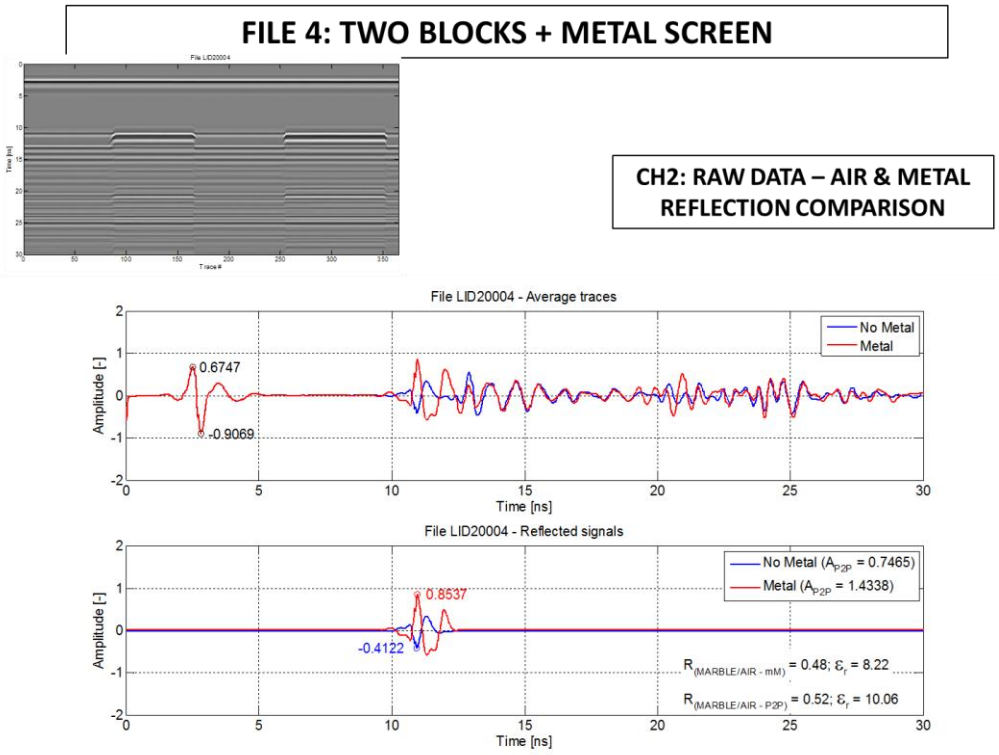

Figure A-13, File 4 (Two blocks_Raw data)

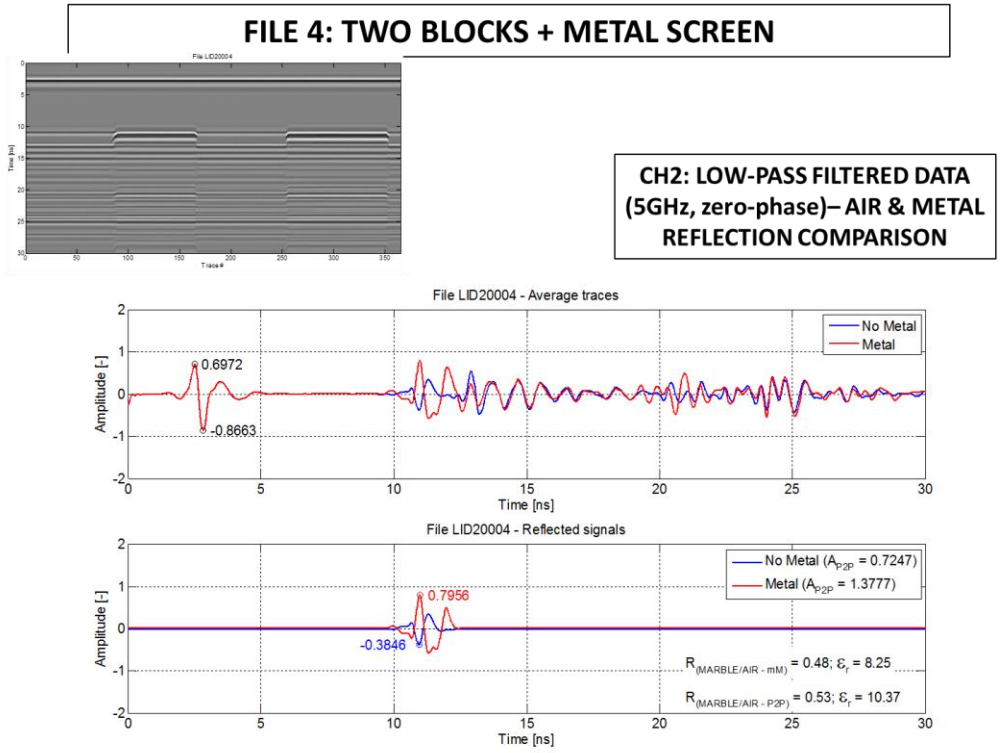

Figure A-14, File 4 (Two blocks_Metal screen_Low-pass filtered data)

FILE 2 & FILE 4

CH2: RAW DATA – VELOCITY & ATTENUATION ANALYSIS

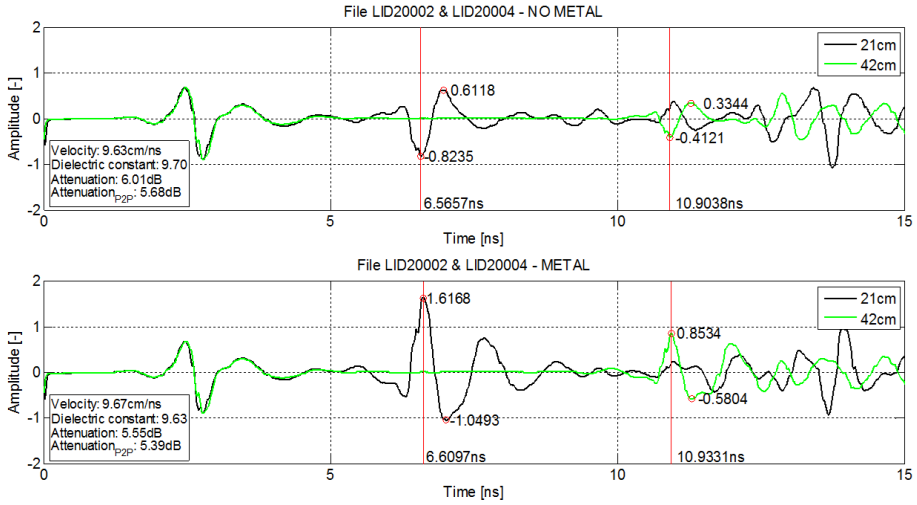

Figure A-15, File 2 & 4 (Velocity & attenuation analysis_Raw data)

FILE 2 & FILE 4

CH2: LOW-PASS FILTERED DATA (5GHz, zero-phase)– VELOCITY & ATTENUATION ANALYSIS

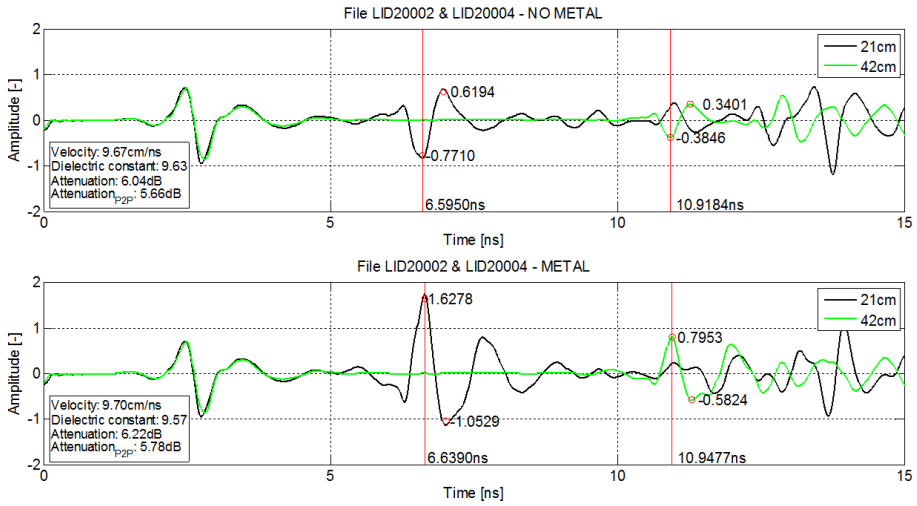

Figure A-16, File 2 & 4 (Velocity & attenuation analysis_Low-pass filtered data)

FILE 22: TWO BLOCKS 1 WAVELENGTH APART

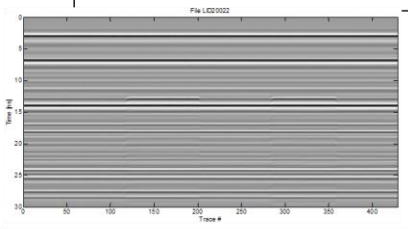

CH2: RAW DATA

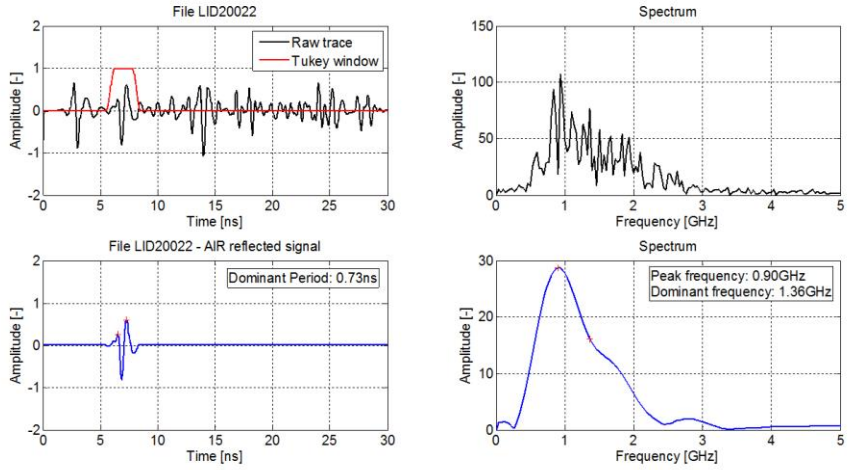

Figure A-17, File 22 (Two blocks_One wavelength apart_Raw data)

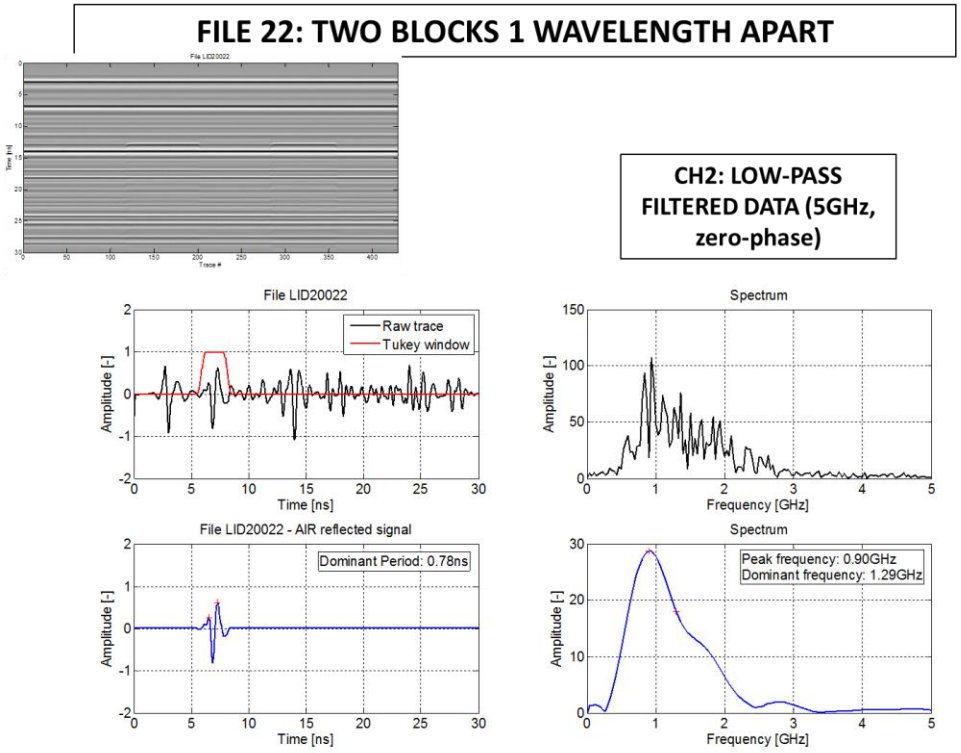

Figure A-18, File 22 (Two blocks_One wavelength apart_Low-pass filtered data)